NUREG/CR-6826
ANL-03/22

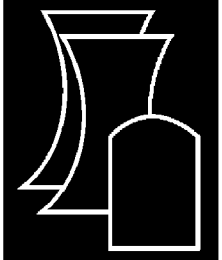

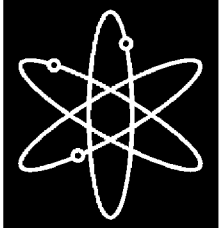

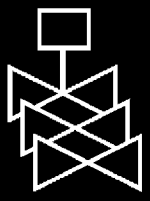

Fracture Toughness and Crack Growth Rates of Irradiated Austenitic Stainless Steels

Argonne National Laboratory

U.S. Nuclear Regulatory Commission
Office of Nuclear Regulatory Research
Washington, DC 20555-0001

AVAILABILITY OF REFERENCE MATERIALS IN NRC PUBLICATIONS

NRC Reference Material

As of November 1999, you may electronically access NUREG-series publications and other NRC records at NRC's Public Electronic Reading Room at http://www.nrc.gov/reading-rm.html. Publicly released records include, to name a few, NUREG-series publications; *Federal Register* notices; applicant, licensee, and vendor documents and correspondence; NRC correspondence and internal memoranda; bulletins and information notices; inspection and investigative reports; licensee event reports; and Commission papers and their attachments.

NRC publications in the NUREG series, NRC regulations, and *Title 10, Energy*, in the Code of *Federal Regulations* may also be purchased from one of these two sources.

1. The Superintendent of Documents
   U.S. Government Printing Office
   Mail Stop SSOP
   Washington, DC 20402–0001
   Internet: bookstore.gpo.gov
   Telephone: 202-512-1800
   Fax: 202-512-2250
2. The National Technical Information Service
   Springfield, VA 22161–0002
   www.ntis.gov
   1–800–553–6847 or, locally, 703–605–6000

A single copy of each NRC draft report for comment is available free, to the extent of supply, upon written request as follows:

Address: Office of the Chief Information Officer,
Reproduction and Distribution
Services Section
U.S. Nuclear Regulatory Commission
Washington, DC 20555-0001
E-mail: DISTRIBUTION@nrc.gov
Facsimile: 301–415–2289

Some publications in the NUREG series that are posted at NRC's Web site address http://www.nrc.gov/reading-rm/doc-collections/nuregs are updated periodically and may differ from the last printed version. Although references to material found on a Web site bear the date the material was accessed, the material available on the date cited may subsequently be removed from the site.

Non-NRC Reference Material

Documents available from public and special technical libraries include all open literature items, such as books, journal articles, and transactions, *Federal Register* notices, Federal and State legislation, and congressional reports. Such documents as theses, dissertations, foreign reports and translations, and non-NRC conference proceedings may be purchased from their sponsoring organization.

Copies of industry codes and standards used in a substantive manner in the NRC regulatory process are maintained at—

The NRC Technical Library
Two White Flint North
11545 Rockville Pike
Rockville, MD 20852–2738

These standards are available in the library for reference use by the public. Codes and standards are usually copyrighted and may be purchased from the originating organization or, if they are American National Standards, from—

American National Standards Institute
11 West 42nd Street
New York, NY 10036–8002
www.ansi.org
212–642–4900

Legally binding regulatory requirements are stated only in laws; NRC regulations; licenses, including technical specifications; or orders, not in NUREG-series publications. The views expressed in contractor-prepared publications in this series are not necessarily those of the NRC.

The NUREG series comprises (1) technical and administrative reports and books prepared by the staff (NUREG–XXXX) or agency contractors (NUREG/CR–XXXX), (2) proceedings of conferences (NUREG/CP–XXXX), (3) reports resulting from international agreements (NUREG/IA–XXXX), (4) brochures (NUREG/BR–XXXX), and (5) compilations of legal decisions and orders of the Commission and Atomic and Safety Licensing Boards and of Directors' decisions under Section 2.206 of NRC's regulations (NUREG–0750).

NUREG/CR-6826
ANL-03/22

Fracture Toughness and Crack Growth Rates of Irradiated Austenitic Stainless Steels

Manuscript Completed: March 2003
Date Published: August 2003

Prepared by
O.K. Chopra, E.E. Gruber, W.J. Shack

Argonne National Laboratory
9700 South Cass Avenue
Argonne, IL 60439

W.H. Cullen, Jr., and C.E. Moyer, NRC Project Managers

Prepared for
Division of Engineering Technology
Office of Nuclear Regulatory Research
U.S. Nuclear Regulatory Commission
Washington, DC 20555-0001
NRC Job Code Y6388

Fracture Toughness and Crack Growth Rates of Irradiated Austenitic Stainless Steels

by

O. K. Chopra, E. E. Gruber, and W. J. Shack

Abstract

Austenitic stainless steels (SSs) are used extensively as structural alloys in the internal components of reactor pressure vessels because of their superior fracture toughness properties. However, exposure to high levels of neutron irradiation for extended periods leads to significant reduction in the fracture resistance of these steels. Experimental data are presented on fracture toughness and crack growth rates (CGRs) of austenitic SSs irradiated to fluence levels up to 2.0 x 10^{21} n/cm^2 (E > 1 MeV) (^{a}3.0 dpa) at ^{a}288°C. Crack growth tests were conducted under cycling loading and long hold time trapezoidal loading in simulated boiling water reactor (BWR) environments, and fracture toughness tests were conducted in air. Neutron irradiation at 288°C decreases the fracture toughness of the steels; the data from commercial heats fall within the scatter band for the data obtained at higher temperatures. In addition, the results indicate significant enhancement of CGRs of the irradiated steels in normal water chemistry BWR environment; the CGRs for irradiated steels are a factor of ^{a}5 higher than the disposition curve proposed for sensitized austenitic SSs. The rates decreased by more than an order of magnitude in low–dissolved–oxygen BWR environment.

Contents

Figures

Tables

Executive Summary

Austenitic stainless steels (SSs) are used extensively as structural alloys in the internal components of reactor pressure vessels because of their high strength, ductility, and fracture toughness. Fracture of these steels occurs by stable tearing at stresses well above the yield stress, and tearing instabilities require extensive plastic deformation. However, exposure to neutron irradiation for extended periods changes the microstructure and degrades the fracture properties of these steels. Irradiation leads to a significant increase in yield strength and reduction in ductility and fracture resistance of austenitic SSs. Existing data on fracture toughness of austenitic SSs indicate substantial decrease in toughness at exposures of 1–10 dpa; the effect is largest in high–toughness steels. However, most of the existing fracture toughness test data have been obtained at temperatures above 350°C; fracture toughness results that are relevant to light water reactors (LWRs) are very limited.

In addition, radiation can exacerbate the corrosion fatigue and stress corrosion cracking (SCC) behavior of SSs by affecting the material microchemistry, e.g., radiation–induced segregation; material microstructure, e.g., radiation hardening; and water chemistry, e.g., radiolysis. Service failures in core components of several operating reactors have been attributed to irradiation assisted stress corrosion cracking (IASCC). While initially considered as a unique form of cracking that would not occur in the absence of radiation, IASCC is now generally considered as a radiation accelerated environmental cracking process. It has been termed as premature subcritical cracking of materials exposed to ionizing irradiation. The factors that influence SCC susceptibility of materials include neutron fluence, cold work, corrosion potential, water purity, temperature, and loading.

This report presents experimental data on fracture toughness and crack growth rate (CGR) for austenitic Types 304 and 316 SS that were irradiated to fluence levels of ^{a}0.3, 0.9, and 2.0 x 10^{21} n/cm^2 (E > 1 MeV) (^{a}0.45, 1.35, and 3.0 dpa) at ^{a}288°C. The irradiations were carried out in a He environment in the Halden heavy water boiling reactor. Fracture toughness tests were conducted in air and CGR tests in normal water chemistry (NWC) and hydrogen water chemistry (HWC) BWR environments at ^{a}288°C. All tests were performed on 1/4–T compact tension specimens.

Neutron irradiation at 288°C to 2.0 x 10^{21} n/cm^2 (E > 1 MeV) (3.0 dpa) decreased the fracture toughness of all of the steels. In general, fracture toughness of the commercial Heats C16 and C19 is superior to that of the laboratory Heats L20 and L2. These differences arise primarily from differences in toughness of the nonirradiated steels, i.e., the fracture toughness of the laboratory heats is significantly lower than that of the commercial heats. The fracture toughness J–R curves for irradiated Types 304 and 316 SS are comparable. The data from commercial heats fall within the scatter band for the data obtained at higher temperatures. For Heat C19 of Type 304 SS irradiated to 0.3, 0.9, and 2.0 x 10^{21} n/cm^2, the J_{Ic} values are 507, 313, and 188 kJ/m^2, respectively.

The results indicate significant enhancement of CGRs of irradiated steel in the NWC BWR environment. The CGRs of irradiated steels are a factor of ^{a}5 higher than the disposition curve proposed in NUREG–0313 for sensitized austenitic SSs in water with 8 ppm dissolved oxygen (DO). The CGRs of Type 304 SS irradiated to 0.9 and 2.0 x 10^{21} n/cm^2 and of Types 304 and 316 SS irradiated to 2.0 x 10^{21} n/cm^2 are comparable.

In low–DO BWR environments, the CGRs of the irradiated steels decreased by an order of magnitude in some tests, e.g., Heat C3 of Type 304 SS irradiated to 0.9 x 10^{21} n/cm^2 and Heat C16 of Type 316 SS irradiated to 2 x 10^{21} n/cm^2. The beneficial effect of decreased DO was not observed for Heat C3 of Type 304 SS irradiated to 2 x 10^{21} n/cm^2; it is possible that this different behavior is associated with the loss of constraint in the specimen due to the high applied load.

Type 304 SS irradiated to 0.3 x 10^{21} n/cm^2 shows very little environmental enhancement of CGRs in the NWC BWR environment; the CGRs under SCC conditions are below the disposition curve for sensitized SSs in water with 8 ppm DO given in NUREG–0313.

Acknowledgments

The authors thank T. M. Galvin, L. A. Knoblich, E. J. Listwan, and R. W. Clark for their contributions to the experimental effort. This work is sponsored by the Office of Nuclear Regulatory Research, U.S. Nuclear Regulatory Commission, under Job Code Y6388; Project Manager: W. H. Cullen, Jr. and C. E. Moyer.

1. Introduction

Austenitic stainless steels (SSs) are used extensively as structural alloys in reactor pressure vessel internal components because of their high strength, ductility, and fracture toughness. Fracture of these steels occurs by stable tearing at stresses well above the yield stress, and tearing instabilities require extensive plastic deformation. However, exposure to neutron irradiation for extended periods changes the microstructure and degrades the fracture properties of these steels. Irradiation leads to a significant increase in yield strength and reduction in ductility and fracture resistance of austenitic SSs.[1–3] Changes in mechanical properties are known to influence fatigue or corrosion fatigue properties of irradiated materials.[4] Irradiation assisted stress corrosion cracking (IASCC) is another degradation process that affects light water reactor (LWR) internals exposed to fast neutron radiation.[1,5,6]

Neutron irradiation of austenitic SSs at temperatures below 400°C leads to the formation of a substructure with very fine defects that consist of small (<5 nm) vacancy and interstitial loops or "black spots" and larger (>5 nm) faulted interstitial loops.[7–9] The latter are obstacles to dislocation motion and lead to matrix strengthening and increase in tensile strength. Also, irradiation–induced defects cause loss of ductility and reduced strain-hardening capacity of the material. The effects of radiation on various austenitic SSs vary significantly and appear to be related to minor differences in the chemical composition of the steels;[1] the chemical composition can influence the stacking fault energy and/or irradiation–induced microstructure. As yield strength approaches ultimate strength, planar slip or dislocation channeling is promoted and leads to pronounced degradation in the fracture resistance of these steels.[3] In general, higher stacking–fault energy enhances and cold working inhibits dislocation channeling.[1]

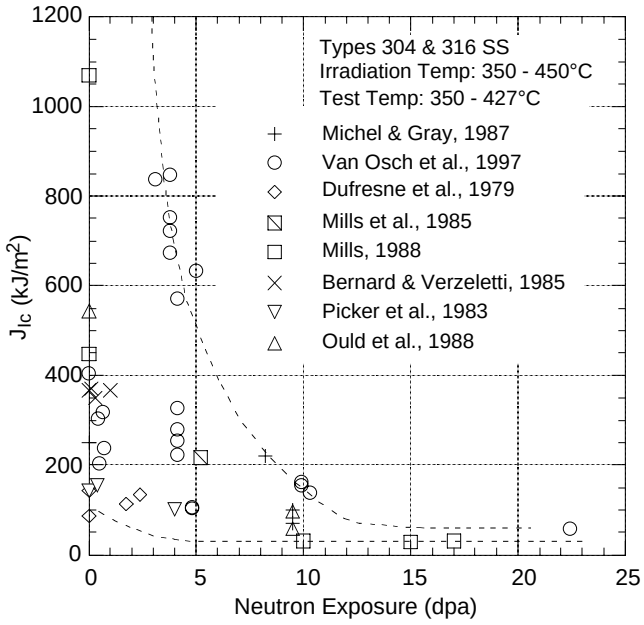

Figure 1.
Fracture toughness J_{Ic} as a function of neutron exposure for austenitic Types 304 and 316 SS

The effect of neutron exposure on the fracture toughness J_{Ic} of austenitic SSs irradiated at 350–450°C is shown in Fig. 1.[10–18] The effects of irradiation may be divided into three regimes: little or no loss of toughness below a threshold exposure of ≈1 dpa, substantial

decrease in toughness at exposures of 1–10 dpa, and no further reduction in toughness above a saturation exposure of 10 dpa. The effect is largest in high–toughness steels. The degradation in fracture properties saturates at a J_{Ic} value of ≈30 kJ/m^2 (or equivalent critical stress intensity factor K_{JC} of 70 MPa $m^{0.5}$). Also, the failure mode changes from dimple fracture to channel fracture. However, most of the existing fracture toughness test data have been obtained at temperatures above 350°C; fracture toughness results that are relevant to LWRs are very limited.[2]

Radiation can exacerbate the corrosion fatigue and stress corrosion cracking (SCC) behavior of SSs by affecting the material microchemistry, e.g., radiation–induced segregation; material microstructure, e.g., radiation hardening; and water chemistry, e.g., radiolysis.[5] Service failures in core components of several boiling water reactors (BWRs)[19,20] and pressurized water reactors (PWRs)[4,21] have been attributed to IASCC. While initially considered as a unique form of cracking that would not occur in the absence of radiation, IASCC is now generally considered as a radiation accelerated environmental cracking process. It has been termed as premature subcritical cracking of materials exposed to ionizing irradiation.

The factors that influence SCC susceptibility of materials include neutron fluence, cold work, corrosion potential, water purity, temperature, and loading. The effects of neutron fluence on IASCC of austenitic SSs has been investigated for BWR control blade sheaths[20] and laboratory tests on BWR–irradiated material;[5,22–24] the extent of intergranular SCC increases with fluence. Although a threshold fluence level of 5 x 10^{20} n/cm^2 (E >1 MeV) has been reported for austenitic SSs in BWR environment, the experimental data show an increase in intergranular cracking above a fluence of ≈2 x 10^{20} n/cm^2 (E >1 MeV) (≈0.3 dpa). The results also show the beneficial effect of reducing the corrosion potential of the environment.[25,26] However, low corrosion potential does not provide immunity to IASCC, e.g., intergranular SCC has been observed in cold worked, irradiated SS baffle bolts in PWRs. The threshold fluence for IASCC is higher under low potential conditions such as HWC in BWRs or PWR primary water chemistry.

This report presents experimental data on fracture toughness, corrosion fatigue, and stress corrosion cracking (SCC) of austenitic SSs that were irradiated to fluence levels of ≈0.3, 0.9, and 2.0 x 10^{21} n/cm^2 (E > 1 MeV) (≈0.45, 1.35, and 3.0 dpa) at ≈288°C. The irradiations were carried out in a He environment in the Halden heavy water boiling reactor. Fracture toughness tests were conducted in air and CGR tests in normal water chemistry (NWC) and low–DO BWR environments at 288°C. The results are compared with the existing data obtained from irradiated reactor internal components removed from operating plants and materials irradiated in test reactors.

2. Experimental

Fracture toughness J–R curve and crack growth rate (CGR) tests have been conducted at 288°C on several austenitic SSs that were irradiated up to 2.0 x 10^{21} n/cm^2 (E > 1 MeV) (≈3.0 dpa) at ≈288°C in a helium environment in the Halden boiling heavy water reactor. The tests were performed on 1/4–T compact tension (CT) specimens; the J–R curve tests were performed in air and CGR tests in BWR environments. A modified configuration of the CT specimen geometry, Fig. 2, was used in the present study. Crack extensions were determined by both DC potential and elastic unloading compliance techniques.

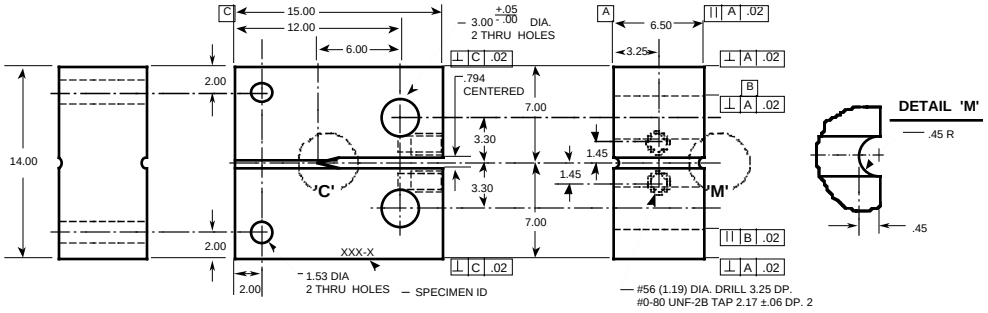

Figure 2. Configuration of compact–tension specimen used for this study (dimensions in mm)

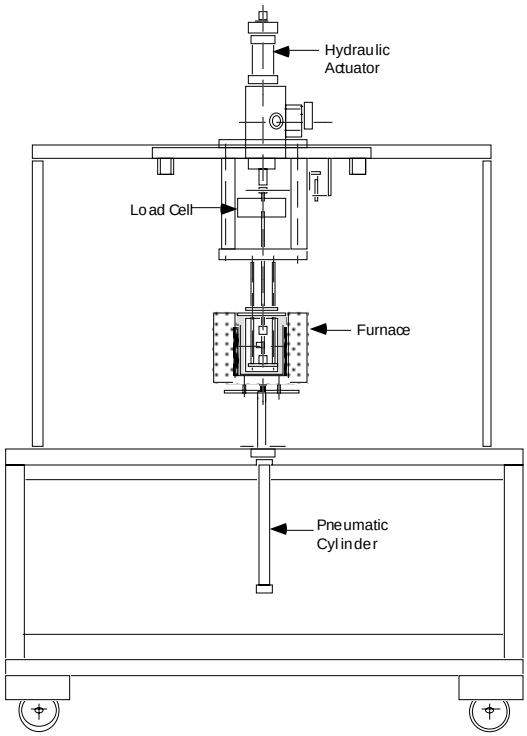

Figure 3. Schematic representation of hot–cell J–R test facility

The facility for conducting the tests is designed for in–cell testing, with the test train, furnace, and other required equipment mounted on top of a portable wheeled cart that can be easily rolled into the cell. A schematic representation of the system is shown in Fig. 3. A small

autoclave is installed inside the furnace for conducting tests in simulated BWR environments. Water is circulated through a port in the autoclave cover plate that serves both as inlet and outlet. The hydraulic actuator is mounted on top of the frame, with the test train components suspended beneath it. A drawing of the actuator, load cell, test train, autoclave, and furnace are shown in Fig. 4. The 22–kN (5–kip) load cell is at the top of the pull rod. The furnace is mounted on a pneumatic cylinder and can be raised to enclose the autoclave with the load cage and the specimen during the test. An Instron Model 8500+ Dynamic Materials Testing System is used for performing the tests.

The load cage that contains the test specimen consists of the cover plate of a 1–liter SS autoclave (from PARR Associates) and a 12.7–mm–thick bottom plate separated by four compression rods. The lower two–piece clevis assembly is fastened to the bottom plate of the cage with the two sections connected by an oxidized zircalloy pin, electrically insulated with mica washers. The same arrangement is used for the upper clevice assembly, connected to the pull rod. A 1/4–T CT specimen is mounted in the clevises with Inconel pins. Platinum wires are used for the current and potential leads. The current leads are attached to SS split pins that are inserted into the holes at the top and bottom of the specimen. The potential leads are attached by screwing short SS pins into threaded holes in the specimen and attaching the platinum wires with in–line SS crimps.

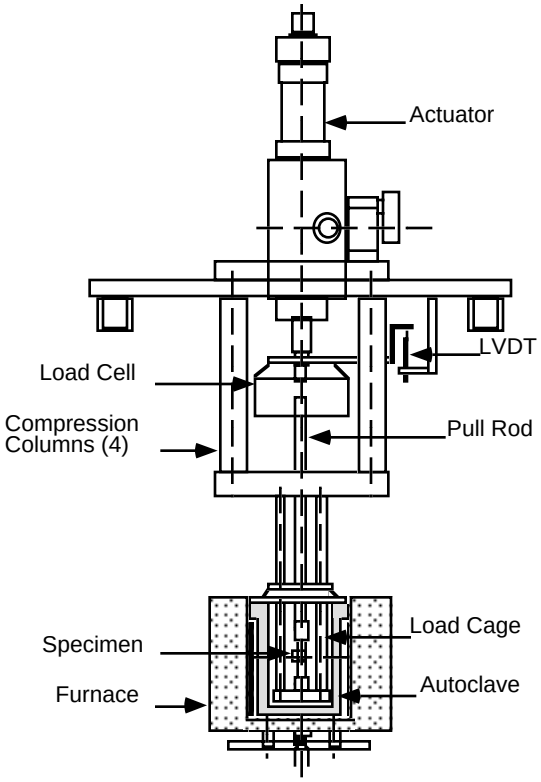

Figure 4. Schematic of the actuator, load cell, test train, autoclave, and furnace

The recirculating water system consists of a storage tank, high pressure pump, regenerative heat exchanger, autoclave preheater, test autoclave, electrochemical potential (ECP) cell preheater, ECP cell, regenerative heat exchanger, Mity Mite^{TM} back-pressure regulator, an ion–exchange cartridge, a 0.2 micron filter, a demineralizer resin bed, another

0.2 micron filter, and return line to the tank. A schematic diagram of the recirculating water system is shown in Fig. 5. Water is circulated at low flow rates, e.g., ≈10 mL/min.

The BWR environments comprise high–purity–deionized water that contains either ≈300 ppb or <30 ppb DO resulting in ECPs for SS that range from 160 to -500 mV. The feedwater is stored in a 135–L SS tank manufactured by Filpaco Industries. The tank is designed for vacuum and over pressure to 60 psig. The deionized water is prepared by passing purified water through a set of filters that comprise a carbon filter, an Organex–Q filter, two ion exchangers, and a 0.2–mm capsule filter. Water samples are taken periodically to measure pH, resistivity, and DO concentration. The DO level in water is established by bubbling nitrogen that contains ≈1% oxygen through the deionized water in the supply tank. The DO is reduced to <10 ppb by bubbling nitrogen through the water; a vacuum is drawn on the tank cover gas to speed deoxygenation. The cover gas of the storage tank is nitrogen plus 1% oxygen for high–DO environment, and either pure nitrogen or nitrogen plus 5% hydrogen for low–DO environment.

1. COVER GAS SUPPLY TANK
2. HIGH-PRESSURE REGULATOR WITH FLASH ARRESTOR
3. LOW-PRESSURE REGULATOR
4. FLOW METER
5. GAS PURIFIER
6. PRESSURE GAUGE
7. PRESSURE RELIEF VALVE
8. VENT TO AIR WITH FLASH ARRESTOR
9. FEEDWATER STORAGE TANK
10. SPARGE TUBE
11. FEEDWATER FILL PORT
12. WATER SAMPLE PORT
13. SOLENOID VALVE
14. 0.2–MICRON FILTER
15. HIGH-PRESSURE PUMP
16. CHECK VALVE
17. RUPTURE DISK
18. HEAT EXCHANGER
19. SYSTEM BLEED PORT
20. HIGH-PRESSURE GAUGE
21. AUTOCLAVE PREHEATER
22. PARR AUTOCLAVE
23. THERMOCOUPLE WELL
24. ECP CELL PREHEATER
25. ECP CELL
26. ECP CELL BYPASS LINE
27. BACK–PRESSURE RELIEF VAVLE
28. ION EXCHANGE CARTRIDGE
29. RECIRCULATING PUMP
30. DEMINERALIZER
31. DEMINERALIZER BYPASS LINE

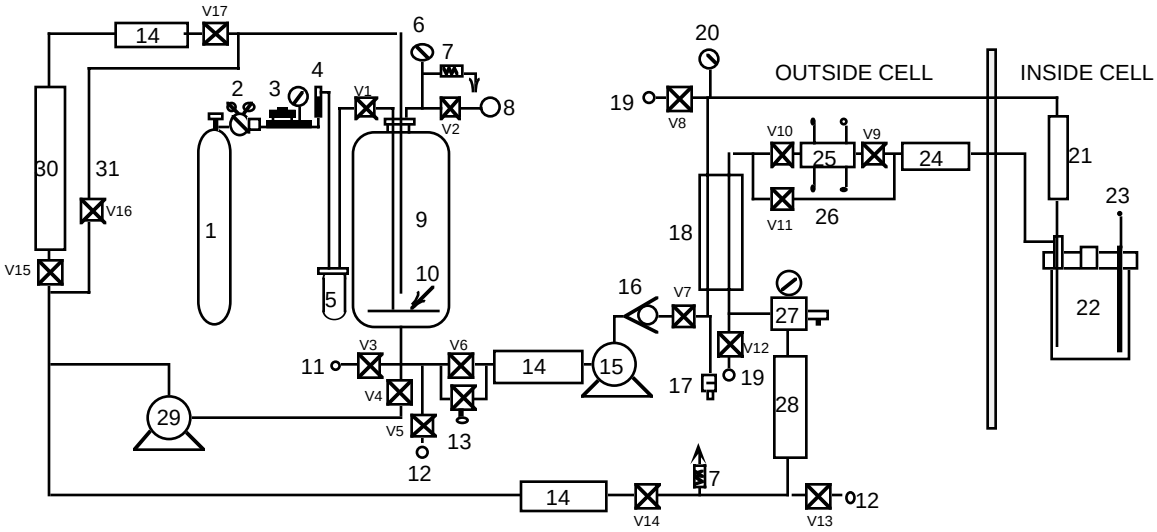

Figure 5. Schematic diagram of recirculating water system

The fracture toughness J–R curve tests were performed in accordance with the requirements of ASTM Specification E 1737 for "J–Integral Characterization of Fracture Toughness." The CGR tests were performed in accordance with ASTM E–647 "Standard Test Method for Measurement of Fatigue Crack Growth Rates" and ASTM E–1681 "Standard Test Method for Determining a Threshold Stress Intensity Factor for Environment–Assisted

Cracking of Metallic Materials Under Constant Load." The composition of the various heats of irradiated austenitic SSs is presented in Table 1. The tensile yield and ultimate stress for the various SSs irradiated to the three fluence levels and in the nonirradiated condition[27,28] are given in Table 2.

Table 1. Composition (wt.%) of austenitic stainless steels irradiated in the Halden reactor

Alloy ID[a]	Vendor Heat ID	Analysis	Ni	Si	P	S	Mn	C	N	Cr	Mo	O[b]
	Type 304 SS											
C3	PNL-C-6	Vendor	8.91	0.46	0.019	0.004	1.81	0.016	0.083	18.55		
		ANL	9.10	0.45	0.020	0.003	1.86	0.024	0.074	18.93		144
C19	DAN–74827	Vendor	8.08	0.45	0.031	0.003	0.99	0.060	0.070	18.21		–
		ANL	8.13	0.51	0.028	0.008	1.00	0.060	0.068	18.05		200
L2	BPC–4–111	Vendor	10.50	0.82	0.080	0.034	1.58	0.074	0.102	17.02		66
L20	BPC–4–101	Vendor	8.91	0.17	0.010	0.004	0.41	0.002	0.002	18.10		–
		ANL	8.88	0.10	0.020	0.005	0.47	0.009	0.036	18.06		940
	Type 316 SS											
C16	PNL–SS–14	Vendor	12.90	0.38	0.014	0.002	1.66	0.020	0.011	16.92		–
		ANL	12.32	0.42	0.026	0.003	1.65	0.029	0.011	16.91	2.18	157

[a]First letters "C" and "L" denote commercial and laboratory heats, respectively.
[b]In wppm.

Table 2. Tensile properties[a] of irradiated austenitic stainless steels at 288°C

			Fluence (E >1 MeV)					
	Nonirradiated		0.3×10^{21} n/cm^2		0.9×10^{21} n/cm^2		2.0×10^{21} n/cm^2	
Steel Type (Heat)	Yield (MPa)	Ultimate (MPa)	Yield (MPa)	Ultimate (MPa)	Yield (MPa)	Ultimate (MPa)	Yield (MPa)	Ultimate (MPa)
304 SS (C3)	(154)	(433)	338	491	632	668	796	826
304 SS (C19)	178	501	554	682	750	769	787	801
304 SS (L2)	193	348	–	–	839	849	–	–
304 SS (L20)	–	–	454	552	670	743	–	–
					632	697		
316 SS (C16)	(189)	(483)	370	527	562	618	766	803

[a]Estimated values within parentheses.

The experimental data for the fracture toughness J–R curves are compiled in the Appendix. Some of the results have been presented earlier.[29–32] Because tensile properties of the material were not available for some irradiation conditions, estimated values of flow stress were used in the earlier presentations. In the present report, the fracture toughness results have been reevaluated using tensile properties determined from comparably irradiated tensile specimens.[27,28]

Also, in earlier publications,[29–33] Heat C16 was erroneously identified as Type 304 SS. Because the flow stress for solution annealed Type 316 SS is typically higher than that for solution annealed Type 304 SS, the experimental data for nonirradiated Heat C16 have been corrected in the present report; the difference is essentially in the slope of the blunting line.

2.1 J–R Curve Characterization

Before testing, the specimens were fatigue–precracked in air at room temperature. The precracked specimens were then tested at 288°C at a constant extension rate; tests were interrupted periodically to determine the crack length. Specimens were held at constant extension to measure crack length by both the DC potential drop and elastic unloading compliance techniques. For most steels, load relaxation occurs during the hold period or

unloading, which causes a time-dependent nonlinearity in the unloading curve. Consequently, before unloading, the specimen was held for ≈1 min to allow load relaxation. Elastic unloading and reloading was carried out in the load control mode.

Specimen extension was monitored and controlled outside the high–temperature zone. The displacement of load points was determined by subtracting the extension of the load train from the measured extension. The load train displacement was determined as a function of applied load using a very stiff specimen. The load–line displacements determined by this method were compared with actual displacements measured optically during J–R curve tests at room temperature. The measured and estimated values were in very good agreement; for load–line displacements up to 2 mm, the error in the estimated values was <0.02 mm.[33] Examples of load-vs.-loadline displacement curves for irradiated SS are shown in Fig. 6.

The J–integral was calculated from the load–vs.–loadline displacement curves according to the correlations for DC(T) specimens in ASTM Specification E 1737. The following correlation, obtained from the best–fit of the experimental data, was used to determine crack lengths by the unloading compliance method.

$$a_i/W = 1.2011 - 7.1572\ u_x + 16.87\ u_x^2 - 13.527\ u_x^3, \quad (1)$$

where

$$u_x = 1\ /\ [(B_{ef}E_{ef}C_{ci})^{1/2} + 1], \quad (2)$$

$$B_{ef} = B - (B - B_N)^2\ /\ B, \quad (3)$$

$$E_{ef} = E\ /\ (1 - \upsilon^2), \quad (4)$$

W is the specimen width, B is the specimen thickness, B_N is the net specimen thickness or distance between the roots of the side grooves, E is the elastic modulus, υ is Poisson's ratio, and C_{ci} is the specimen elastic compliance corrected for rotation of the crack centerline. The effective elastic modulus E_{ef} was adjusted with the measured initial crack length a_i, i.e., E_{ef} was determined from Eqs. 1 and 2 by using the measured fatigue precrack length a_i and the corresponding corrected specimen elastic compliance C_{ci}.

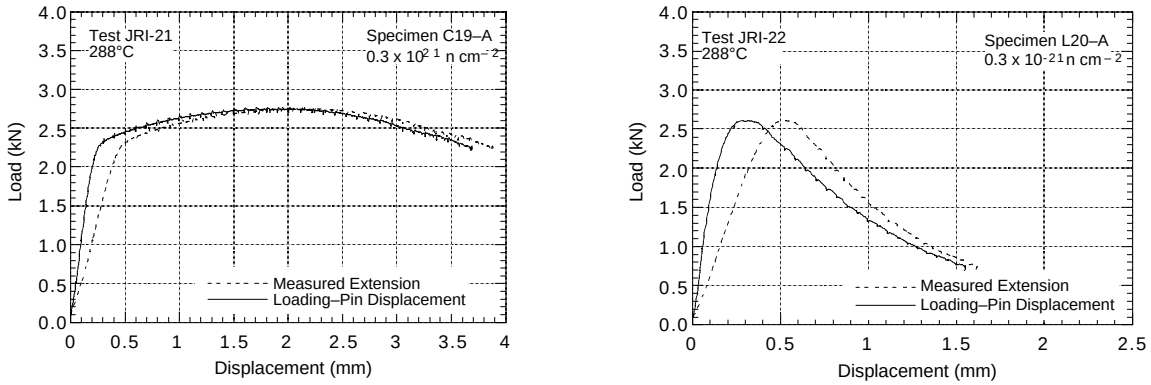

Figure 6. Examples of load-vs.-loadline displacement curves for irradiated specimens of Heats (a) C19 and (b) L20 of Type 304 SS tested at 288°C

The following correlation, obtained from the best–fit of the experimental data for normalized crack length and normalized DC potential, was used to determine crack lengths by the DC potential method.

$$\frac{a_i}{W} = \left[0.28887 \left(\frac{U}{U_0} - 0.5 \right) \right]^{0.34775}, \tag{5}$$

where W is the specimen width, and U and U_0 are the current and initial potentials. Equation 5 is comparable to the ASTM E 1737 correlation for a CT specimen with current inputs at the W/4 position and DC potential lead connections at the W/3 position.

The DC potential data were corrected for the effects of plasticity on the measured potential, i.e., large crack–tip plasticity can increase measured potentials due to resistivity increases without crack extension. As per ASTM E 1737, the change in potential before crack initiation was ignored, and the remainder of the potential change was used to establish the J–R curve. A plot of normalized potential vs. loadline displacement generally remains linear until the onset of crack extension. For all data within the linear portion of the curve, crack extension was calculated from the blunting–line relationship $\Delta a = J/(4\sigma_f)$, where σ_f is the flow stress defined as the average of the 0.2% offset yield stress and ultimate tensile stress. The exclusion lines are parallel to the blunting line intersecting the abscissa at 0.15 and 1.50 mm.

Although ASTM E 813 specifies a slope of two times the effective yield stress (or flow stress) for the offset line, a slope of four times the flow stress was used to define the offset and exclusion lines. For high–strain–hardening materials, e.g., nonirradiated austenitic SSs, a slope that is four times the flow stress ($4\sigma_f$) represents the blunting line better than the slope of $2\sigma_f$ defined in ASTM E 1737.[3] In irradiated materials, the increase in yield stress is primarily due to a high density of barriers to dislocation motion. During deformation as dislocations sweep through the irradiated matrix, they annihilate the very fine scale of barriers, thus creating a "channel" for easy dislocation motion. This may result in marked work softening. To account for possible strain softening that may occur in irradiated materials, an effective flow stress defined as the average of the nonirradiated and irradiated flow stress was used in J–R curve data analysis. Because the effective flow stress discounts the irradiation–induced increase in flow stress by a factor of 2, the slope of the blunting line was defined as $4\sigma_f$ even for the irradiated materials.

The final crack size was marked by fatigue cycling at room temperature. The specimens were then fractured and the initial (i.e., fatigue precrack) and final (test) crack lengths of both halves of the fractured specimen were measured optically. The crack lengths were determined by the 9/8 averaging technique, i.e., the two near–surface measurements were averaged and the resultant value was averaged with the remaining seven measurements.

The elastic unloading compliance measurements were adjusted only with the measured initial crack length, whereas the crack length measurements obtained by the DC potential–drop technique were adjusted with both the initial and final crack lengths. The two-point pinning method was used to correct the measured potentials from the test data. The corrected normalized potentials $\overline{NP}$ are expressed in terms of the measured normalized potentials *NP* (U/U_0 in Eq. 5) by the relationship

$$\overline{NP} = \frac{NP - P_1}{P_2 - P_1}. \tag{6}$$

The variables P_1 and P_2 are solutions of the expressions

$$\overline{NP_i} = \frac{NP_i - P_i}{P_2 - P_1}, \tag{7}$$

and

$$\overline{NP_f} = \frac{NP_f - P_i}{P_2 - P_1}, \tag{8}$$

where $\overline{NP_i}$ and $\overline{NP_f}$ are normalized potentials that correspond to initial and final crack lengths determined from Eq. 5, and NP_i and NP_f are the measured values. The fracture toughness J_{Ic} values were determined from ASTM E–813 as the intersection of the 0.2–mm offset line with the power law fit (of the form $J = \Delta a^n$) of the test data between the 0.15– and 1.50–mm exclusion lines.

Several fracture toughness J–R curve tests were conducted at room temperature and 288°C on thermally aged CF–8M cast SS and on a 50% cold–worked (CW) Type 316LN SS to develop correlations for estimating crack lengths and to validate the test procedure. Experimental data for the tests at 288°C are given in the Appendix, Tables A–1 to A–7.

For materials with relatively low fracture toughness, e.g., J_{Ic} <300 kJ/m^2, the measurements of crack extension by the elastic unloading compliance method showed excellent agreement with those obtained by DC potential methods. The J–R curves obtained from DC potential and elastic unloading compliance methods for thermally aged cast CF–8M SSs and 50% cold–worked Type 316NG SS at 288°C are shown in Figs. 7–9. Replicate tests on different specimens of the same material show good reproducibility of the J–R curves.

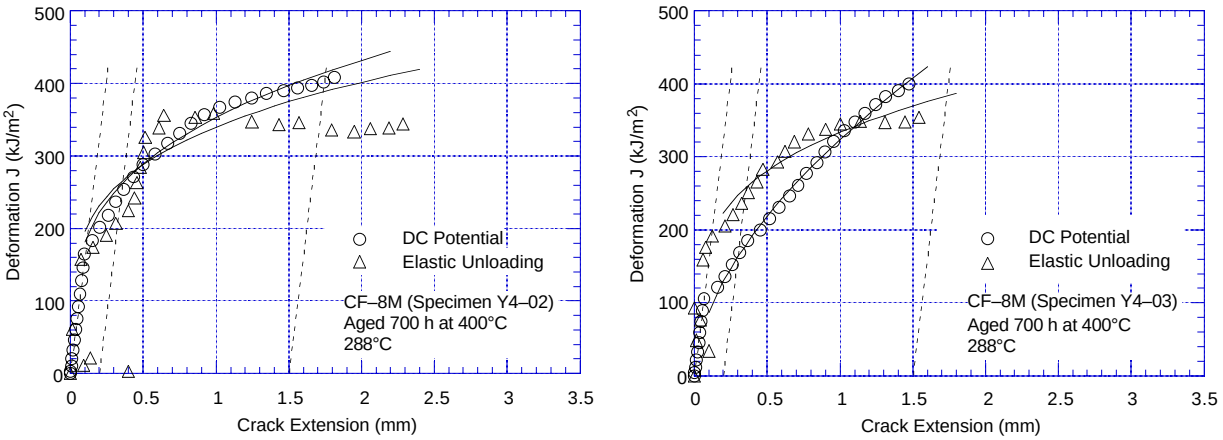

Figure 7. Fracture toughness J–R curves obtained from DC potential and elastic unloading compliance methods for specimens (a) Y4–02 and (b) Y4–03 of thermally aged cast CF–8M SS

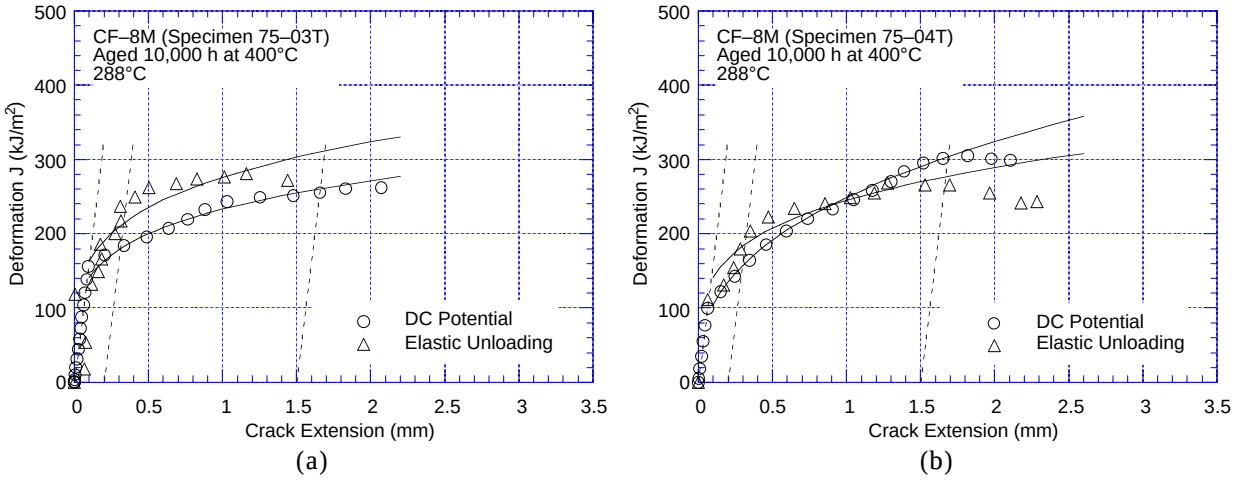

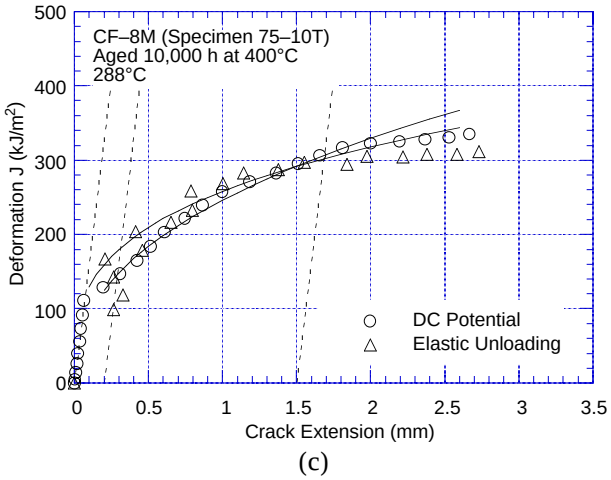

Figure 8.
Fracture toughness J–R curves obtained from DC potential and elastic unloading compliance methods for thermally aged Heat 75 of cast CF–8M SS; specimen (a) 75–03T, (b) 75–04T, and (c) 75–10T

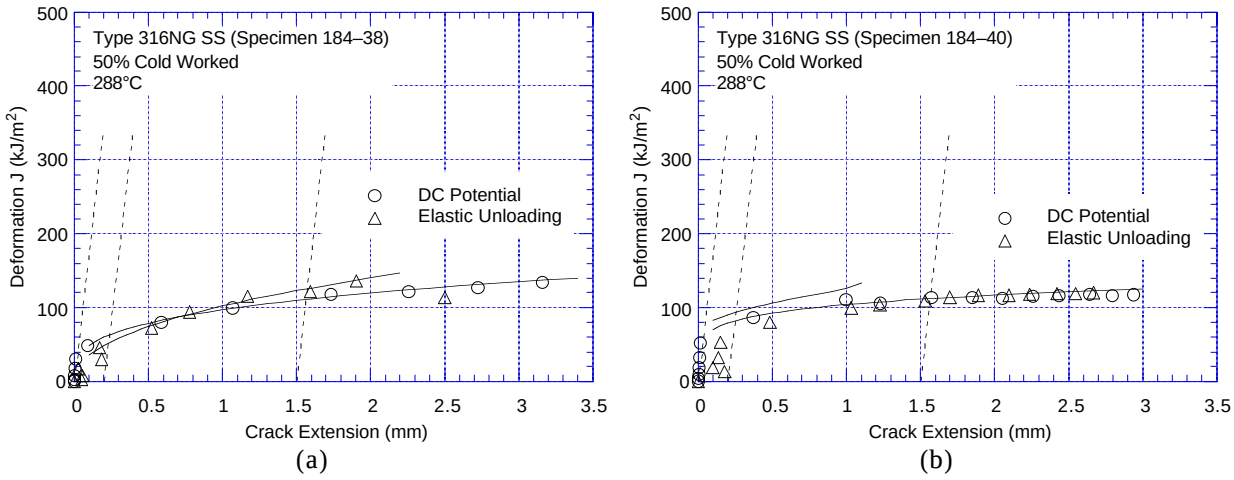

Figure 9. Fracture toughness J–R curves obtained from DC potential and elastic unloading compliance methods for 50% cold–worked Type 316NG; specimen (a) 184–38 and (b) 184–40

The J–R curves obtained from 1/4–T CT specimens of thermally aged Heat 75 of CF–8M cast SS are compared with those obtained from 1–T CT specimens of the same heat in Fig. 10. The curves for the 1/4–T CT specimens show good agreement with the curve for the 1–T CT specimen with the same orientation, e.g., transverse orientation.

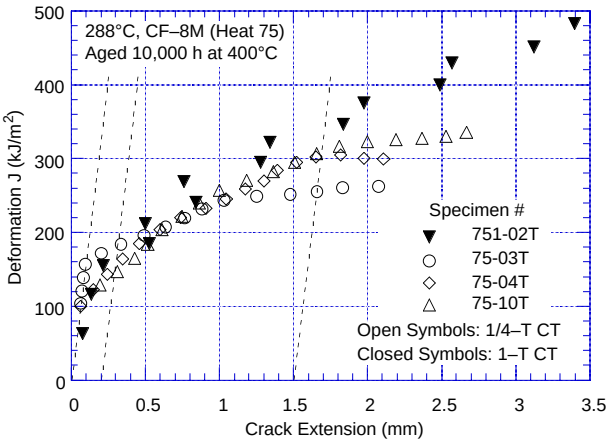

Figure 10.
Fracture toughness J–R curves for 1/4–T and 1–T CT specimens of aged Heat 75 of CF–8M cast stainless steel at 288°C. The last digit in the specimen number represents orientation;
T = transverse.

2.2 Crack Growth Rate Tests

2.2.1 Procedure

All specimens were fatigue precracked in the test environment at temperature and load ratio R = 0.2, ≈1 Hz frequency, and maximum stress intensity factor K_{max} ≈15 MPa $m^{1/2}$. After ≈0.5–mm extension, R was increased incrementally to 0.7, and the loading waveform changed to a slow/fast sawtooth with rise times of 30–1000 s. Constant–load tests were conducted with the trapezoidal waveform, R = 0.7, 1– or 2–h hold period at peak, and either 4– or 24–s unload/reload period. During individual test periods, K_{max} was maintained approximately constant by periodic load shedding (less than 2% decrease in load at any given time).

The stress intensity factor range ΔK was calculated as follows:

$$\Delta K = \frac{\Delta P}{\left(BB_N W\right)^{1/2}} \frac{\left(2+\frac{a}{W}\right)}{\left(1-\frac{a}{W}\right)^{3/2}} f\left(\frac{a}{W}\right) \tag{9}$$

$$\Delta P = P_{max} - P_{min} \qquad \text{for R > 0} \tag{10}$$

$$f\left(\frac{a}{W}\right) = 0.886 + 4.64\left(\frac{a}{W}\right) - 13.32\left(\frac{a}{W}\right)^2 + 14.72\left(\frac{a}{W}\right)^3 - 5.6\left(\frac{a}{W}\right)^4 . \tag{11}$$

where P_{max} and P_{min} are maximum and minimum applied load, a is crack length, W is the specimen width, and effective thickness $B_{eff} = (B\ B_N)^{0.5}$. Also, because a modified configuration of disc–shaped CT specimen was used in the present study, crack length was calculated from Eq. 5 that was developed from the best fit of the experimental data for normalized crack length and normalized DC potential.

Under cyclic loading, the CGR (m/s) can be expressed as the superposition of the rate in air (i.e., mechanical fatigue) and the rates due to corrosion fatigue and SCC, given as

$$\dot{a}_{env} = \dot{a}_{air} + \dot{a}_{cf} + \dot{a}_{scc} . \tag{12}$$

During crack growth tests in high–temperature water, environmental enhancement of CGRs does not occur from the start of the test. Under more rapid cyclic loading, the crack growth is dominated by mechanical fatigue. The CGRs during precracking and initial periods of cyclic loading were primarily due to mechanical fatigue. For the present tests on irradiated SSs, environmental enhancement typically was observed under loading conditions that would lead to CGRs between 10^{-10} and 10^{-9} m/s in air. For K_{max} values of 15–18 MPa $m^{1/2}$, these values correspond to a load ratio $R \geq 0.5$ and rise time ≥ 30 s.

All tests were started in high–purity water that contained 250–300 ppb DO (i.e., NWC BWR environment). The ECPs of a Pt electrode and a SS sample located at the exit of the autoclave were monitored continuously during the test while the water DO level and conductivity were determined periodically. After data were obtained for high–DO water, the DO level in the feedwater was decreased to <30 ppb by sparging the feedwater with pure N_2, and in some cases, this was followed by sparging with N_2 + 5% H_2 [to simulate hydrogen water chemistry (HWC) BWR environment]. Because of the very low water flow rates, it took several days for the environmental conditions to stabilize. In general, the changes in ECP of the SS sample were slower than in the ECP of the Pt electrode.

After the test the final crack size was marked by fatigue cycling in air at room temperature. The specimens were then fractured, and the fracture surface of both halves of the specimen was photographed with a telephoto lens through the hot cell window. The final crack length of each half of the fractured specimen was measured from the photograph by the 9/8 averaging technique.

2.2.2 Data Qualification

The ASTM specifications for specimen K/size criteria are intended to ensure applicability and transferability of the cracking behavior of a component or specimen of a given thickness under a specific loading condition to a crack associated with a different geometry, thickness, and loading condition.

The CGR test results were validated in accordance with the specimen size criteria of ASTM E 1681 and E 647. These criteria require that the plastic zone at the tip of a fatigue crack is small relative to the specimen geometry. For constant load tests, ASTM E 1681 requires that

$$B_{eff} \text{ and } (W-a) \geq 2.5\,(K/\sigma_{ys})^2, \tag{13}$$

and for cyclic loading ASTM 647 requires that

$$(W-a) \geq (4/\pi)\,(K/\sigma_{ys})^2, \tag{14}$$

where K is the applied stress intensity factor, and σ_{ys} is the yield stress of the material. For tests on irradiated material, side grooved specimens are strongly recommended, with a depth for each side groove between 5 and 10% of the specimen thickness. The effective thickness B_{eff} of side–grooved specimen should be calculated as a root mean square, i.e., $(B \cdot B_N)^{0.5}$. In high–temperature water, because the primary mechanism for crack growth during continuous cycling is not mechanical fatigue, Eq. 13 is probably the more appropriate criterion, but Eq. 14 may give acceptable results. For high–strain hardening materials, i.e., materials with an

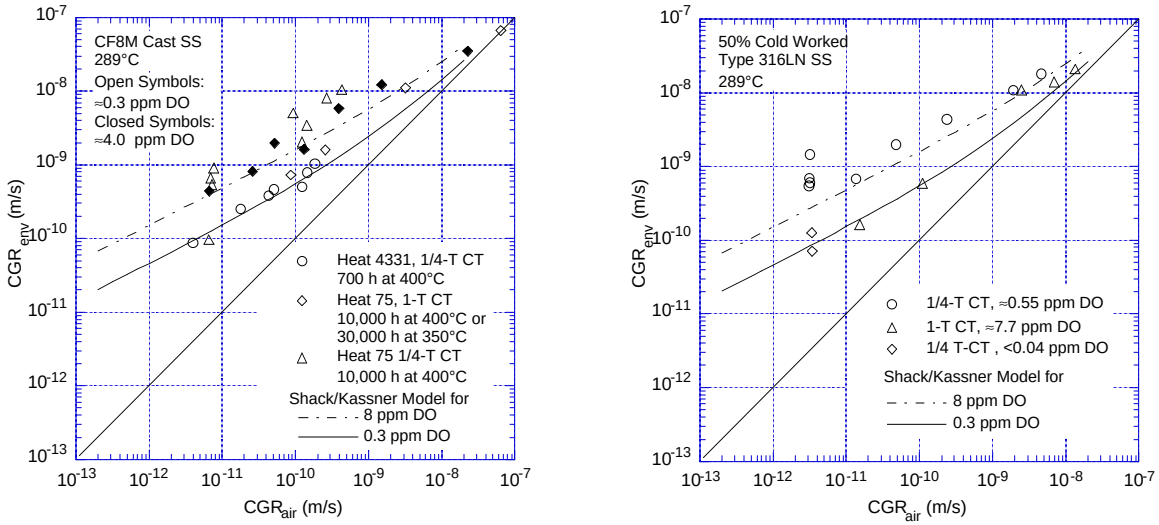

Figure 11. Crack growth rate data under continuous cycling for thermally aged cast SS and 50% cold–worked Type 316LN SS in high–purity water at 289°C.

ultimate to yield stress ratio (σ_{ult}/σ_{ys}) ≥1.3, both criteria allow the use of the flow stress defined as $\sigma_f = (\sigma_{ult} + \sigma_{ys})/2$ rather than the yield stress.

The K/size criteria were developed for materials that show work hardening and, therefore, may not be valid for materials irradiated to fluence levels where, on a local level, they do not strain harden. This lack of strain hardening, or strain softening, is most dramatic when dislocation channeling occurs but may also occur at lower fluences. For moderate to highly irradiated material, it has been suggested that an effective yield stress, defined as the average of the nonirradiated and irradiated yield stresses, be used;[34] this discounts the irradiation–induced increase in yield stress by a factor of 2. This modification of the K/size criteria has been used in the current analysis.

2.2.3 Effect of Specimen Size

Several CGR tests were conducted on thermally aged CF–8M cast SS and on a 50% CW Type 316LN SS in BWR environments to establish the test procedures and determine the possible effect of specimen size. The experimental CGRs for the materials in water and those predicted in air for the same loading conditions are plotted in Fig. 11. The results obtained earlier on a 1–T CT specimen of the same heat of 50% CW Type 316LN SS and Heat 75 of CF8M cast SS in high–DO water are also included in the figure.[35] The CGRs in air, $\dot{a}_{air}$ (m/s), were determined from the correlations developed by James and Jones;[36] it is expressed as

$$\dot{a}_{air} = C_{SS}\ S(R)\ \Delta K^{3.3}/T_R\,, \qquad (15)$$

where R is the load ratio (K_{min}/K_{max}), ΔK is $K_{max} - K_{min}$ in MPa $m^{1/2}$, T_R is the rise time (s) of the loading waveform, and function S(R) is expressed in terms of the load ratio R as follows:

$$\begin{aligned} S(R) &= 1.0 && R < 0 \\ S(R) &= 1.0 + 1.8R && 0 < R < 0.79 \\ S(R) &= -43.35 + 57.97R && 0.79 < R < 1.0, \end{aligned} \qquad (16)$$

and function C_{SS} is given by a third–order polynomial of temperature T (°C), expressed as

$$C_{SS} = 1.9142 \times 10^{-12} + 6.7911 \times 10^{-15}\, T - 1.6638 \times 10^{-17}\, T^2 + 3.9616 \times 10^{-20}\, T^3. \quad (17)$$

The two curves in the figure represent the best–fit curves for sensitized austenitic SSs in high–purity water at 289°C.[35] The CGRs in water with ≈0.3 ppm DO are given by the expression

$$\dot{a}_{env} = \dot{a}_{air} + 4.5 \times 10^{-5} (\dot{a}_{air})^{0.5} \quad (18)$$

and in water with ≈8 ppm DO by the expression

$$\dot{a}_{env} = \dot{a}_{air} + 1.5 \times 10^{-4} (\dot{a}_{air})^{0.5}. \quad (19)$$

The experimental CGRs for the 1/4–T CT specimen of Heat 4331 are in good agreement with the data obtained on the 1–T CT specimen of Heat 75. The rates for the 1/4–T CT specimen of Heat 75 and 50% CW Type 316LN SS are somewhat higher. However, the K/size criteria were generally exceeded for these tests, i.e., the values of K_{max} were higher than those allowed by Eqs. 13 or 14.

For the 50% CW Type 316LN SS, the CGR under constant load conditions in high–DO water at 289°C is plotted in Fig. 12; the maximum stress intensity for the test was within the K/size–validity criteria. Data obtained earlier on 1–T CT specimens of several heats of Types 304 and 316 SS are also included in the figure. In ≈250–ppb–DO water, the CGRs for a 1/4–T CT specimen of 50% CW Type 316LN SS are higher than those for a 1–T CT specimen of sensitized Type 304 SS. Rates for the 1/4–T specimen are comparable to those of sensitized Type 304 SS in very high–DO water (>6000 ppb DO).

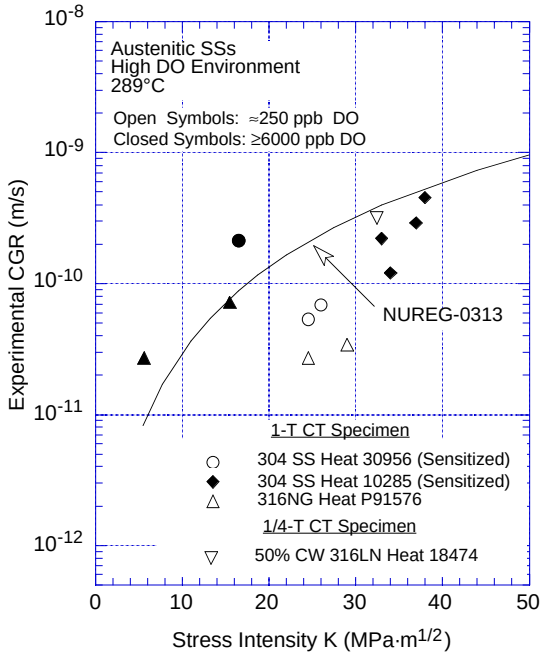

Figure 12.
Stress corrosion cracking data for austenitic stainless steels in high–DO water at 289°C.

3. Results

3.1 Fracture Toughness

3.1.1 Nonirradiated Type 304 Stainless Steel

The fracture toughness J–R curves for nonirradiated specimens of Heats L2, L20, C16, and C19, obtained in air by the DC potential and elastic unloading compliance methods, are shown in Figs. 13–16; experimental data for the tests are given in the Appendix. Duplicate tests were conducted for Heats L2 and C16. The results indicate that the fracture toughness of the laboratory Heats L2 and L20 is very low. The J–R curves are significantly lower than those typically observed for Type 304 SSs, Fig. 17.[15,38–41] For wrought austenitic SSs,[3] the J_{Ic} values at temperatures up to 550°C are typically >400 kJ/m^2; experimental J_{Ic} for Heats L2 and L20 is in the range of 150–230 and 80–120 kJ/m^2, respectively. The commercial Heats C16 and C19 show the very high fracture toughnesses expected for Type 304 SSs. For both steels, the J–R curve could not be obtained; the experimental curve is composed only of the blunting line. Fracture toughness J_{Ic} is >830 kJ/m^2 for C19, and it could not be determined for Heat C16.

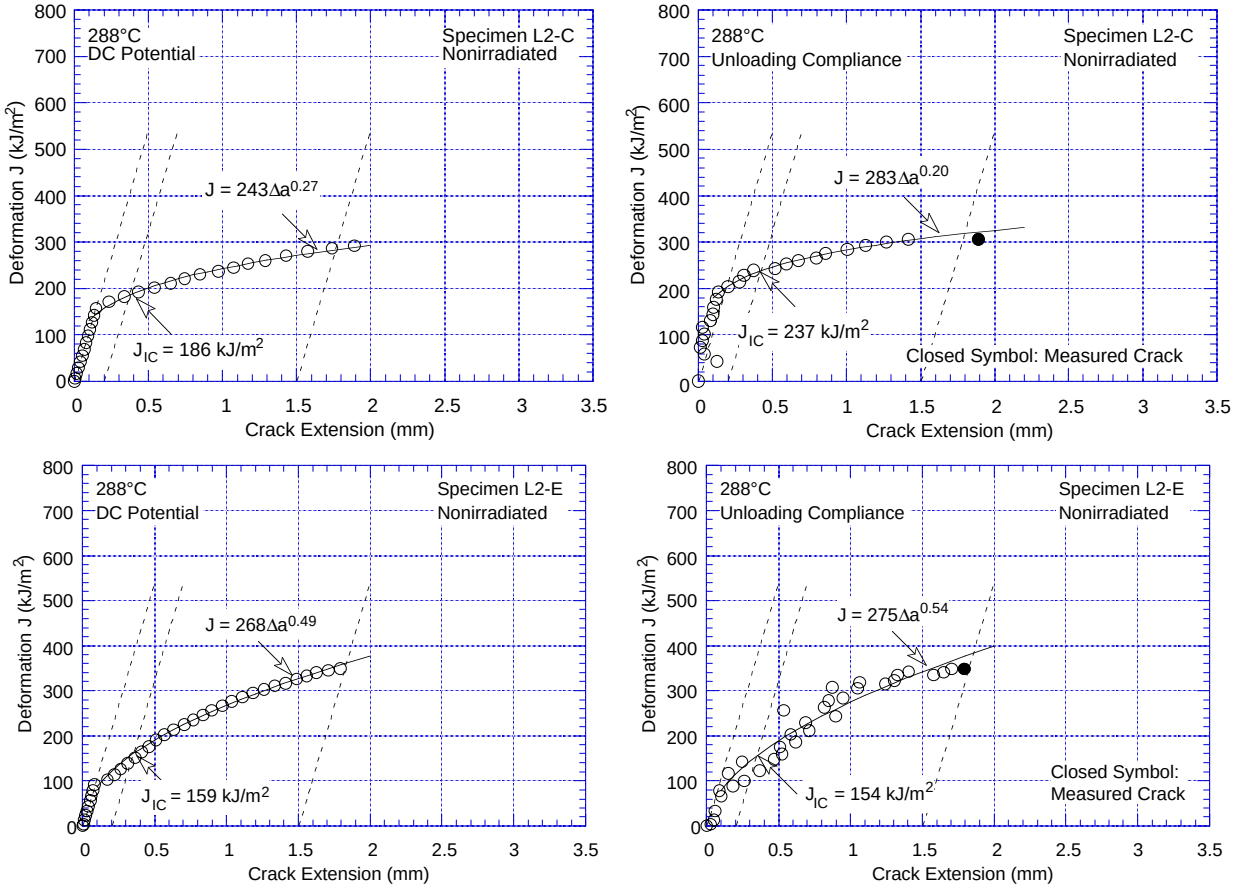

Figure 13. Fracture toughness J–R curve obtained by DC potential and unloading compliance methods for nonirradiated specimens L2–C and L2–E of Heat L2 of Type 304 SS at 288°C.

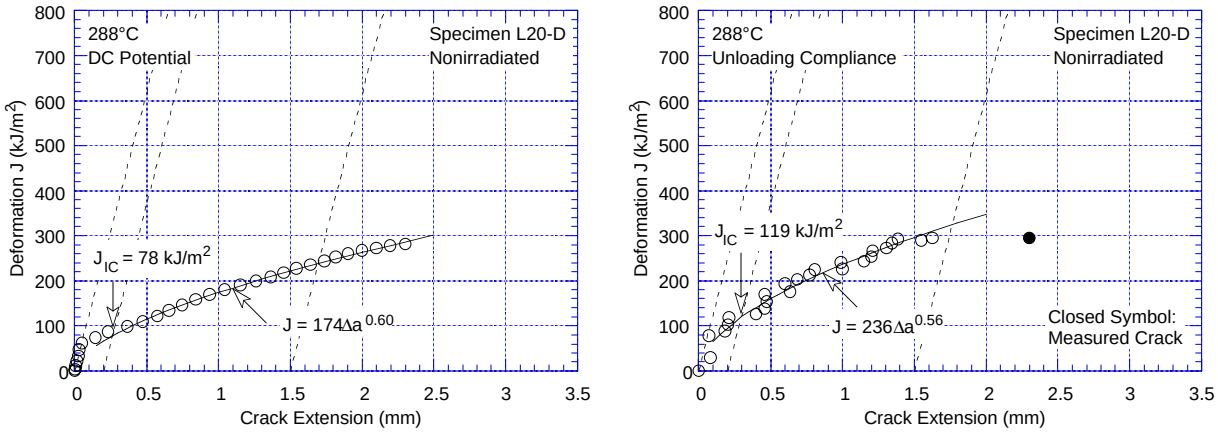

Figure 14. Fracture toughness J–R curve obtained by DC potential and unloading compliance methods for nonirradiated specimen L20–D of Heat L20 of Type 304 SS at 288°C.

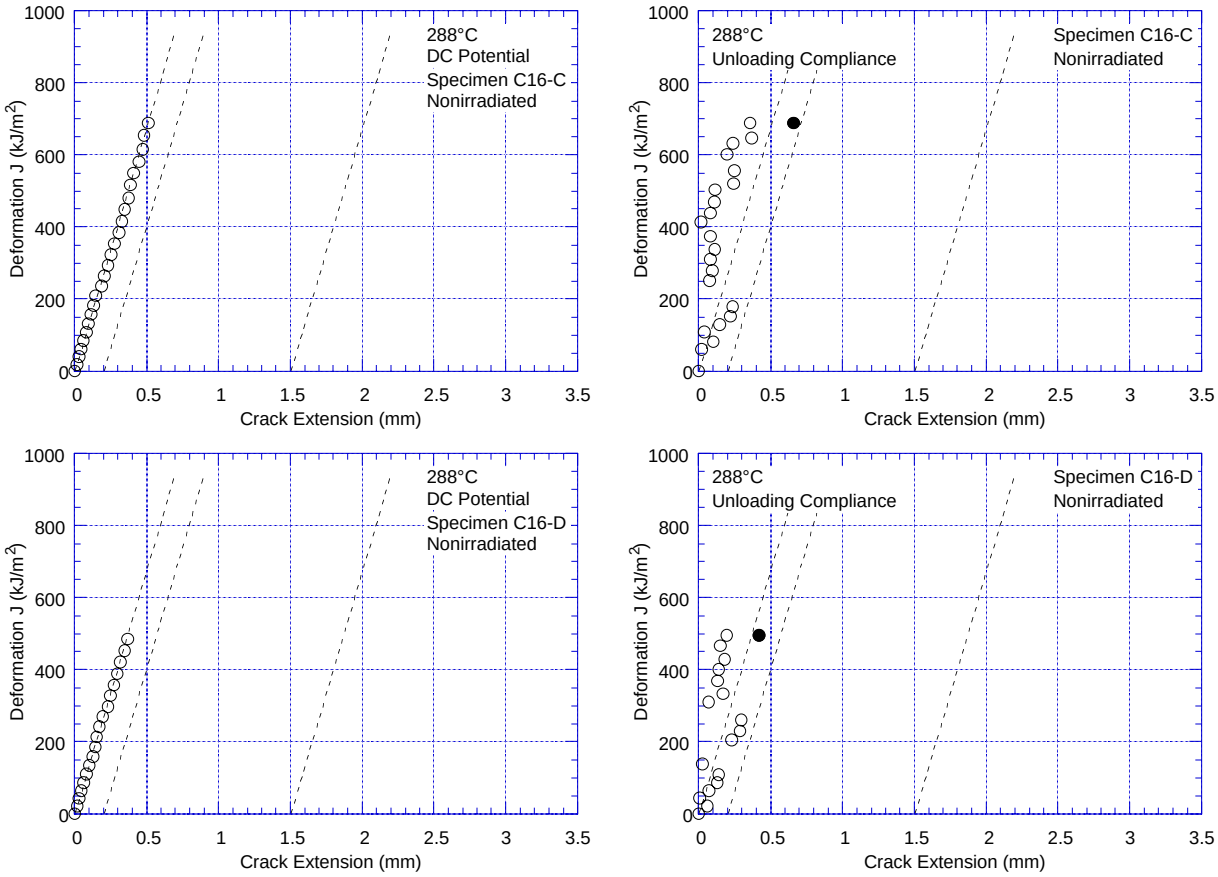

Figure 15. Fracture toughness J–R curve obtained by DC potential and unloading compliance methods for nonirradiated specimens C16–C and C16–D of Heat C16 of Type 316 SS at 288°C.

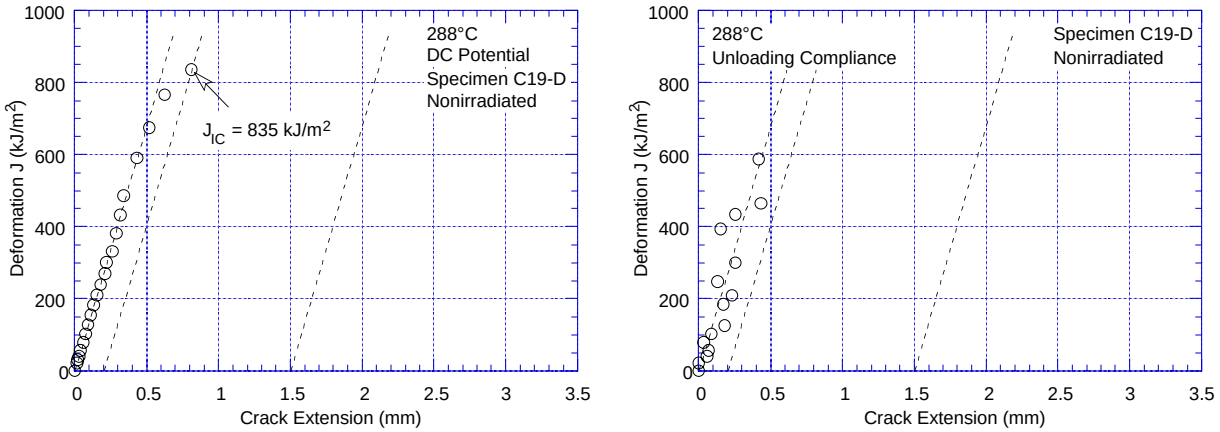

Figure 16. Fracture toughness J–R curve obtained by DC potential and unloading compliance methods for nonirradiated specimen C19–D of Heat C19 of Type 304 SS at 288°C.

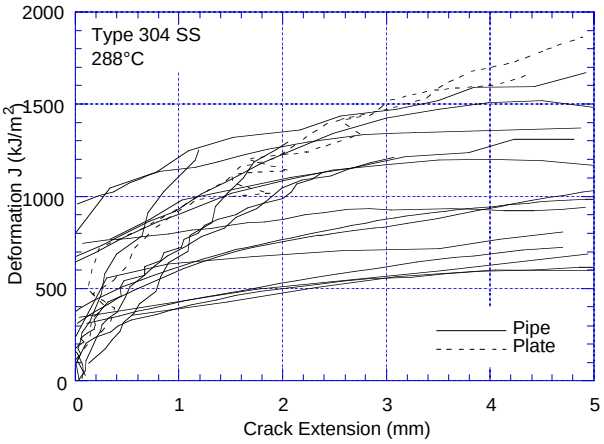

Figure 17.
Fracture toughness J–R curves for nonirradiated Type 304 stainless steels at 288°C.

The differences between the fracture toughness of laboratory and commercial heats are reflected in their fracture behavior. Photomicrographs of the fracture surface of broken nonirradiated specimens of laboratory Heats L2 and L20 and commercial Heat C19 are shown in Figs. 18 and 19, respectively. Heat L2 contains relatively high S and P contents and many clusters of MnS inclusions. Failure occurs primarily via grain–boundary separation, which is

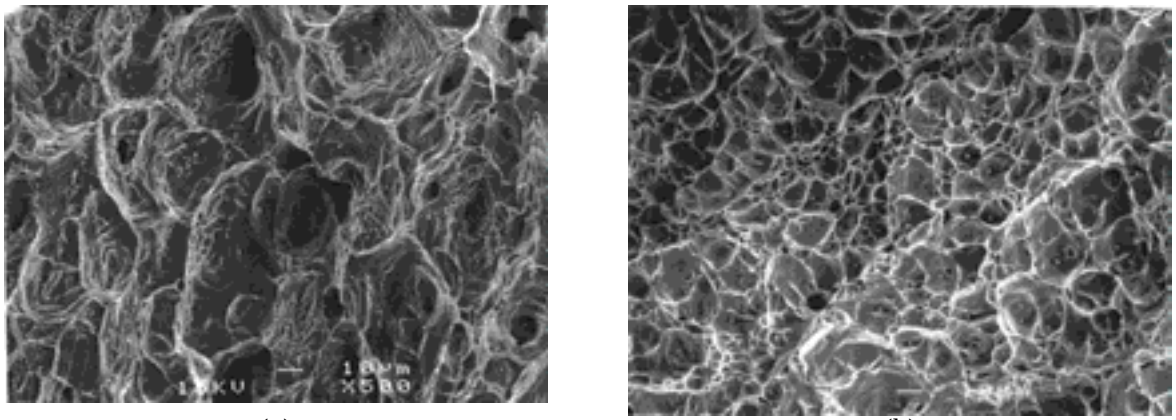

(a) (b)

Figure 18. Photomicrographs of fracture surfaces of nonirradiated specimens of Heats (a) L2 and (b) L20 tested at 288°C.

accompanied by some plastic deformation and decohesion along the MnS clusters (Fig. 20). Heat L20 exhibits a dimple fracture; failure occurs by nucleation and growth of microvoids and rupture of remaining ligaments. Heat L20 contains relatively high oxygen and many oxide particle inclusions. In Fig. 18b, nearly every dimple appears to have been initiated by decohesion of an oxide inclusion. An identical fracture behavior was observed for Heat L20 irradiated to 0.9 x 10^{21} n·cm^{-2} (1.35 dpa). In contrast, commercial heats exhibit ductile failure with some dimple fracture, as shown for Heat C19 in Fig. 19.

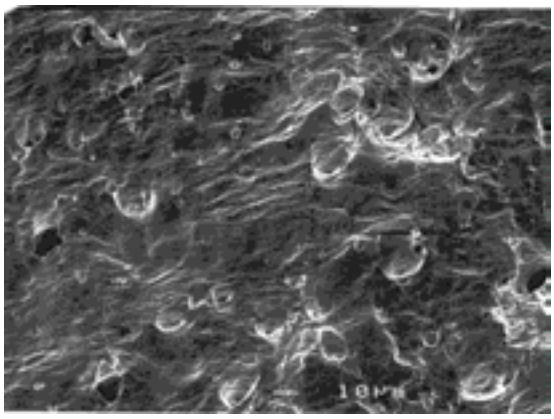

Figure 19.
Photomicrograph of fracture surface of nonirradiated specimen of Heat C19 tested at 288°C.

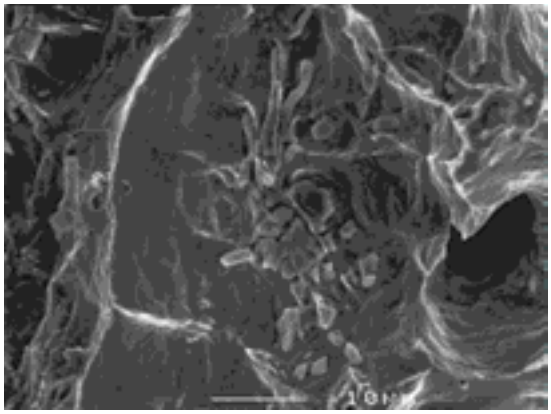

Figure 20.
Photomicrograph of MnS inclusions on the fracture surface of nonirradiated specimen of Heat L2 tested at 288°C.

3.1.2 Irradiated Type 304 Stainless Steels

Fracture toughness J–R curve tests were conducted at 288°C on Heats C19, L20, and L2 of Type 304 SS and Heat C16 of Type 316 SS irradiated to 2.0 x 10^{21} n·cm^{-2} (E > 1 MeV) (3.0 dpa). The J–R curves for the various steels are shown in Figs. 21–24; experimental data for the tests are given in the Appendix. For specimen C19–C, the J–R curve could not be determined from the DC potential method because of broken potential leads. Note that the rather flat J–R curve determined for specimen C19–A most likely is due to the small specimen size used in these tests; the maximum allowed J values were exceeded for the test.

Neutron irradiation at 288°C decreases the fracture toughness of all steels. In general, fracture toughness of the commercial Heats C16 and C19 is superior to that of the laboratory Heats L20 and L2. These differences arise primarily from differences in toughness of the nonirradiated steels, i.e., the fracture toughness of the laboratory heats is significantly lower than that of the commercial heats. The fracture toughness J–R curves for irradiated Types 304 and 316 SS are comparable.

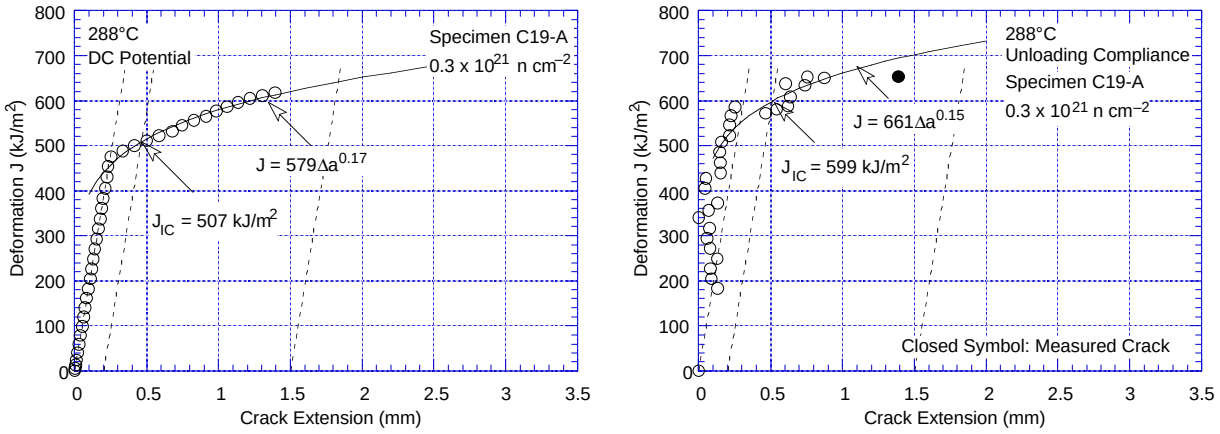

(a)

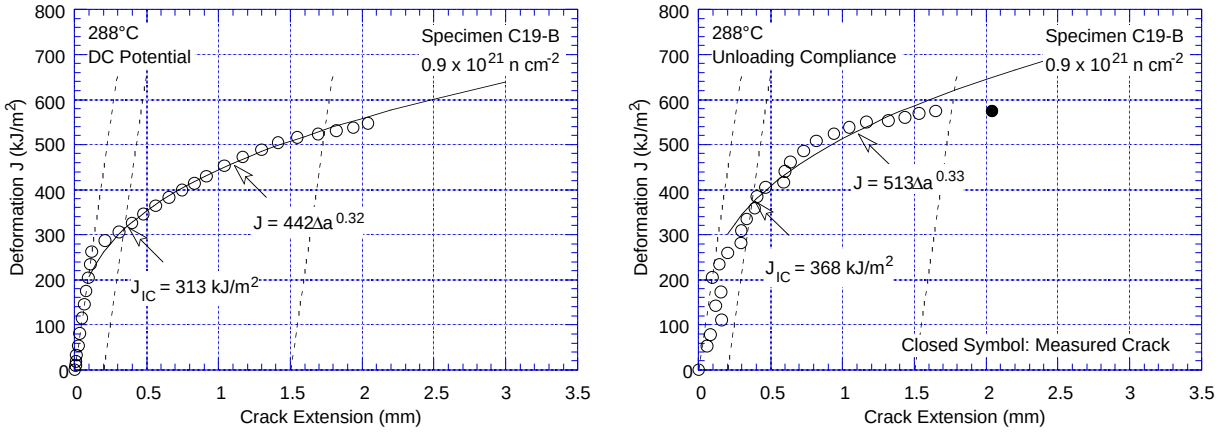

(b)

Specimen C19–C – DC Potential method
Data not obtained

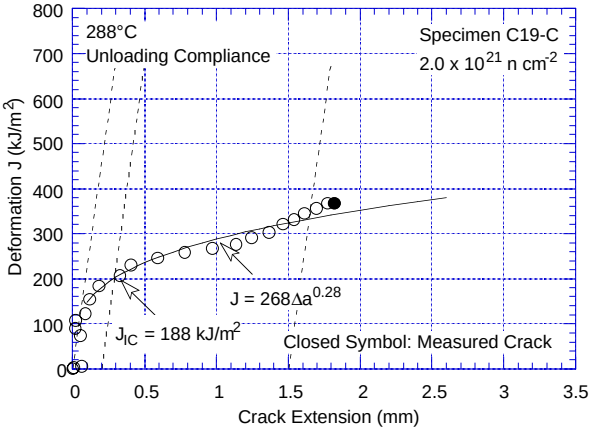

(c)

Figure 21. Fracture toughness J–R curve obtained by DC potential and unloading compliance methods at 288°C for Heat C19 of Type 304 SS irradiated to a fluence level of (a) 0.3, (b) 0.9, and (c) 2.0 x 10^{21} n/cm^2.

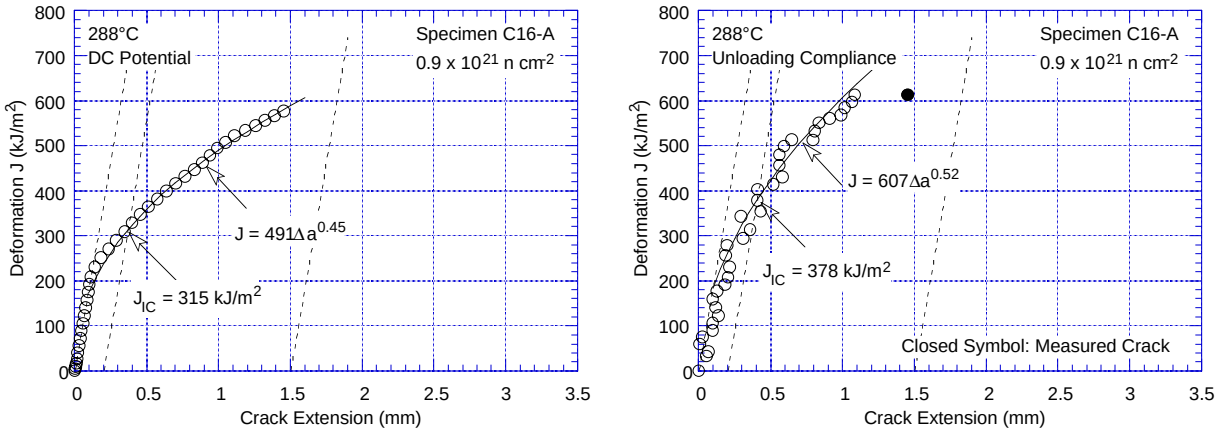

Figure 22. Fracture toughness J–R curve obtained by DC potential and unloading compliance methods at 288°C for Heat C16 of Type 316 SS irradiated to a fluence level of 0.9 x 10^{21} n/cm^2.

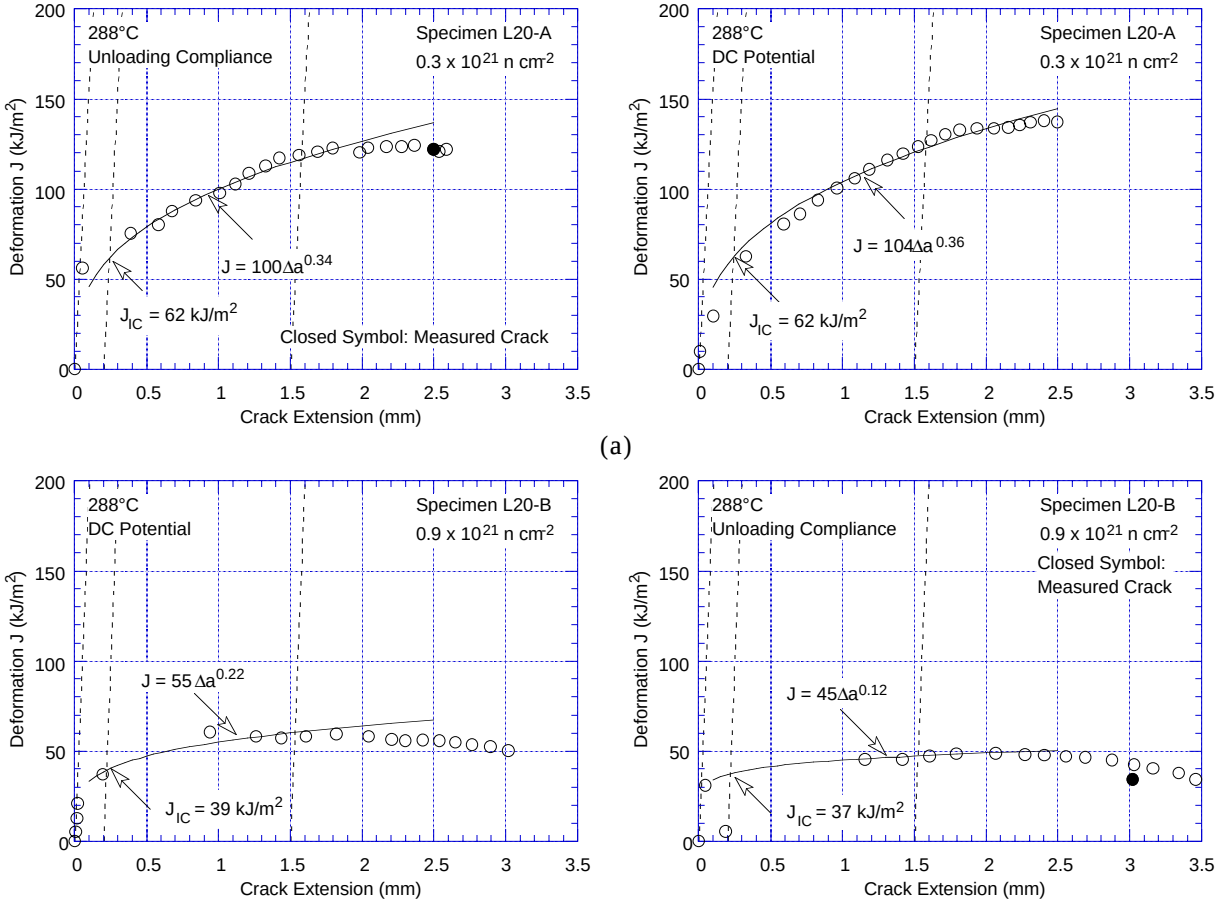

Figure 23. Fracture toughness J–R curve obtained by DC potential and unloading compliance methods at 288°C for Heat L20 of Type 304 SS irradiated to a fluence level of (a) 0.3 and (b) 0.9 x 10^{21} n/cm^2.

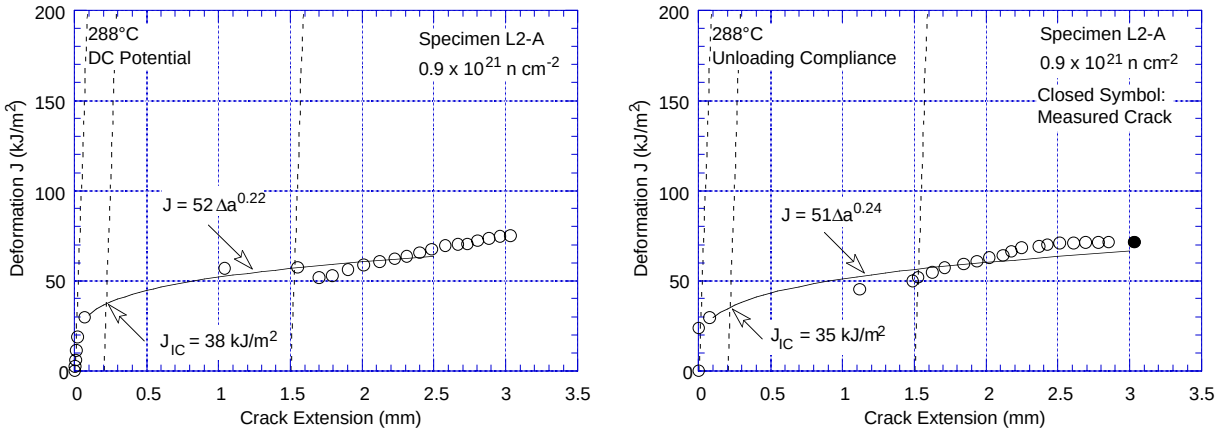

Figure 24. Fracture toughness J–R curve obtained by DC potential and unloading compliance methods at 288°C for Heat L2 of Type 304 SS irradiated to a fluence level of 0.9 x 10^{21} n/cm^2.

The experimental J_{Ic} values for the two commercial heats of austenitic SSs are plotted as a function of neutron exposure in Fig. 25. Results from tests on Type 304 SS reactor internal materials from operating BWRs[2] are also included in the figure. All CT specimen data from commercial heats fall within the scatter band for the data obtained at temperatures higher than 288°C.

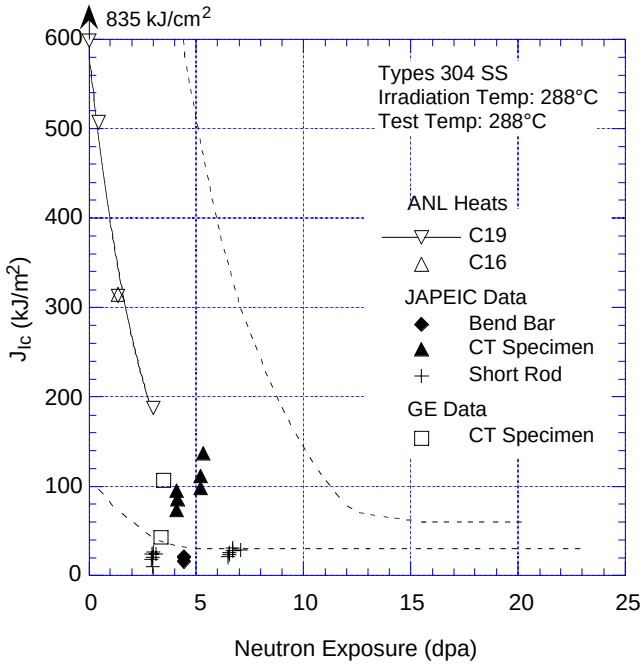

Figure 25.
Fracture toughness J_{Ic} of austenitic stainless steels as a function of neutron exposure at 288°C. Dashed lines represent upper and lower bounds for change in J_{Ic} for austenitic SSs irradiated at 350–450°C.
JAPEIC = Japan Power Engineering and Inspection Corporation, GE = General Electric Nuclear Energy

3.2 Crack Growth Tests on Irradiated Stainless Steels in BWR Environments

Crack growth tests have been completed at 289°C on 1/4–T CT specimens of Type 304 SS (Heat C3) irradiated to 0.3, 0.9, and 2.0 x 10^{21} n/cm^2 and Type 316 SS (Heat C16) irradiated to 2.0 x 10^{21} n/cm^2. The significant results for the various tests are summarized below.

3.2.1 Specimen C3-B Irradiated to 0.9 x 10^{21} n/cm^2

The environmental and loading conditions, experimental CGRs, allowed K_{max} from K/size criterion in Eq. 13, and the deviation of applied K_{max} from the allowed value are given in Table 3. Allowed K_{max} was determined using effective yield stress in Eq. 13. Precracking was initiated at R = 0.2 and K_{max} = 16 MPa $m^{1/2}$. During most test periods, K_{max} was maintained approximately constant by periodic load shedding.

Table 3. Crack growth results for Specimen C3–B of Type 304 SS[a] in high–purity water at 289°C

Test Period	Test Time, h	ECP mV (SHE)[b] Pt	ECP mV (SHE)[b] Steel	O_2 Conc.,[b] ppb	Load Ratio	Rise Time, s	Down Time, s	Hold Time, s	K_{max}, MPa·$m^{1/2}$	ΔK, MPa·$m^{1/2}$	Growth Rate, m/s	K_{max} from Eq. 13 MPa $m^{1/2}$	Deviation in K_{max}, %
1	28	230	154	300	0.20	0.5	0.5	0	19.14	15.31	6.83E-08	18.4	4
2	172	239	189	300	0.51	60	2	0	18.96	9.29	1.75E-10	18.3	3
3	287	233	187	300	0.70	300	2	0	19.79	5.94	6.38E-10	18.0	10
4	335	235	191	300	0.70	2	2	7200	20.10	0	1.06E-09	17.7	14
5	376	238	195	300	0.70	2	2	7200	22.07	0	1.04E-09	17.4	27
6	624	-475	–595	≈10	0.70	2	2	7200	22.27	0	4.02E-11	17.2	30
7	696	-482	–607	≈10	0.70	300	2	0	22.10	6.63	8.56E-11	17.1	29
8	935	-495	–614	≈10	0.70	2	2	3600	22.66	0	6.42E-12	17.1	32
9	1031	-499	–609	≈10	0.70	300	2	0	22.53	6.76	3.37E-11	17.1	32
10a	1127	-495	–613	≈10	0.70	1000	2	0	22.19	6.66	negligible	17.1	30
10b	1271	-507	–620	≈10	0.70	1000	2	0	23.04	6.91	1.20E-11	17.1	35
11	1295	-507	–624	≈10	0.70	30	2	0	22.87	6.86	5.17E-11	17.1	34
12	1343	-498	–617	≈10	0.70	300	2	0	23.10	6.93	1.55E-11	17.1	36
14	1608	248	151	250	0.70	1000	2	0	24.17	7.25	5.93E-10	16.7	45
15	1655	244	155	250	0.70	2	2	3600	24.42	0	8.70E-10	16.4	49

[a] Heat C3, irradiated to 0.9 x 10^{21} n cm^{-2}.
[b] Represents values in the effluent.
Conductivity was 0.07 and 0.3–0.45 μS/cm in feedwater and effluent, respectively. Feedwater pH at room temperature was 6.5.

The test was initiated in high–purity water with ≈300 ppb DO. After ≈375 h, the DO level in the feedwater was decreased to ≈10 ppb by sparging it with pure nitrogen. After 1380 h, the DO level was increased from ≈10 to ≈300 ppb by sparging the feedwater with nitrogen plus 1% oxygen gas mixture. Because of the very low flow rates for the recirculating water system it took several days for the environmental conditions to stabilize. Changes in crack length and ECP of Pt and SS electrodes during these transient periods are shown in Fig. 26. During the transition periods, changes in the steel ECP were slower than those in the Pt ECP. For example, in Fig. 26a, although the Pt ECP decreased below –400 mV (SHE) within 40 h, it took more than 150 h for the steel ECP to decrease below –400 mV. Also, because of an unexpected power bump the test tripped after ≈1390 h (during the second transition period); it was restarted at 1470 h. The ECPs of both electrodes were below –200 mV before the interruption and above 100 mV after the test was restarted.

A photomicrograph of the fracture surface of both halves of the specimen is shown in Fig. 27. The final crack length, determined from the photograph, showed very good agreement with the value estimated from the DC potential measurements. Changes in crack length and K_{max} with time during various test periods are shown in Fig. 28a–e. In general, the DC potential measurements show very little scatter, particularly for measured growth rates >5 x 10^{-11} m/s. Some fluctuations in DC potential measurements were observed when either the autoclave temperature varied ±3°C (e.g., 170–260 h) or the DO level in the water was being changed (e.g., 450–530 h and 1370–1510 h).

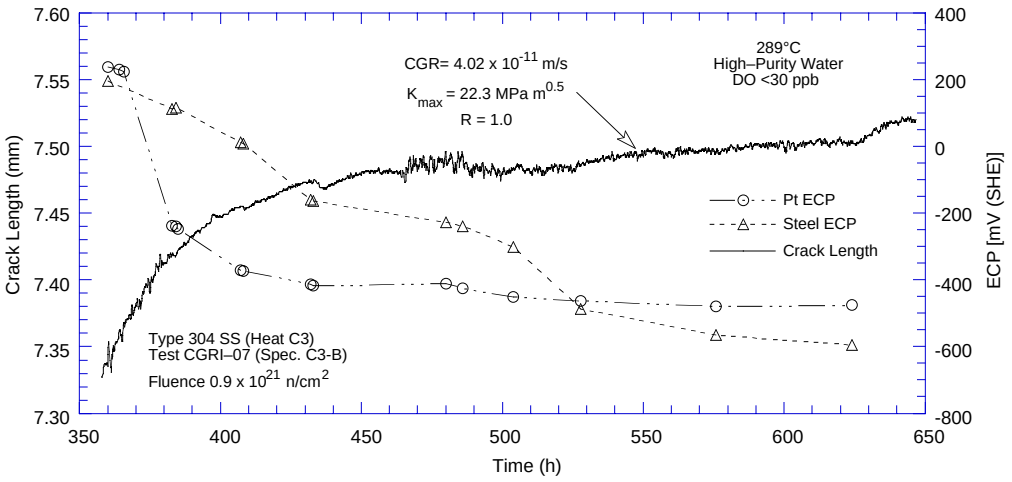

(a)

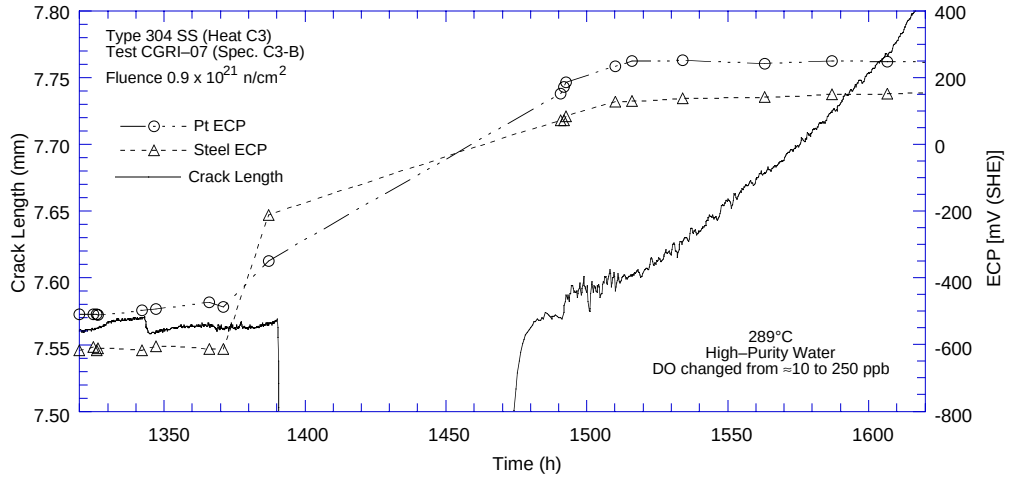

(b)

Figure 26. Changes in crack length and ECP after the dissolved oxygen level in the feedwater was (a) decreased from ≈500 to 10 ppb and (b) increased from ≈10 to 300 ppb

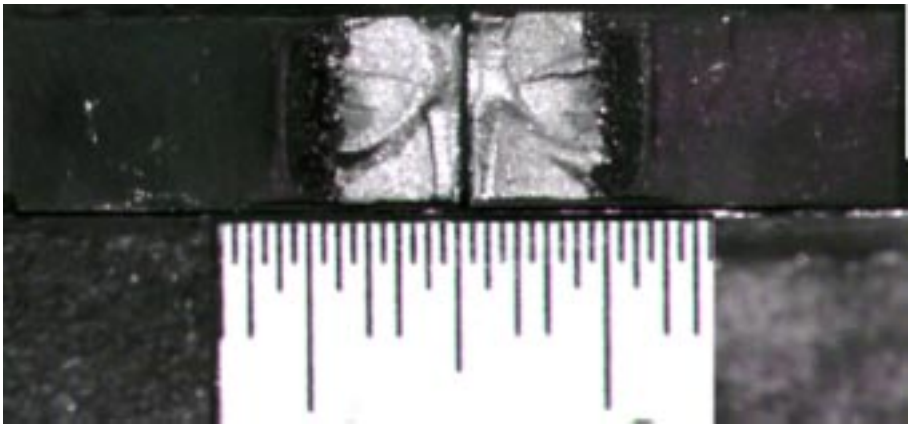

Figure 27. Photomicrographs of the fracture surface of specimen C3–B tested in high–purity water at 289°C

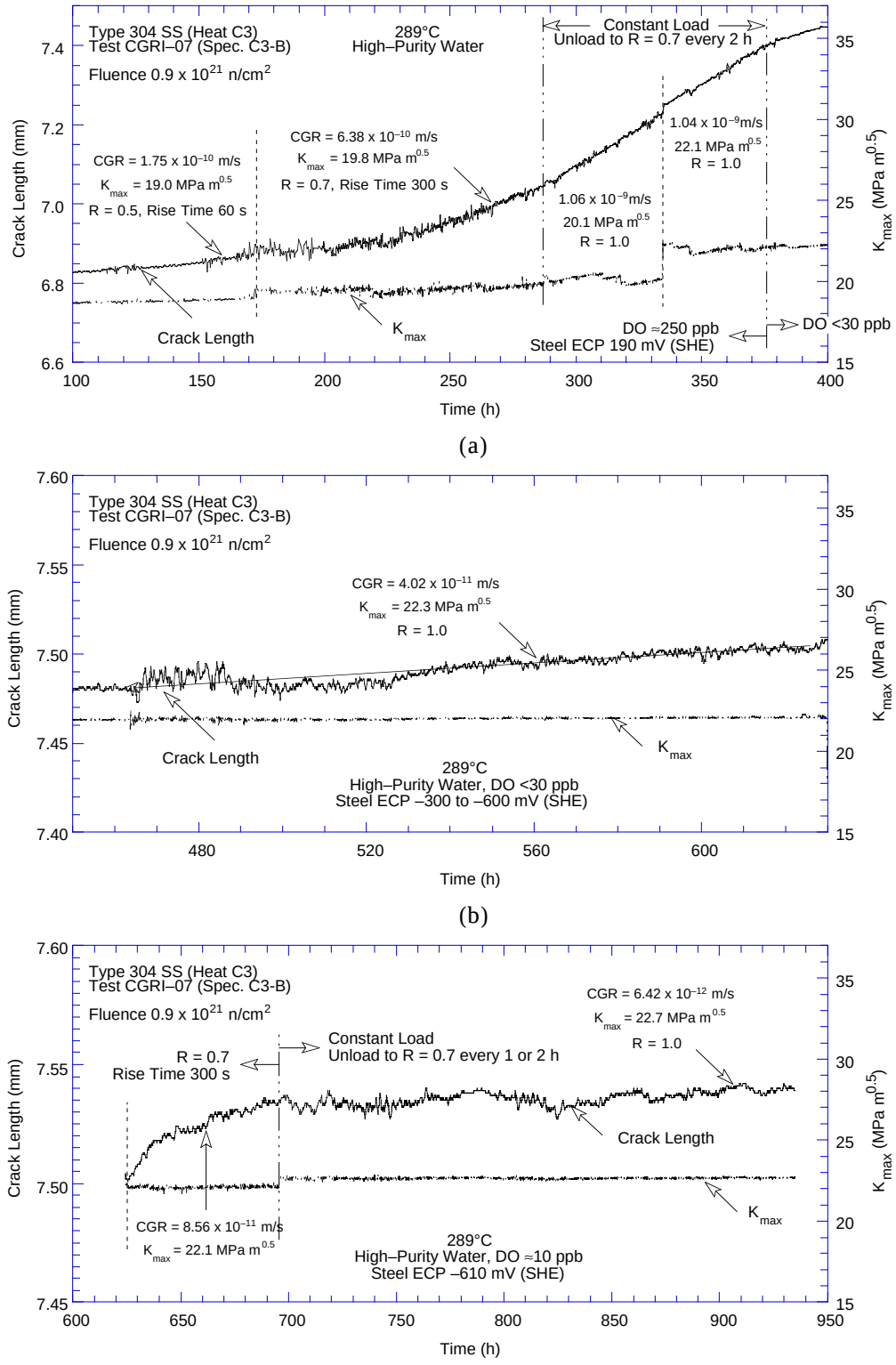

Figure 28. Crack–length–vs.–time plots for irradiated Type 304 SS (Heat C3) in high–purity water at 289°C during test periods (a) 2–5, (b) 6, (c) 7–8, (d) 9–12, and (e) 14–15

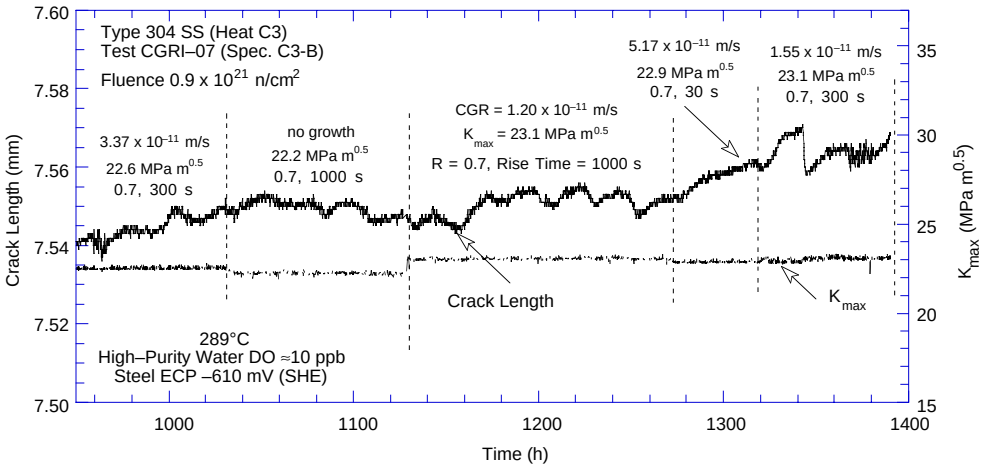

(d)

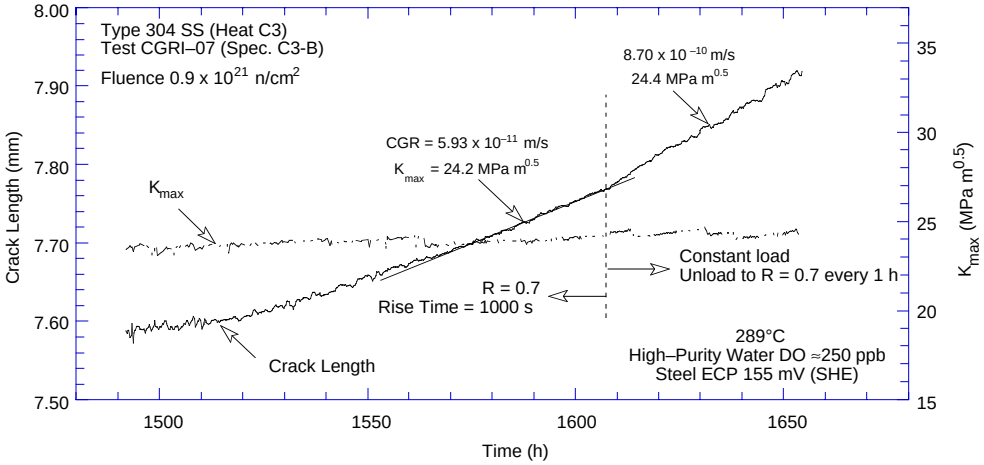

(e)

Figure 28. (Cont'd.)

For this specimen, environmental enhancement occurred after ≈170 h (Fig. 28a), when the load ratio and rise time, respectively, were changed from 0.5 and 60 s to 0.7 and 300 s. For the new loading condition, although the predicted CGR in air decreased by a factor of ≈15 (Eqs. 15–17), the measured rate in the environment increased by a factor of ≈3. The results indicate the benefit of low–DO environment on growth rates; CGRs decreased by more than an order of magnitude when the DO level was decreased to <10 ppb and increased when the DO level was raised back to ≈300 ppb.

The results also suggest a possible effect of loading history on growth rates, e.g., during test periods 6 and 8, the CGRs under the same trapezoidal waveform were 4.0×10^{-11} and 6.4×10^{-12} m/s, respectively. The higher rate was observed following a long period of growth at a higher ECP under a trapezoidal waveform. The lower rate was observed following cycling under a sawtooth waveform with a 300–s rise time at low DO. It is possible that the cyclic loading changed the mode of fracture. The reason for such apparent differences in CGRs under similar loading conditions will be investigated by metallographic evaluation of the fracture surfaces; if a transition in fracture mode is observed, additional precautions to avoid such transitions will be observed in future tests.

For specimen C3–B, during Test Periods 1–4 the experimental K_{max} values were 4–14% higher than the allowable value based on the effective yield stress and 30–50% higher during Periods 5–15. For this specimen, loading conditions for all test periods would satisfy the K/size criterion of Eq. 13 if the actual yield stress instead of effective yield stress is used. The crack–length–vs.–time plots in Figs. 26a and 28a and b show that environmental factors still strongly influenced the CGR at these K levels. For example, the CGRs decreased by a factor of ≈20 when the DO level was decreased from ≈300 to 10 ppb. Thus in this case, it is not clear that the violation of the K size criterion after Test Period 3 actually led to a significant loss of specimen constraint.

3.2.2 Specimen C3-C Irradiated to 2.0 x 10^{21} n/cm^2

The environmental and loading conditions, experimental CGRs, allowed K_{max} from K/size criterion in Eq. 13, and the deviation of applied K_{max} from the allowed value are given in Table 4. Allowed K_{max} was determined using effective yield stress. Precracking was carried out at R = 0.3 and K_{max} = 17 MPa $m^{1/2}$; the applied K_{max} was maintained approximately constant during individual test periods by periodic load shedding. The test was initiated in high–purity water with ≈300 ppb DO. After ≈240 h, the DO level in the feedwater was decreased to ≈10 ppb by sparging the feedwater tank first with pure nitrogen and then with nitrogen plus 5% hydrogen. The changes in crack length and ECP of Pt and SS electrodes during the transient period are shown in Fig. 29. As seen earlier for Specimen C3–B, it took several days for the DO level to decrease below 20 ppb, and changes in the steel ECP were slower than that in the Pt ECP. For example, the Pt ECP decreased to –450 mV (SHE) within a couple of days while the steel ECP remained above –250 mV for a long time; it decreased below –400 mV only after the feedwater tank was sparged with nitrogen plus 5% hydrogen gas mixture. The test was terminated after 810 h because the range of valid K_{max} was significantly exceeded.

Table 4. Crack growth results for Specimen C3–C of Type 304 SS[a] in high–purity water at 289°C

Test Period	Test Time, h	ECP mV (SHE)[b] Pt	ECP mV (SHE)[b] Steel	O_2 Conc.,[b] ppb	Load Ratio	Rise Time, s	Down Time, s	Hold Time, s	K_{max}, MPa·$m^{1/2}$	ΔK, MPa·$m^{1/2}$	Growth Rate, m/s	K_{max} from Eq. 13 MPa $m^{1/2}$	Deviation in K_{max}, %
1	46	241	164	300	0.26	2	2	0	17.89	13.24	2.00E-08	22.4	-20
2	71	223	155	300	0.53	30	2	0	18.40	8.65	2.22E-09	22.1	-17
3	99	235	167	300	0.70	300	2	0	18.80	5.64	1.73E-09	21.8	-14
4	142	232	164	300	0.69	1000	2	0	19.21	5.96	1.25E-09	21.4	-10
5	191	233	164	300	0.70	2	2	3600	19.42	0	6.83E-10	21.1	-8
6	311	-450	7	100	0.70	2	2	3600	23.67	0	5.07E-10	20.5	16
7	560	-547	-294	10	0.70	2	2	3600	27.49	0	6.91E-10	19.1	44
8	706	-551	-502	10	0.70	2	2	3600	34.74	0	2.04E-09	16.4	111
9	724	-557	-457	10	0.70	2	2	3600	36.96	0	3.70E-09	15.8	134

[a]Heat C3, irradiated to 2.0 x 10^{21} n/cm^2.
[b]Represents values in the effluent.
Conductivity was 0.07 and 0.3–0.45 μS/cm in feedwater and effluent, respectively. Feedwater pH at room temperature was 6.5.

A photomicrograph of the fracture surface of both halves of the specimen is shown in Fig. 30. The final crack length was determined from the photograph of both halves of the fractured specimen. Several unbroken ligaments can be seen extending back from the final crack front. Because of these unbroken ligaments the crack lengths were determined from an average of 16 evenly spaced measurements. A total 17 measurements were made, the two near–surface measurements were averaged, and the resultant value was averaged with the remaining 15 measurements. The actual crack extension was ≈40% greater than the value

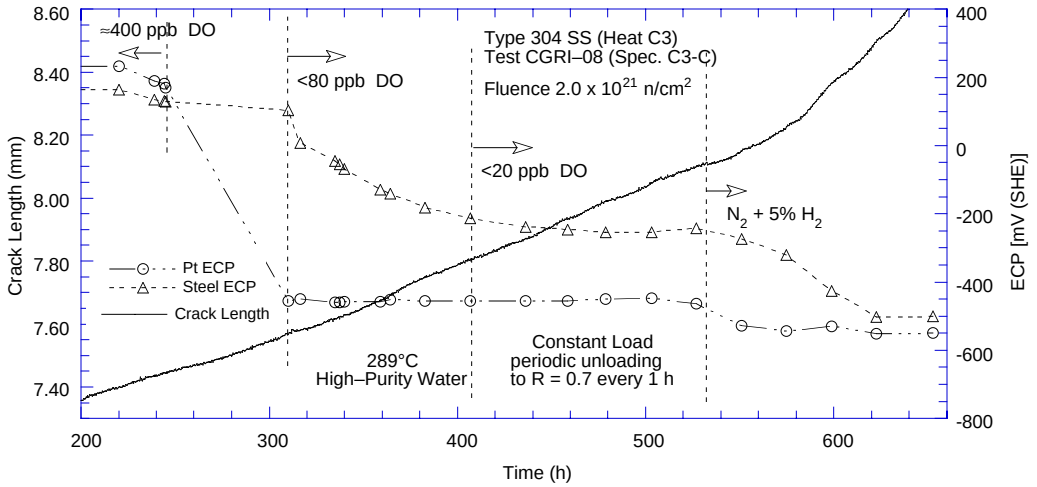

Figure 29. Change in crack length and ECP of Pt and SS electrodes for Specimen C3–C after the dissolved oxygen level in the feedwater was decreased from ≈300 to 10 ppb

determined from the DC potential measurements. This difference is larger than is typically observed in most of our CGR tests, and is most likely due to the presence of the unbroken ligaments. Crack extensions estimated from the DC potential method were scaled proportionately. The values given in Table 4 are the corrected values of K_{max} and growth rate.

The changes in the (corrected) crack length and K_{max} with time during various test periods are shown in Figs. 31a–d. For this specimen, significant environmental enhancement occurred after ≈100 h (Fig. 31b) during continuous cycling at R = 0.7 when the rise time was changed from 30 s to 300 s. For the new loading condition, although the predicted CGR in air decreased by a factor of ≈10, the rate in water did not change.

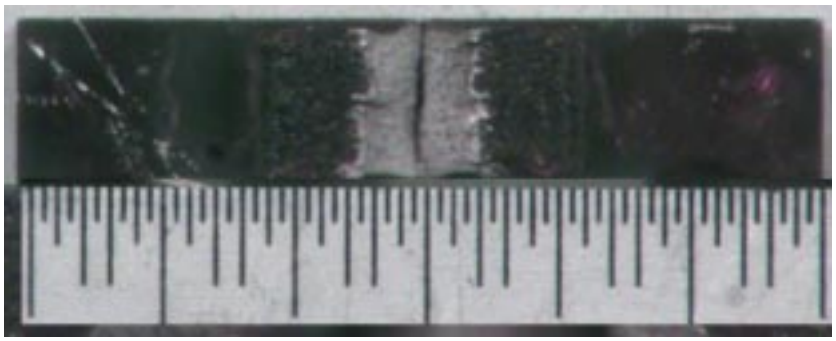

Figure 30. Photomicrographs of the fracture surface of Specimen C3–C

Figures 29 and 31c show that when the DO level was decreased from ≈300 to 10 ppb, the steel ECP decreased from ≈240 to -255 mV (SHE), but the CGR did not decrease. For a similar decrease in DO, the CGR of specimen C3–B, irradiated to 0.9 x 10^{21} n/cm^2, decreased by more than an order of magnitude. For specimen C3–C, the CGR actually increased at ≈570 h when the cover gas was changed from pure nitrogen to nitrogen plus 5% hydrogen and the steel ECP decreased below –500 mV (Fig. 31d). However, during the whole time at low ECP, the specimen K/size criteria were exceeded. Thus the apparent absence of a beneficial effect of reduced DO content on growth rates thus may be a test artifact.

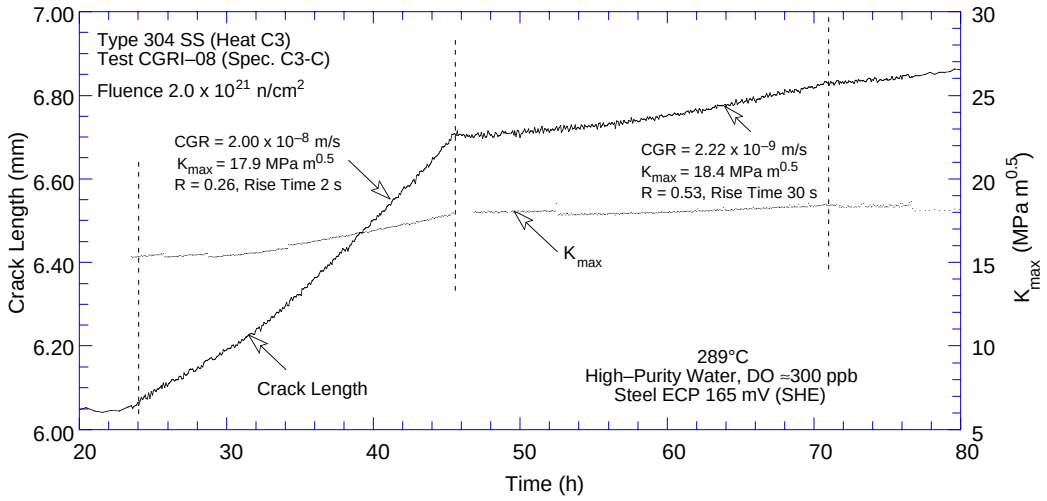

(a)

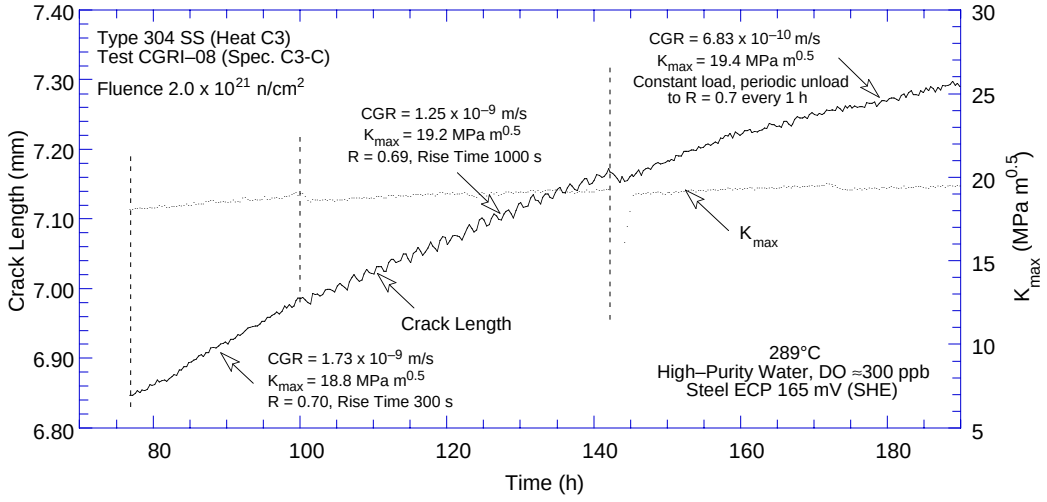

(b)

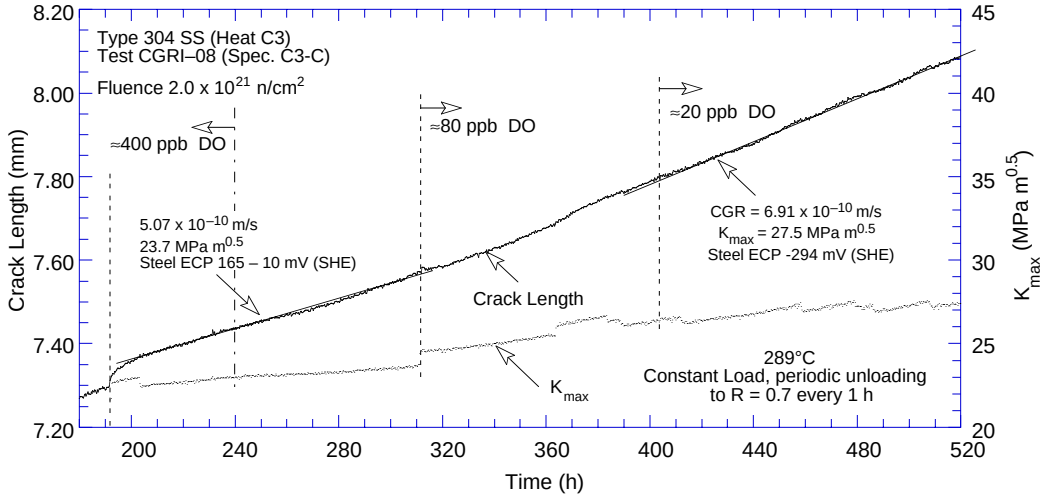

(c)

Figure 31. Crack–length–vs.–time plots for irradiated Type 304 SS (Heat C3) in high–purity water at 289°C during test periods (a) 1–2, (b) 3–5, (c) 6–7, and (d) 7–8

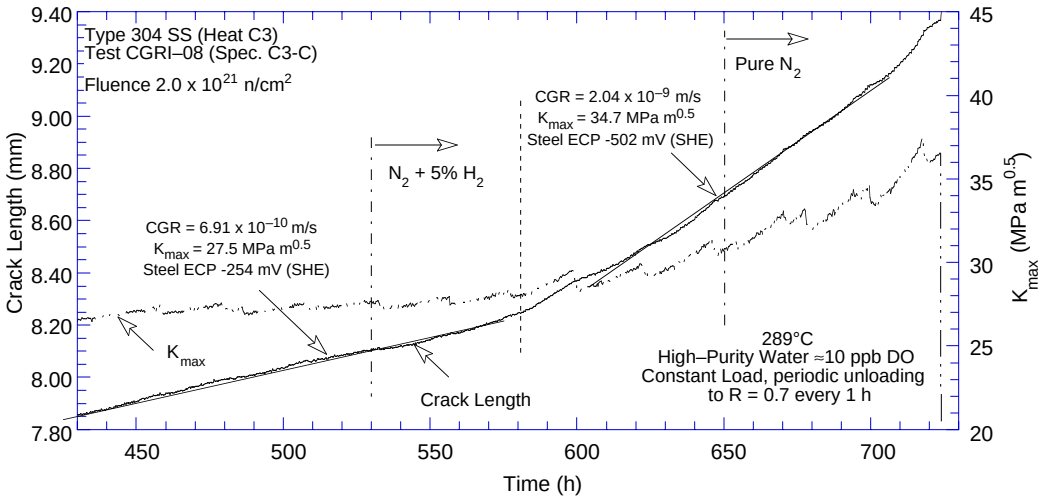

(d)

Figure 31. (Cont'd.)

3.2.3 Specimen C16-B Irradiated to 2.0 x 10^{21} n/cm^2

The environmental and loading conditions, experimental CGRs, allowed K_{max} from K/size criterion in Eq. 13, and the deviation of applied K_{max} from the allowed value are given in Table 5. Allowed K_{max} was determined using effective yield stress in Eq. 13. Precracking was initiated at R = 0.3 and K_{max} = 14 MPa $m^{1/2}$. After ≈0.4 mm advance, R was increased incrementally to 0.7, and rise time increased to 30 s. The maximum stress intensity factor K_{max} was maintained approximately constant by periodic load shedding. After ≈265 h, the DO level in the feedwater was decreased from ≈250 ppb to <30 ppb by sparging the feedwater tank initially with pure nitrogen and then with nitrogen plus 5% hydrogen gas mixture. After 780 h,

Table 5. Crack growth results for Specimen C16–B of Type 316 SS[a] in high–purity water at 289°C

Test Period	Test Time, h	ECP [b] mV (SHE) Pt	ECP [b] mV (SHE) Steel	O_2 Conc.,[b] ppb	Load Ratio	Rise Time, s	Down Time, s	Hold Time, s	K_{max}, MPa·$m^{1/2}$	ΔK, MPa·$m^{1/2}$	Growth Rate, m/s	K_{max} from Eq. 13 MPa $m^{1/2}$	Deviation in K_{max}, %
Pre a	6	–	–	250	0.32	1	1	0	14.3	9.8	1.75E-08		
Pre b	30	232	144	250	0.30	2	2	0	14.0	9.8	7.54E-09		
Pre c	52	227	144	250	0.31	2	2	0	14.2	9.8	8.94E-09		
1	94	224	148	250	0.56	12	2	0	14.6	6.4	4.94E-10	22.2	-35
2	132	226	147	250	0.73	30	2	0	14.8	4.0	8.65E-10	22.0	-33
3	173	228	151	250	0.71	300	2	0	15.0	4.4	8.16E-10	21.8	-31
4	198	224	153	250	0.70	1000	12	0	15.0	4.5	7.33E-10	21.7	-31
5	265	162	117	250	0.70	12	12	3600	15.2	0	4.62E-10	21.4	-29
6	410	-547	-298	<30	0.70	12	12	3600	15.2	0	1.90E-11	21.3	-28
7	504	-562	-410	<30	0.70	1000	12	0	15.2	4.54	2.76E-11	21.3	-29
8	527	-560	-449	<30	0.73	30	2	0	15.2	4.10	6.07E-11	21.3	-29
9	552	-557	-502	<30	0.70	30	2	0	17.3	5.18	2.51E-10	21.2	-18
10	600	-554	-545	<30	0.69	1000	12	0	17.2	5.34	3.59E-11	21.2	-19
11	672	-557	-554	<30	0.70	12	12	3600	17.3	0	1.73E-11	21.1	-18
12	792	-438	-597	<30	0.70	12	12	3600	19.7	0	4.11E-11	21.1	-7
13	866	219	139	250	0.70	12	12	3600	19.6	0	7.14E-10	21.0	-7
14	871	224	148	250	0.70	12	12	3600	21.9	0	1.10E-09	20.9	5
15	888	224	148	250	1.00[c]	0	0	–	21.9	–	5.27E-10	20.9	5

[a]Heat C16, irradiated to 2.0 x 10^{21} n/cm^2.
[b]Represents values in the effluent. Effluent conductivity was ≈0.45 μS/cm and DO was ≈250 ppb during high–DO test and <40 ppb during low–DO test. Feedwater conductivity was 0.07 μS/cm and pH at room temperature was 6.5.
[c]Constant displacement test.

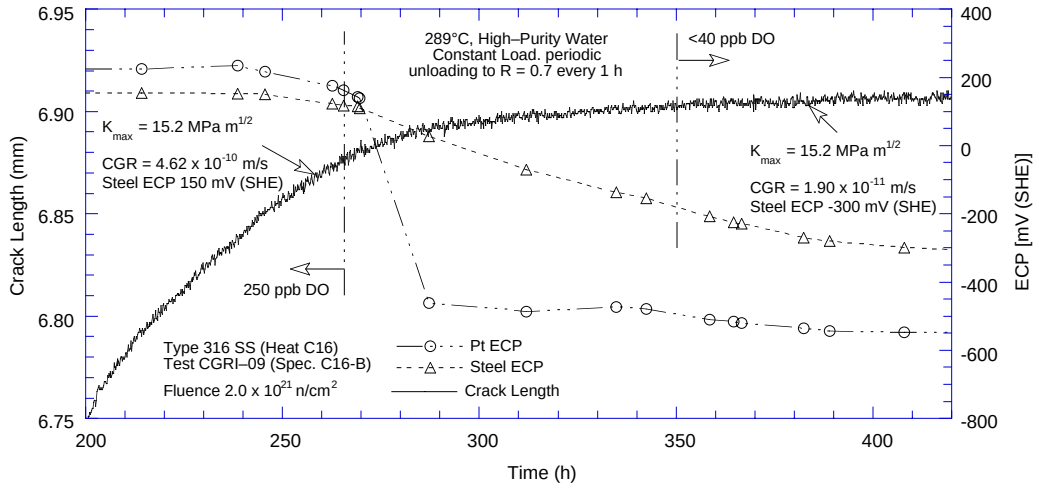

(a)

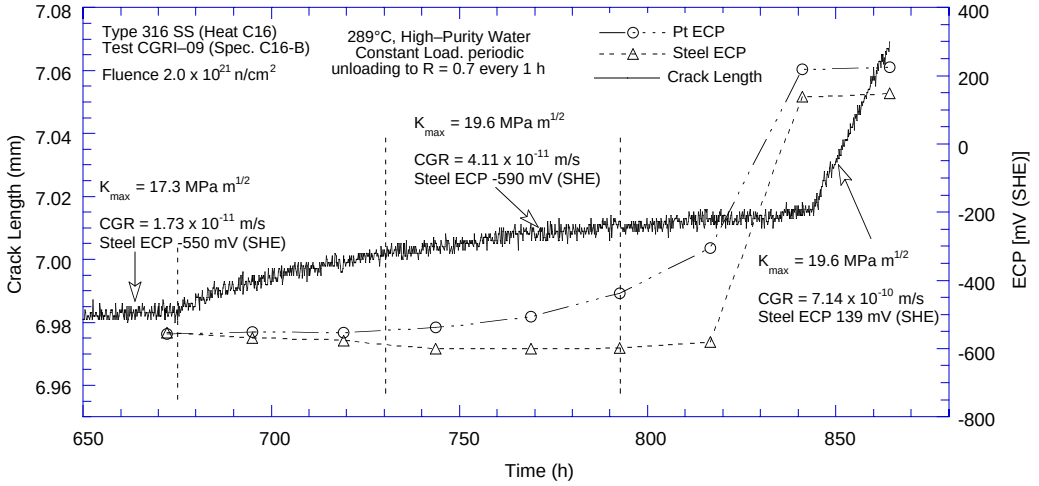

(b)

Figure 32. Change in crack length and ECP of Pt and SS electrodes when the DO level in feedwater was (a) decreased from ≈300 to <40 ppb and (b) increased from <40 to ≈300 ppb.

the DO level was increased back to ≈250 ppb by sparging the feedwater with nitrogen plus 1% oxygen. Change in crack length and ECP of Pt and SS electrodes during the transient periods are shown in Fig. 32. In both cases, it took more than 100 h for the changes to occur.

A photomicrograph of the fracture surface of both halves of the specimen is shown in Fig. 33. The final crack length, determined from the photograph, showed very good agreement with the value estimated from the DC potential measurement. Also, the results in Table 5 indicate that for specimen C16–B, loading conditions for all test periods satisfied the K/size criterion of Eq. 13.

The changes in corrected crack length and K_{max} with time during various test periods are shown in Figs. 34a–g. For this specimen, environmental enhancement occurred at ≈150 h (Fig. 34b) during continuous cycling at R = 0.7 when the rise time was changed from 30 s to 300 s. For the new loading condition, although the predicted CGR in air decreased by a factor of ≈10, the rate in water did not change.

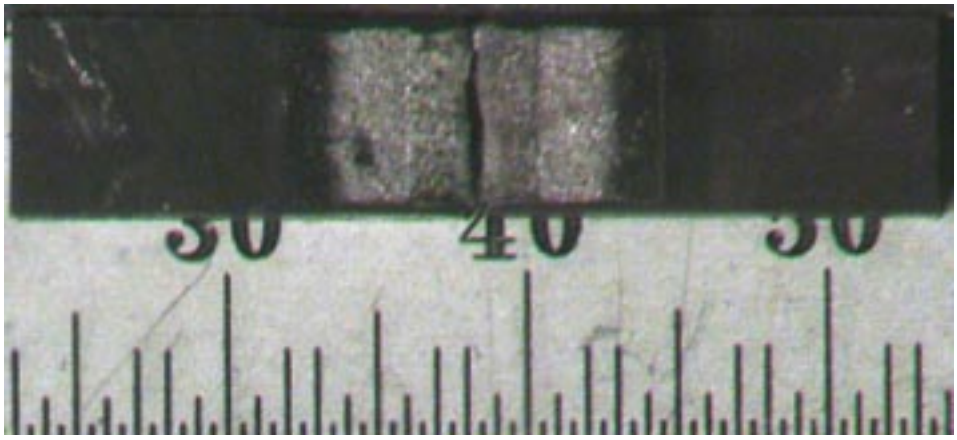

Figure 33. Photomicrographs of the fracture surface of Specimen C16–B

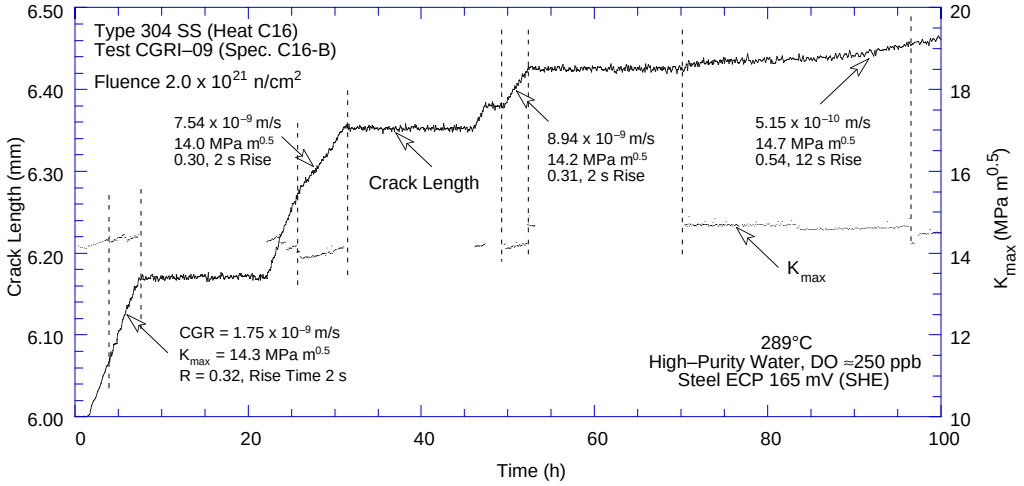

Figure 34. Crack–length–vs.–time plots for irradiated Type 316 SS (Heat C16) in high–purity water at 289°C during test periods (a) up to 1, (b) 2–3, (c) 4–5, (d) 6–7, (e) 8–10, (f) 11–12, and (g) 13–15.

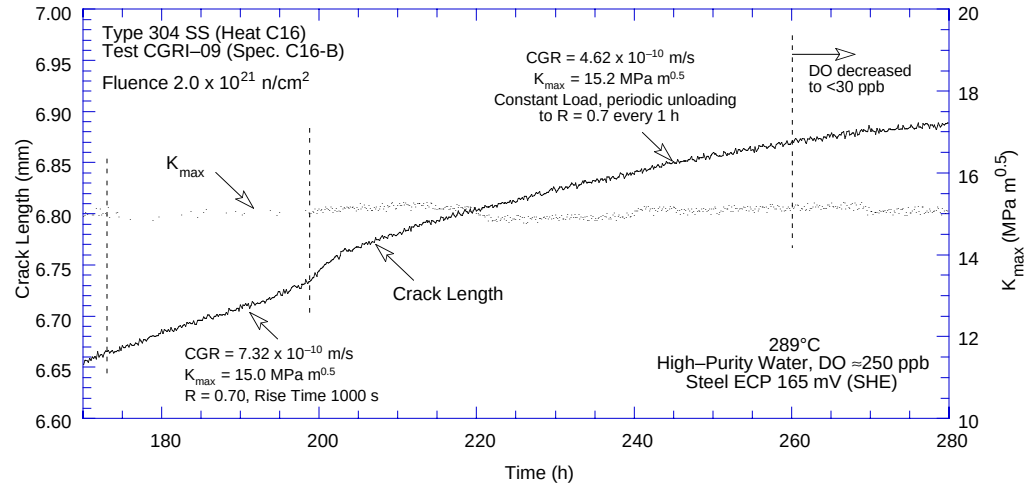

(c)

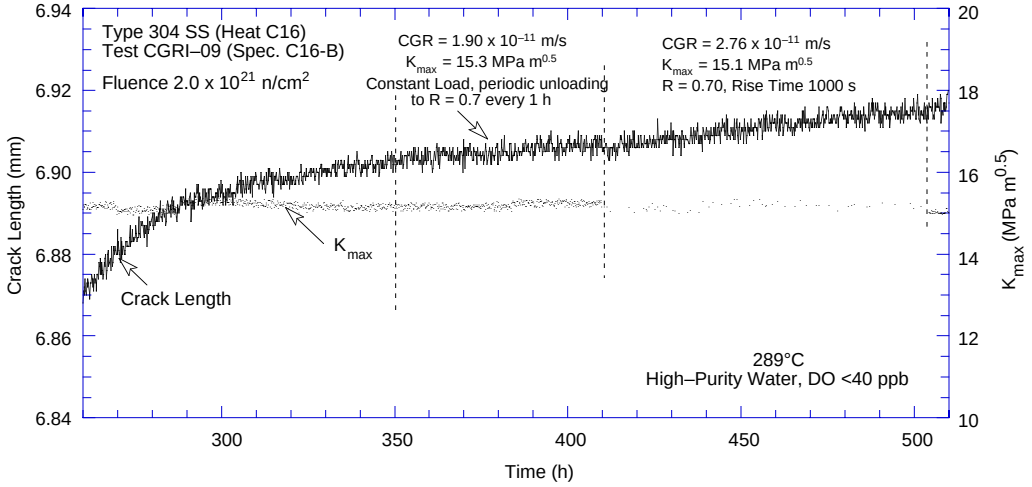

(d)

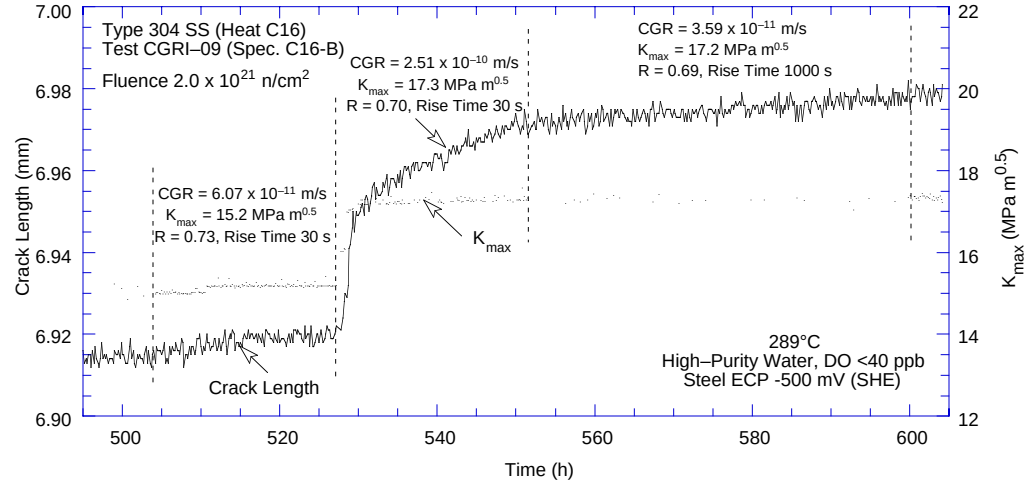

(e)

Figure 34. (Cont'd.)

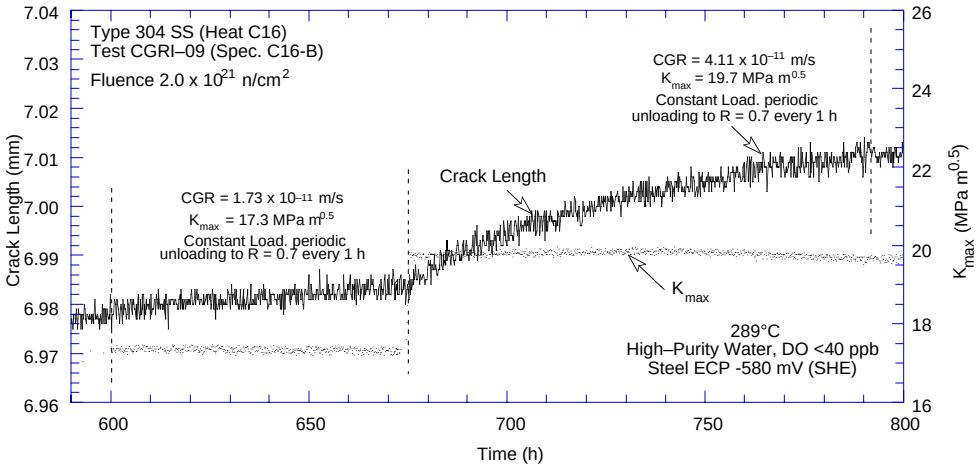

(f)

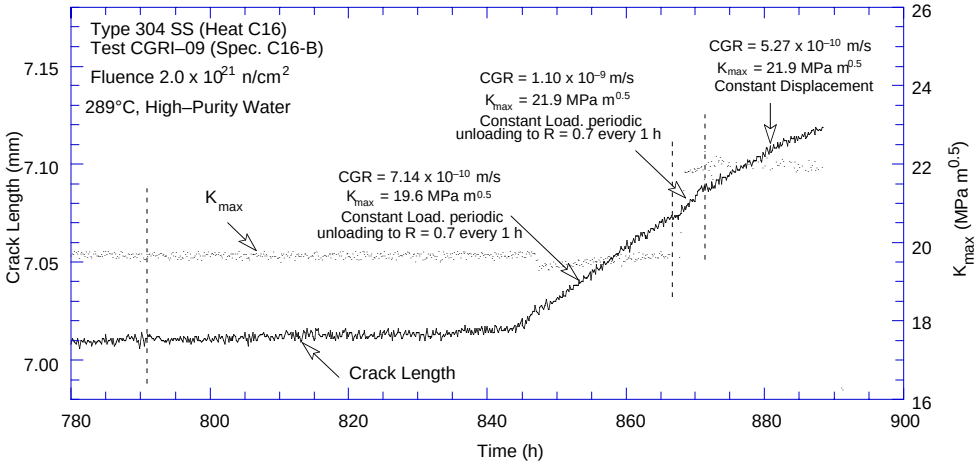

(g)

Figure 34. (Cont'd.)

For this test, a change in loading conditions from continuous cycling to nearly constant load (e.g., at 198 h), or an increase in applied K_{max} (e.g., at 527 h), resulted in a transition period of somewhat high CGRs; the growth rates gradually decrease later with time. At 527 h, the increase in K_{max} was accomplished by three load increments over a relatively short period of ≈0.5 h. It resulted in a crack advance of ≈0.03 mm (Fig. 34e). To avoid such crack advances, the increase in load at 675 h was achieved using a ramp loading with 2–h rise time (Fig. 34f). The sudden increase in crack length was not observed with gradual increase in load.

In addition, the crack growth behavior with a decrease in DO differed distinctly from that when the DO level was increased (Fig. 32a and b). With decreasing DO, the CGRs decreased by a factor of about 25, but the change was relatively gradual, extending over 60 h. With increasing DO, the growth rates increased abruptly from 4.11×10^{-11} to 7.14×10^{-10} m/s, a factor of 17 increase in CGRs. The ECPs of both the Pt and steel electrodes were above 100 mV at the time of this increase in growth rate.

Irradiated to the same fluence level as Type 304 SS specimen C3–C, the Type 316 SS specimen C16–B clearly does show a benefit of reduced DO level on CGRs (Fig. 32a). The growth rates decreased by more than an order of magnitude when DO was decreased from 250

to <30 ppb. Additional data will be obtained to establish the effect of decreased DO level on the CGRs of irradiated austenitic SSs from testing samples from the Halden II irradiation.

3.2.4 Specimen C3-A Irradiated to 0.3 x 10^{21} n/cm^2

The environmental and loading conditions, experimental CGRs, allowed K_{max} from K/size criterion in Eq. 13, and the deviation of applied K_{max} from the allowed value are given in Table 6. For this specimen, because the ultimate–to–yield stress ratio was >1.3 (Table 2), effective flow stress instead of effective yield stress was used to determine the allowed K_{max} from Eq. 13. The test was started in a high–DO environment (≈300 ppb DO in effluent), and the water flow rate was ≈10 mL/min. The ECPs of Pt and SS electrodes in the effluent stream were monitored continuously. Precracking was carried out at R = 0.3 and K_{max} = 13–14 MPa $m^{1/2}$. After ≈0.3 mm crack advance, R was increased incrementally to 0.7, and the waveform was changed from triangular to saw-tooth with rise times of 12–500 s.

A photomicrograph of the fracture surface of both halves of the specimen is shown in Fig. 35. The final crack length, determined from the photograph, showed very good agreement with the value estimated from the DC potential measurement. Also, the results in Table 6 indicate that for specimen C3–A, loading conditions for all test periods, except 11 and 12, satisfied the K/size criterion of Eq. 13.

The changes in crack length and K_{max} with time during various test periods are shown in Figs. 36a–e. For this specimen, crack growth could not be maintained for loading conditions with high values of R and relatively low K_{max}. For example, at K_{max} = 14 MPa $m^{1/2}$ increasing R from 0.3 to 0.5 essentially stopped crack growth (Fig. 36a). Changing R back to the earlier value did not restore crack growth; K_{max} had to be increased to start crack growth. To promote environmentally enhanced crack growth, the rise time for the cyclic loading at R = 0.3 was increased from 0.5 to 300 s before increasing R (Fig. 36b). For R = 0.7, crack growth occurred only at K_{max} greater than 17 MPa $m^{1/2}$.

Table 6. Crack growth results for Specimen C3–A of Type 304 SS[a] in high–purity water at 289°C

Test Period	Test Time, h	ECP [b] mV (SHE) Pt	ECP [b] mV (SHE) Steel	O_2 Conc.,[b] ppb	Load Ratio	Rise Time, s	Down Time, s	Hold Time, s	K_{max}, MPa·$m^{1/2}$	ΔK, MPa·$m^{1/2}$	Growth Rate, m/s	K_{max} from Eq. 13 MPa $m^{1/2}$	Deviation in K_{max}, %
Pre	55	226	167	300	0.31	0.5	0.5	0	12.9	8.9	2.94E-09	18.4	-30
1	165	212	166	300	0.30	0.5	0.5	0	14.0	9.8	8.37E-09	17.9	-22
2a	189	221	169	300	0.50	5	5	0	13.9	6.9	negligible	17.9	-23
2b	193	211	169	300	0.50	0.5	0.5	0	13.8	6.9	negligible	17.9	-23
2c	214	209	161	300	0.30	0.5	0.5	0	13.9	9.7	negligible	17.9	-23
2d	219	211	163	300	0.30	0.5	0.5	0	15.0	10.5	1.48E-08	17.7	-15
3	364	218	171	300	0.30	1	1	0	15.9	11.1	1.39E-08	17.5	-9
4	380	218	171	300	0.30	30	4	0	16.0	11.2	1.33E-09	17.4	-8
5	404	219	177	300	0.29	300	4	0	15.9	11.3	3.29E-10	17.4	-8
6	479	204	173	300	0.48	300	4	0	15.7	8.2	4.75E-11	17.4	-10
7	596	235	187	300	0.70	12	12	0	15.7	4.7	negligible	17.4	-10
8	670	228	188	300	0.70	12	12	0	17.6	5.3	6.23E-11	17.3	2
9	717	231	186	300	0.70	12	12	3600	17.8	–	–	17.3	3
10	910	234	197	300	0.70	500	12	3600	17.9	–	8.65E-11	17.2	4
11	1080	232	200	300	0.70	500	12	3600	22.0	–	1.11E-10	17.1	29
12	1175	226	203	300	0.70	500	1	9500	22.3	–	1.28E-10	17.0	31

[a]Heat C3, irradiated to 2.0 x 10^{21} n/cm^2.
[b]Represents values in the effluent. Conductivity was 0.07 and 0.3–0.45 μS/cm in feedwater and effluent, respectively. Feedwater pH at room temperature was 6.5.

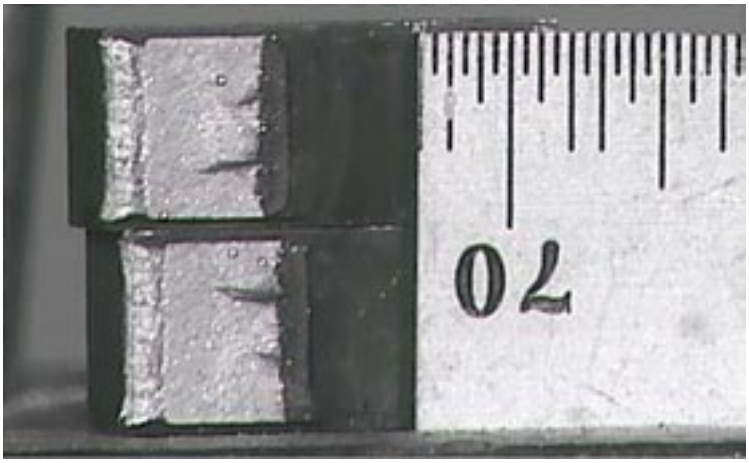

Figure 35. Photomicrographs of the fracture surface of Specimen C3–A

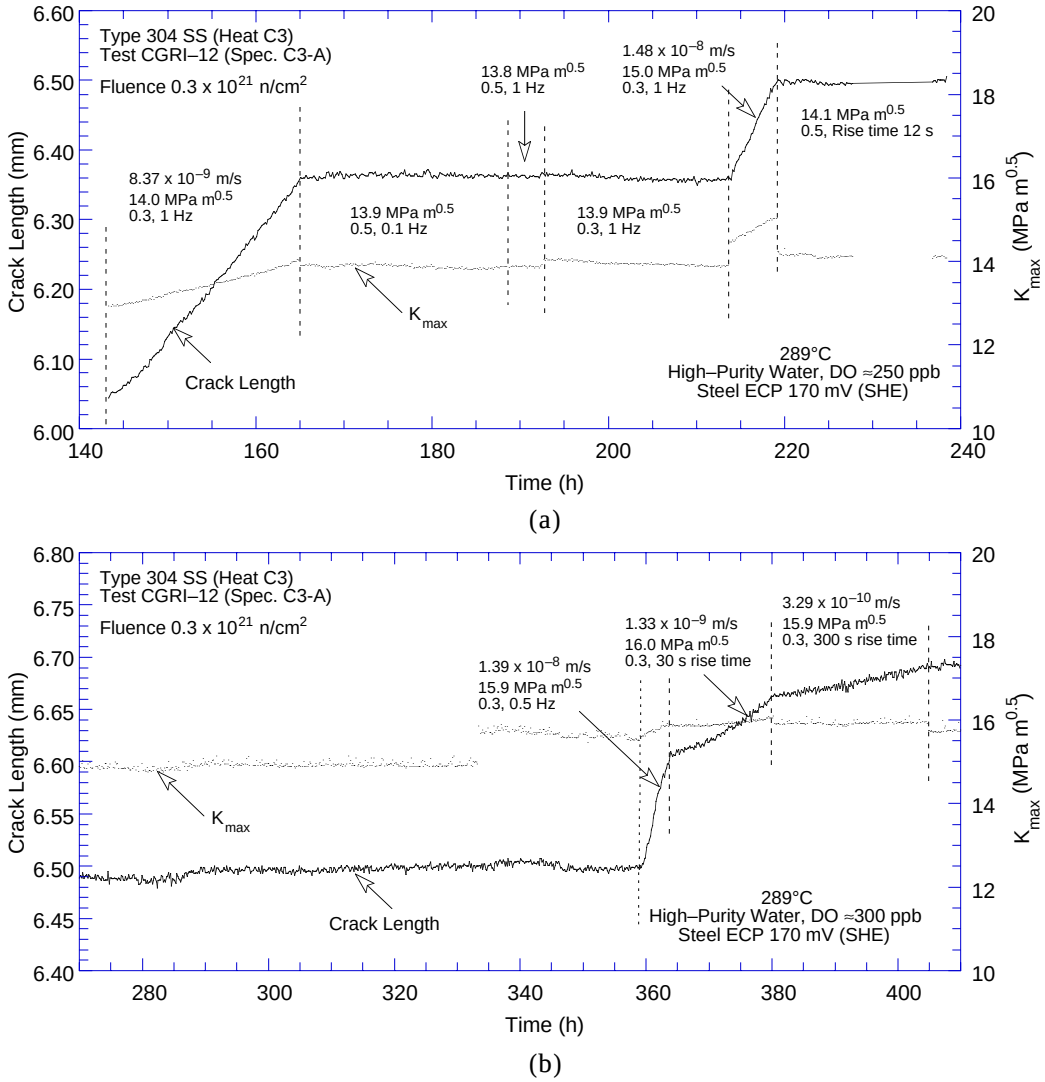

Figure 36. Crack–length–vs.–time plots for irradiated Type 316 SS (Heat C16) in high–purity water at 289°C during test periods (a) 1–2, (b) 3–5, (c) 6–7, (d) 8–10, and (e) 11–12.

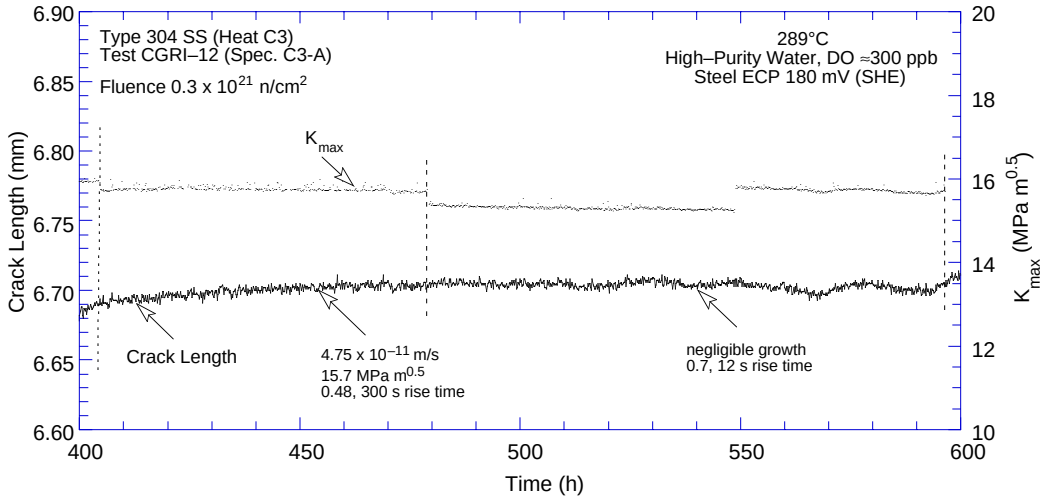

(c)

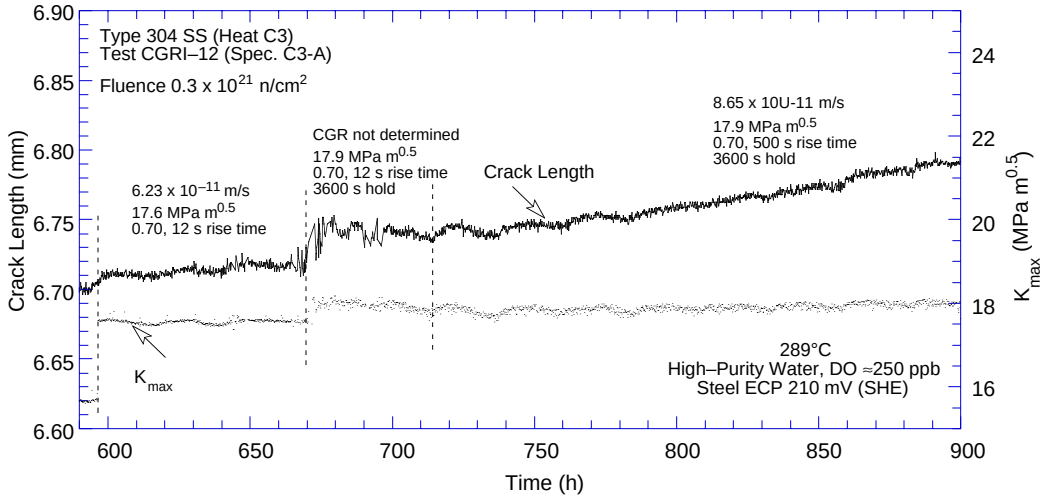

(d)

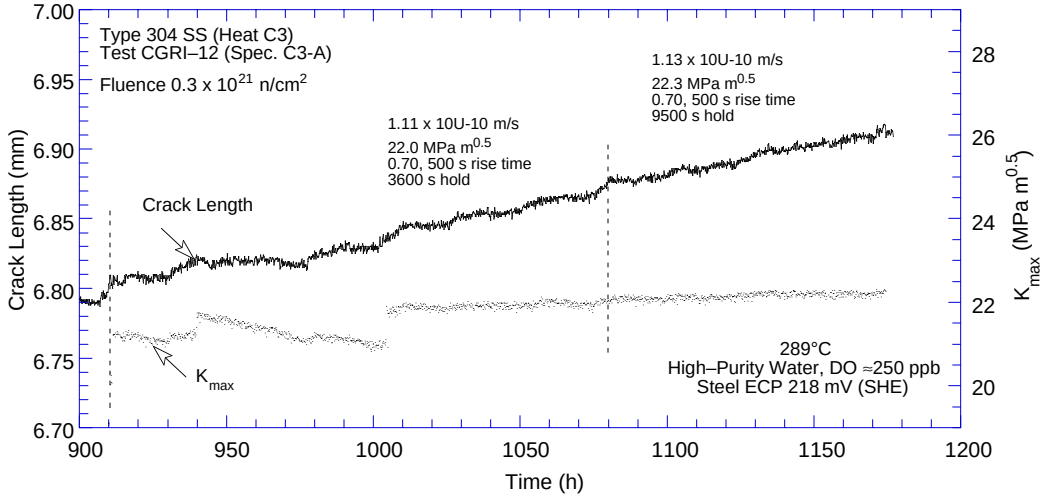

(e)

Figure 36. (Cont'd)

Crack growth rates could not be measured during test period 9 because of significant variations in the autoclave temperature, which resulted in large fluctuations in the DC potential measurements (Fig. 36d). Also, during test period 11 (Fig. 36e), applied K_{max} gradually decreased from the desired value of 22 to 20.5 MPa $m^{1/2}$ over a 50–h period because of faulty back–pressure regulator. Specimen C3–A irradiated to 0.3 x 10^{21} n/cm^2 showed very little environmental enhancement of CGRs both under continuous cycling and SCC conditions. There was no change in CGR when the hold time was increased from 3600 to 9500 s (Fig. 36e test period 11 and 12).

3.2.5 CGRs of Irradiated Austenitic SSs under Continuous Cycling

For continuous cyclic loading, the experimental CGRs for irradiated austenitic SSs in high– and low–DO environments and those predicted in air for the same loading conditions are plotted in Fig. 37. The curves represent the Shack/Kassner model for nonirradiated austenitic SSs in high–purity water with either 8 or 0.2 ppm DO (Eqs. 18 and 19, respectively) and are included to provide a comparison with the irradiated CGR data. The CGRs in air $\dot{a}_{air}$ (m/s) were determined from the correlations developed by James and Jones,[36] e.g., Eqs. 15–17.

The results for SSs irradiated to 0.9 or 2.0 x 10^{21} n/cm^2 (1.35 or 3.0 dpa) indicate significant enhancement of the CGRs in high–DO water under cyclic loading with long rise times. The CGRs for Type 304 SS irradiated to either 0.9 or 2.0 x 10^{21} n·cm^{-2}, and Type 316 SS irradiated to 2.0 x 10^{21} n·cm^{-2} are comparable. For these irradiation conditions, the CGRs in water with ≈ 300 ppb DO are slightly higher than the rates predicted by the Shack/Kassner model for nonirradiated austenitic SSs in high–purity water with 8 ppm DO (Fig. 37a).

Type 304 SS irradiated to 0.3 x 10^{21} n/cm^2 (0.45 dpa) shows very little environmental enhancement of CGRs in high–DO water (open diamonds in Fig. 37a); the CGRs in water with ≈ 300 ppb DO may be represented by the Shack/Kassner model for nonirradiated austenitic SSs in high–purity water with 0.2 ppm DO.

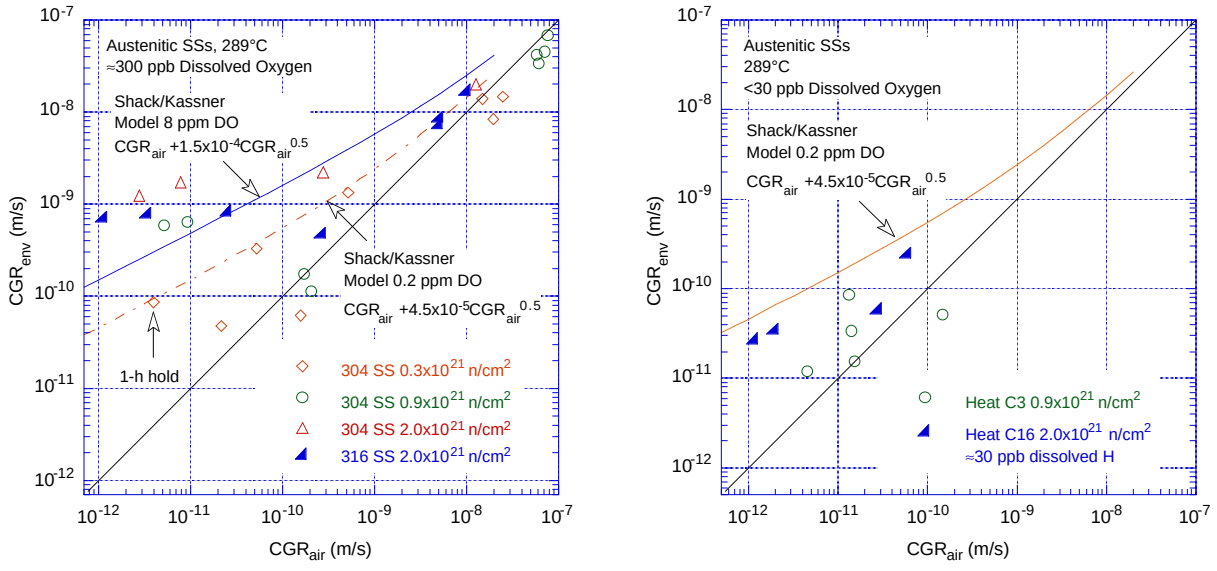

Figure 37. CGR data for irradiated austenitic SSs under continuous cycling at 289°C in high–purity water with (a) ≈300 ppb and (b) <30 ppb dissolved oxygen.

For continuous cyclic loading, decreasing the DO level has a beneficial effect on CGRs, e.g., decreasing the DO from ≈300 ppb DO to <30 ppb DO results in a factor of 25 decrease in the CGR. The growth rates are slightly lower for the irradiated steels in water with <30 ppb DO than for nonirradiated austenitic SSs in high–purity water with 0.2 ppm DO (Fig. 37b). The CGR data in low–DO environment was not obtained for Type 304 SS specimen C3–C irradiated to 2 x 10^{21} n/cm^2. As discussed below, a benefit of reduced DO environment was not observed for this specimen under SCC conditions.

3.2.6 CGRs of Irradiated Austenitic SSs under Cycling with Long Hold Periods

For CGR tests with a trapezoidal waveform (i.e., constant load with periodic partial unloading), the experimental CGRs for irradiated SSs in high– and low–DO water are plotted in Fig. 38. In high–DO water, the CGRs obtained in the present study of Types 304 and 316 SS irradiated to either 0.9 or 2.0 x 10^{21} n/cm^2 are a factor of ≈5 higher than the disposition curve for sensitized SSs in water with 8 ppm DO given in NUREG–0313.[37] The growth rates for the two steels at the same fluence level, as well as those for Type 304 SS irradiated to 0.9 and 2.0 x 10^{21} n/cm^2 fluence levels, are comparable. In high–DO water, the CGRs for Type 304 irradiated to 0.3 x 10^{21} n/cm^2 are below the disposition curve for sensitized SSs in water with 8 ppm DO given in NUREG–0313.

The results also indicate a benefit from a low–DO environment. For Heat C3 irradiated to 0.9 x 10^{21} n/cm^2 and Heat C16 irradiated to 2.0 x 10^{21} n/cm^2 (circles and open diamonds in Fig. 38), the CGRs decreased more than an order of magnitude when the DO level was decreased from ≈300 to <30 ppb.

No benefit of low–DO environment was observed for Heat C3 irradiated to 2.0 x 10^{21} n/cm^2 (open and closed triangles in Fig. 38). However, the applied K_{max} for the test period in low–DO water was 44% greater than the allowable value based on the K/size criterion in Eq. 13. Additional data will be obtained on Type 316 SS Heat C21 irradiated to 0.3, 0.9, and 2.0 x 10^{21} n/cm^2, to better establish the effect of decreased DO level on the CGRs of irradiated austenitic SSs.

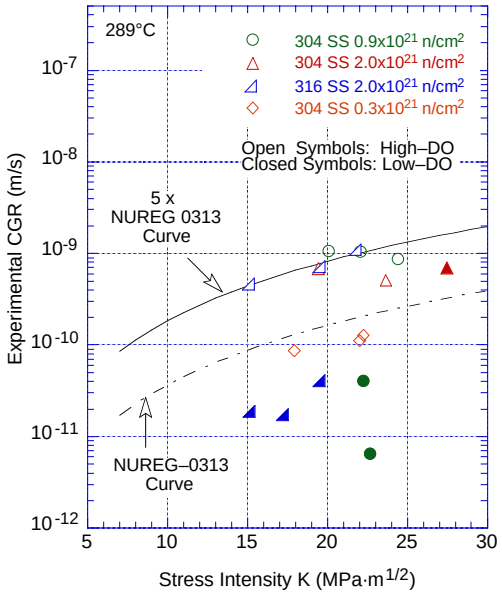

Figure 38.
CGR data under constant load with periodic partial unloads for irradiated austenitic SSs in high–purity water at 289°C

4. Summary

Fracture toughness J–R curve tests have been conducted on four heats of Type 304 SS that were irradiated to fluence levels of ≈0.3, 0.9, and 2.0 x 10^{21} n/cm^2 (E > 1 MeV) (≈0.45, 1.35, 3.00 dpa) at ≈288°C in a helium environment in the Halden boiling heavy water reactor. The tests were performed on 1/4–T compact tension specimens in air at 288°C; crack extensions were determined by both DC potential and elastic unloading compliance techniques.

Neutron irradiation at 288°C to 2.0 x 10^{21} n/cm^2 (E > 1 MeV) (3.0 dpa) decreased the fracture toughness of all of the steels. For these materials, minor differences in the chemical composition of the steels, e.g., differences in nickel content for Heats C16 and C19 or silicon content for heats L2 and L20, have little or no effect on the fracture toughness of irradiated steels.

In general, fracture toughness of the commercial Heats C16 and C19 is superior to that of the laboratory Heats L20 and L2. These differences arise primarily from differences in toughness of the nonirradiated steels, i.e., the fracture toughness of the laboratory heats is significantly lower than that of the commercial heats. The fracture toughness J–R curves for irradiated Types 304 and 316 SS are comparable. The data from commercial heats fall within the scatter band for the data obtained at higher temperatures. For Heat C19 of Type 304 SS irradiated to 0.3, 0.9, and 2.0 x 10^{21} n/cm^2, the J_{Ic} values are 507, 313, and 188 kJ/m^2, respectively.

Crack growth tests have been performed in simulated BWR environments at ≈289°C on Type 304 SS (Heat C3) irradiated to 0.3, 0.9, and 2.0 x 10^{21} n/cm^2 and Type 316 SS (Heat C16) irradiated to 2.0 x 10^{21} n/cm^2 at ≈288°C in a helium environment. The tests were conducted under cyclic loading with a slow/fast sawtooth waveform and long rise times or a trapezoidal waveform. The latter essentially represents constant load with periodic partial unloads.

The results for the steels irradiated to either 0.9 or 2.0 x 10^{21} n/cm^2 indicate significant enhancement of CGRs in the NWC BWR environment. For these irradiation conditions, the CGRs under continuous cycling are slightly higher than the rates predicted by the Shack/Kassner model for nonirradiated austenitic SSs in high–purity water with 8 ppm DO. The CGRs under SCC conditions are a factor of ≈5 higher than the disposition curve proposed in NUREG–0313 for sensitized austenitic SSs. The CGRs of Type 304 SS irradiated to 0.9 and 2.0 x 10^{21} n/cm^2 and of Types 304 and 316 SS irradiated to 2.0 x 10^{21} n/cm^2 are comparable.

In low–DO BWR environments, the CGRs of the irradiated steels decreased by an order of magnitude in tests where K values clearly met the validity criteria, e.g., Heat C3 of Type 304 SS irradiated to 0.9 x 10^{21} n/cm^2 and Heat C16 of Type 316 SS irradiated to 2 x 10^{21} n/cm^2. The beneficial effect of decreased DO was not observed for Heat C3 of Type 304 SS irradiated to 2 x 10^{21} n/cm^2; it is possible that this different behavior is associated with the loss of constraint in the specimen due to the high K.

Type 304 SS irradiated to 0.3 x 10^{21} n/cm^2 (0.45 dpa) shows very little environmental enhancement of CGRs in the NWC BWR environment; under continuous cycling, the CGRs are comparable to those predicted by the Shack/Kassner model for nonirradiated austenitic SSs in

high–purity water with 0.2 ppm DO. The CGRs for Type 304 irradiated to 0.3×10^{21} n/cm^2 under SCC conditions are below the disposition curve for sensitized SSs in water with 8 ppm DO given in NUREG–0313.

References

1. S. M. Bruemmer et al., "Critical Issue Reviews for the Understanding and Evaluation of Irradiation–Assisted Stress Corrosion Cracking," EPRI TR–107159, Electric Power Research Institute, Palo Alto, CA (1996).

2. M. L. Herrera, et al., "Evaluation of the Effects of Irradiation on the Fracture Toughness of BWR Internal Components," in Proc. ASME/JSME 4th Intl. Conf. on Nucl. Eng. (ICONE–4) Vol. 5, A. S. Rao, R. M. Duffey, and D. Elias, eds., American Society of Mechanical Engineers, New York, pp. 245–251 (1996).

3. W. J. Mills, "Fracture Toughness of Type 304 and 316 Stainless Steels and their Welds," Intl. Mater. Rev. 42, 45–82 (1997).

4. H. Kanasaki, I. Satoh, M. Koyama, T. Okubo, T. R. Mager, and R. G. Lott, "Fatigue and Stress Corrosion Cracking Behaviors of Irradiated Stainless Steels in PWR Primary Water," Proc. 5th Intl. Conf. On Nuclear Engineering, ICONE5-2372, pp. 1–7 (1997).

5. P. L. Andresen, F. P. Ford, S. M. Murphy, and J. M. Perks, "State of Knowledge of Radiation Effects on Environmental Cracking in Light Water Reactor Core Materials," Proc. 4th Intl. Symp. on Environmental Degradation of Materials in Nuclear Power Systems – Water Reactors, NACE, pp. 1.83–1.121 (1990).

6. A. Jenssen and L. G. Ljungberg, "Irradiation Assisted Stress Corrosion Cracking of Stainless Alloys in BWR Normal Water Chemistry and Hydrogen Water Chemistry," Proc. Sixth Intl. Symp. on Environmental Degradation of Materials in Nuclear Power Systems – Water Reactor, R. E. Gold and E. P. Simonen, eds., Minerals, Metals & Materials Society, 547–553 (1993).

7. P. J. Maziasz and C. J. McHargue, "Microstructural Evolution in Annealed Austenitic Steels during Neutron Irradiation," Int. Met. Rev. 32, 190 (1987).

8. P. J. Maziasz, "Overview of Microstructural Evolution in Neutron–Irradiated Austenitic Stainless Steels," J. Nucl. Mater. 205, 118–145 (1993).

9. F. A. Garner, "Evolution of Microstructures in Face–Centered Cubic Metals during Neutron Irradiation," J. Nucl. Mater. 205, 98–111 (1993).

10. J. Dufresne, B. Henry, and H. Larsson, "Fracture Toughness of Irradiated AISI 304 and 316L Stainless Steels," in Effects of Radiation on Structural Materials, ASTM STP 683, J. A. Sprague and D. Kramer, eds., American Society for Testing and Materials, Philadelphia, pp. 511–528 (1979).

11. C. Picker, A. L. Stott, and H. Cocks, "Effects of Low–Dose Fast Neutron Irradiation on the Fracture Toughness of Type 316 Stainless Steel and Weld Metal," in Proc. Specialists Meeting on Mechanical Properties of Fast Reactor Structural Materials, Chester, UK, Paper IWGFR 49/440–4 (1983).

12. F. H. Huang, “The Fracture Characterization of Highly Irradiated Type 316 Stainless Steel,” Int. J. Fracture 25, 181–193 (1984).

13. J. Bernard and G. Verzeletti, “Elasto–Plastic Fracture Mechanics Characterization of Type 316H Irradiated Stainless Steel up to 1 dpa,” in Effects of Radiation on Materials: 12th Intl. Symp., ASTM STP 870, F. A. Garner and J. S. Perrin, eds., American Society for Testing and Materials, Philadelphia, pp. 619–641 (1985).

14. W. J. Mills, L. A. James, and L. D. Blackburn, 1985, “Results of Fracture Mechanics Tests on PNC SU 304 Plate,” Westinghouse Hanford Report HEDL–7544, Hanford Engineering Development Laboratory, Richland, WA.

15. W. J. Mills, “Fracture Toughness of Irradiated Stainless Steel Alloys,” Nucl. Technol. 82, 290–303 (1988).

16. D. J. Michel and R. A. Gray, “Effects of Irradiation on the Fracture Toughness of FBR Structural Materials,” J. Nucl. Mater. 148, 194–203 (1987).

17. P. Ould, P. Balladon, and Y. Meyzaud, Bull. Cercle Etud. Metaux 15, 31.1–31.12 (1988).

18. E. V. Van Osch, M. G. Horsten, and M. I. De Vries, “Fracture Toughness of PWR Internals,” ECN Contribution to CEC Contract on PWR Internals–Part 2 (ETNU/CT/94/0136–F), ECN–I–97–010 (71747/NUC/EvO/mh/006274), Netherlands Energy Research Foundation ECN, Petten, the Netherlands (1997).

19. K. S. Brown and G. M. Gordon, “Effects of BWR Coolant Chemistry on the Propensity for IGSCC Initiation and Growth in Creviced Reactor Internals Components,” Proc. Third Intl. Symp. on Environmental Degradation of Materials in Nuclear Power Systems – Water Reactor, AIME, pp. 243–248 (1987).

20. G. M. Gordon and K. S. Brown, “Dependence of Creviced BWR Component IGSCC Behavior on Coolant Chemistry,” Proc. 4th Intl. Symp. on Environmental Degradation of Materials in Nuclear Power Systems – Water Reactor, Daniel Cubicciotti, ed., NACE, pp. 14.46–14.61 (1990).

21. F. Garzarolli, D. Alter, and P. Dewes, “Deformability of Austenitic Stainless Steels and Nickel–Base Alloys in the Core of a Boiling and a Pressurized Water Reactor,” Proc. Intl. Symp. on Environmental Degradation of Materials in Nuclear Power Systems – Water Reactor, ANS, pp. 131–138 (1986).

22. M. Kodama et al., “IASCC Susceptibility of Austenitic Stainless Steels Irradiated to High Neutron Fluence,” Proc. Sixth Intl. Symp. on Environmental Degradation of Materials in Nuclear Power Systems – Water Reactor, R. E. Gold and E. P. Simonen, eds., Minerals, Metals & Materials Society, pp. 583–588 (1993).

23. M. Kodama et al., “Effects of Fluence and Dissolved Oxygen on IASCC in Austenitic Stainless Steels,” Proc. Fifth Intl. Symp. on Environmental Degradation of Materials in Nuclear Power Systems – Water Reactor, American Nuclear Society, pp. 948–954 (1991).

24. W. L. Clark and A. J. Jacobs, “Effect of Radiation Environment on SCC of Austenitic Materials,” Proc. First Intl. Symp. on Environmental Degradation of Materials in Nuclear Power Systems – Water Reactor, NACE, p. 451 (1983).

25. A. Jenssen and L. G. Ljungberg, “Irradiation Assisted Stress Corrosion Cracking of Stainless Alloys in BWR Normal Water Chemistry and Hydrogen Water Chemistry,” Proc. Sixth Intl. Symp. on Environmental Degradation of Materials in Nuclear Power Systems – Water Reactor, R. E. Gold and E. P. Simonen, eds., Minerals, Metals & Materials Society, pp. 547–553 (1993).

26. A. Jenssen and L. G. Ljungberg, “Irradiation Assisted Stress Corrosion Cracking. Post Irradiation CERT Tests of Stainless Steels in a BWR Test Loop,” Proc. Seventh Intl. Symp. on Environmental Degradation of Materials in Nuclear Power Systems – Water Reactor, G. Airey et al., eds., NACE, pp. 1043–1052 (1995).

27. H. M. Chung, W. E. Ruther, R. V. Strain, and W. J. Shack, “Irradiated–Assisted Stress Corrosion Cracking of Model Austenitic Stainless Steel Alloys,” NUREG/CR–6687, ANL–00/21 (Oct. 2000).

28. H. M. Chung, R. V. Strain, and R. W. Clark, “Slow–Strain–Rate–Tensile Test of Model Austenitic Stainless Steels Irradiated in the Halden Reactor,” in Environmentally Assisted Cracking in Light Water Reactors Annual Report January–December 2001, NUREG/CR–4667, Vol. 32, ANL–02/33, pp. 19–28 (2003).

29. O. K. Chopra, E. E. Gruber, and W. J. Shack, “Fracture Toughness Characterization of Type 304 Stainless Steel Irradiated in the Halden Reactor,” Proc. of the 8th Intl. Conf. on Nuclear Engineering, ICONE8–8301, ASME (2000).

30. E. E. Gruber and O. K. Chopra, “Fracture Toughness J–R Test of Austenitic Stainless Steels Irradiated in Halden Reactor,” in Environmentally Assisted Cracking in Light Water Reactors Semiannual Report January 1999–June 1999, NUREG/CR–4667, Vol. 28, ANL–00/7, pp. 27–35 (July 2000).

31. E. E. Gruber and O. K. Chopra, “Fracture Toughness J–R Test of Austenitic Stainless Steels Irradiated in Halden Reactor,” in Environmentally Assisted Cracking in Light Water Reactors Semiannual Report July 1999–December 1999, NUREG/CR–4667, Vol. 29, ANL–00/23, pp. 30–38 (Nov. 2000).

32. E. E. Gruber and O. K. Chopra, “Fracture Toughness J–R Test of Austenitic Stainless Steels Irradiated in Halden Reactor,” in Environmentally Assisted Cracking in Light Water Reactors Semiannual Report July 1998–December 1998, NUREG/CR–4667, Vol. 31, ANL–01/09, pp. 33–37 (April 2002).

33. E. E. Gruber and O. K. Chopra, “Fracture Toughness J–R Test of Austenitic Stainless Steels Irradiated in Halden Reactor,” in Environmentally Assisted Cracking in Light Water Reactors Semiannual Report July 1998–December 1998, NUREG/CR–4667, Vol. 27, ANL–99/11, pp. 39–45 (Oct. 1999).

34. P. L. Andresen, “Similarity of Cold Work and Radiation Hardening in Enhancing Yield Strength and SCC Growth of Stainless Steel in Hot Water,” Corrosion/02, Paper 02509, NACE (2002).

35. W. J. Shack and T. F. Kassner, “Review of Environmental Effects on Fatigue Crack Growth of Austenitic Stainless Steels,” NUREG/CR–6176, ANL–94/1 (May 1994).

36. L. A. James and D. P. Jones, “Fatigue Crack Growth Correlation for Austenitic Stainless Steels in Air,” Proc. Conf. on Predictive Capabilities in Environmentally–Assisted Cracking, PVP Vol. 99, R. Rungta, ed., American Society of Mechanical Engineers, New York, pp. 363–414 (1985).

37. W. S. Hazelton and W. H. Koo, “Technical Report on Material Selection and Processing Guidelines for BWR Coolant Pressure Boundary Piping, Final Report,” NUREG–0313, Rev. 2 (1988).

38. A. L. Hiser, “Fracture Toughness Characterization of Nuclear Piping Steels,” NUREG/CR–5118, MEA–2325, Materials Engineering Associates, Inc., Lanham, MD (1989).

39. G. M. Wilkowski et al., “Degraded Piping Program – Phase II, Semiannual Report,” NUREG/CR–4082, Vol. 2 (1985).

40. Mills, W. J., “Heat–to–Heat Variations in the Fracture Toughness of Austenitic Stainless Steels,” Eng. Fracture Mech. 30, 469–492 (1988).

41. M. G. Vassilaros, R. A. Hays, and J. P. Gudas, “Investigation of the Ductile Fracture Properties of Type 304 Stainless Steel Plate, Welds, and 4–Inch Pipe,” in Proc. 12th Water Reactor Safety Information Meeting, NUREG/CP–0058, Vol. 4, U.S. Nuclear Regulatory Commission, pp. 176–189 (1985).

Appendix

Table A-1. Test data for specimen Y4–03 of thermally aged CF–8M cast SS tested at 288°C

Test Number	: JR–18	Test Temp.	: 288°C
Material Type	: CF–8M Cast SS	Heat Number	: 4331
Aging Temp.	: 400°C	Aging Time	: 700 h
Irradiation Temp.	: –	Fluence	: –
Thickness	: 6.515 mm	Net Thickness	: 5.879 mm
Width	: 12.005 mm	Flow Stress	: 410.5 MPa
Modulus E	: 180 GPa		
Initial Crack	: 7.43 mm	Init. a/W	: 0.62 (Measured)
Final Crack	: 8.90 mm	Final a/W	: 0.74 (Measured)
Final Crack	: 8.97 mm	Final a/W	: 0.75 (Compliance)

No.	Load (kN)	Deflection (mm)	Unloading Compliance		DC Potential Method	
			J (kJ/m^2)	Δa (mm)	J (kJ/m^2)	Δa (mm)
0	0.0885	0.000				
1	1.6352	0.309	34.5	0.103	32.9	0.021
2	1.7575	0.398	48.6	0.016	45.6	0.030
3	1.8598	0.490	63.3	-0.030	59.3	0.039
4	1.9474	0.583	76.7	0.042	74.0	0.047
5	2.0168	0.678	93.2	-0.001	89.5	0.057
6	2.0747	0.774	110.1	-0.014	105.7	0.067
7	2.1142	0.871	126.9	-0.013	120.7	0.159
8	2.1325	0.971	144.1	-0.003	136.2	0.211
9	2.1641	1.069	158.8	0.061	152.2	0.262
10	2.1930	1.169	175.9	0.077	168.6	0.309
11	2.1907	1.269	192.1	0.120	185.0	0.365
12	2.1627	1.373	205.9	0.209	200.2	0.451
13	2.1592	1.475	220.9	0.266	215.4	0.517
14	2.1463	1.577	235.9	0.325	230.8	0.584
15	2.1369	1.679	251.6	0.370	245.9	0.652
16	2.1329	1.781	266.0	0.432	261.3	0.712
17	2.1169	1.884	282.4	0.468	276.9	0.771
18	2.0898	1.988	293.2	0.569	291.6	0.841
19	2.0822	2.091	307.6	0.621	306.6	0.897
20	2.0395	2.196	321.1	0.688	321.9	0.956
21	1.9870	2.302	331.2	0.781	335.5	1.027
22	1.9336	2.408	337.5	0.903	347.7	1.104
23	1.8696	2.515	345.5	1.004	359.9	1.174
24	1.8184	2.621	348.7	1.139	371.5	1.243
25	1.7353	2.731	347.2	1.309	382.5	1.316
26	1.6788	2.837	348.2	1.444	390.6	1.399
27	1.6272	2.943	354.2	1.541	399.1	1.471

Power–Law Fit	$J = C(\Delta a)^n$		
Unloading Compliance	J_{Ic} : 258 kJ/m^2		(15 Data)
Coeff. C : 334 kJ/m^2	Exponent n : 0.25		Fit Coeff. R : 0.907
DC Potential Method	J_{Ic} : 162 kJ/m^2		(20 Data)
Coeff. C : 324 kJ/m^2	Exponent n : 0.57		Fit Coeff. R : 0.997

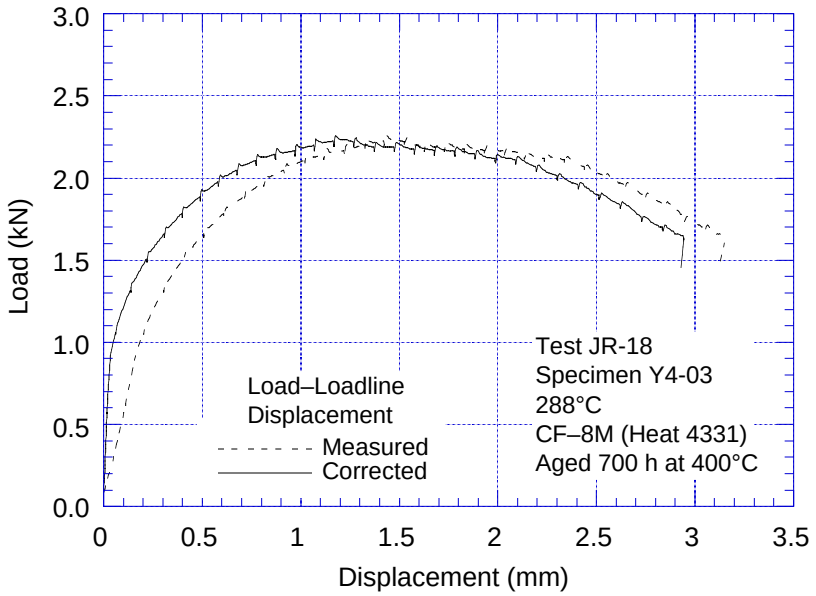

Figure A-1.1. Load-vs.-loadline displacement curve for specimen Y4–03 of thermally aged CF–8M cast SS tested at 288°C

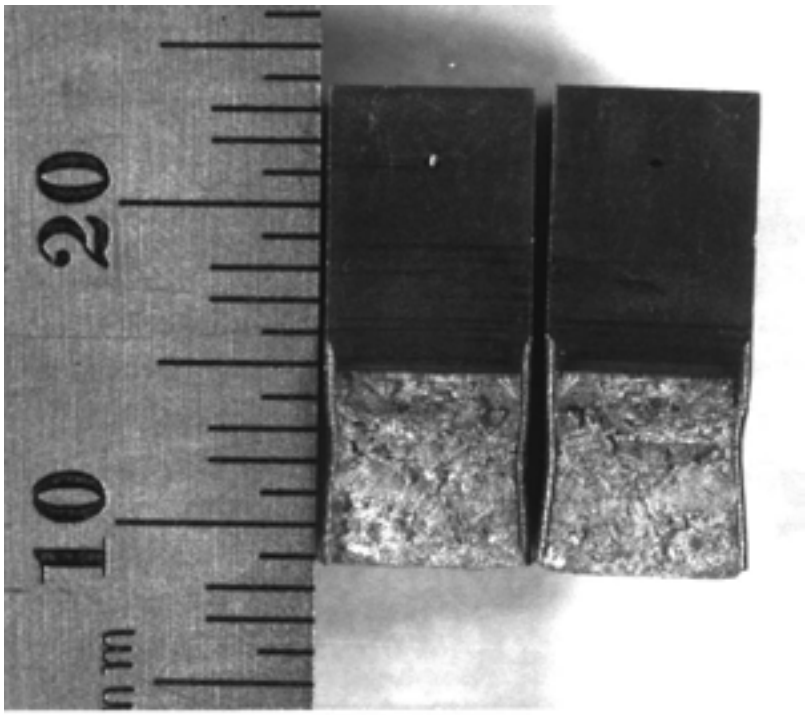

Figure A-1.2. Fracture surface of specimen Y4–03 tested at 288°C

Table A-2. Test data for specimen Y4–02 of thermally aged CF–8M cast SS tested at 288°C

Test Number	: JR–10	Test Temp.	: 288°C
Material Type	: CF–8M Cast SS	Heat Number	: 4331
Aging Temp.	: 400°C	Aging Time	: 700 h
Irradiation Temp.	: –	Fluence	: –
Thickness	: 6.515 mm	Net Thickness	: 5.857 mm
Width	: 12.003 mm	Flow Stress	: 410.5 MPa
Modulus E	: 180 GPa		
Initial Crack	: 7.51 mm	Init. a/W	: 0.63 (Measured)
Final Crack	: 9.32 mm	Final a/W	: 0.78 (Measured)
Final Crack	: 9.79 mm	Final a/W	: 0.82 (Compliance)

	Load	Deflection	Unloading Compliance		DC Potential Method	
No.	(kN)	(mm)	J (kJ/m^2)	Δa (mm)	J (kJ/m^2)	Δa (mm)
0	0.0454	0.000				
1	1.3318	0.126	11.3	0.090	10.2	0.006
2	1.5435	0.207	21.7	0.135	20.3	0.012
3	1.8447	0.380	49.2	-0.127	45.7	0.027
4	1.9550	0.471	61.3	0.015	60.3	0.036
5	2.2615	0.846	129.8	-0.147	127.6	0.076
6	2.3153	0.942	142.5	-0.003	146.1	0.087
7	2.3602	1.039	158.0	0.075	165.0	0.098
8	2.3776	1.139	174.3	0.158	183.5	0.148
9	2.3923	1.240	190.4	0.245	201.3	0.202
10	2.4221	1.338	207.1	0.313	218.4	0.259
11	2.4132	1.440	224.0	0.395	236.7	0.311
12	2.4189	1.537	242.1	0.441	253.7	0.367
13	2.4221	1.638	263.4	0.454	270.7	0.433
14	2.3963	1.741	284.2	0.479	287.4	0.502
15	2.3313	1.846	304.8	0.504	303.1	0.581
16	2.2815	1.951	325.9	0.516	317.4	0.668
17	2.2210	2.056	338.7	0.607	331.3	0.750
18	2.1712	2.161	356.1	0.644	344.9	0.828
19	2.0689	2.270	353.6	0.856	357.3	0.920
20	1.9830	2.379	359.4	0.981	366.8	1.023
21	1.8812	2.488	347.5	1.245	374.5	1.133
22	1.7815	2.597	343.0	1.435	380.2	1.245
23	1.7143	2.704	345.7	1.569	385.9	1.347
24	1.6143	2.815	335.4	1.797	389.5	1.465
25	1.5329	2.923	333.6	1.950	394.1	1.560
26	1.4724	3.029	337.5	2.060	397.5	1.658
27	1.4208	3.136	338.5	2.188	402.4	1.740
28	1.3745	3.241	343.7	2.284	408.5	1.813

Power–Law Fit $J = C(\Delta a)^n$

Unloading Compliance	J_{Ic} : 252 kJ/m^2	(14 Data)	
Coeff. C : 341 kJ/m^2	Exponent n : 0.29	Fit Coeff. R : 0.620	
DC Potential Method	J_{Ic} : 254 kJ/m^2	(14 Data)	
Coeff. C : 351 kJ/m^2	Exponent n : 0.31	Fit Coeff. R : 0.976	

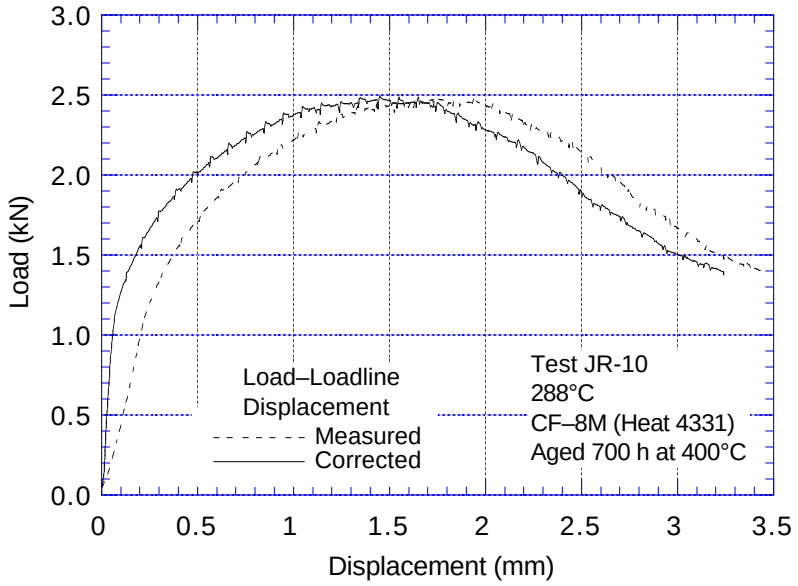

Figure A-2.1. Load-vs.-loadline displacement curve for specimen Y4–02 of thermally aged CF–8M cast SS tested at 288°C

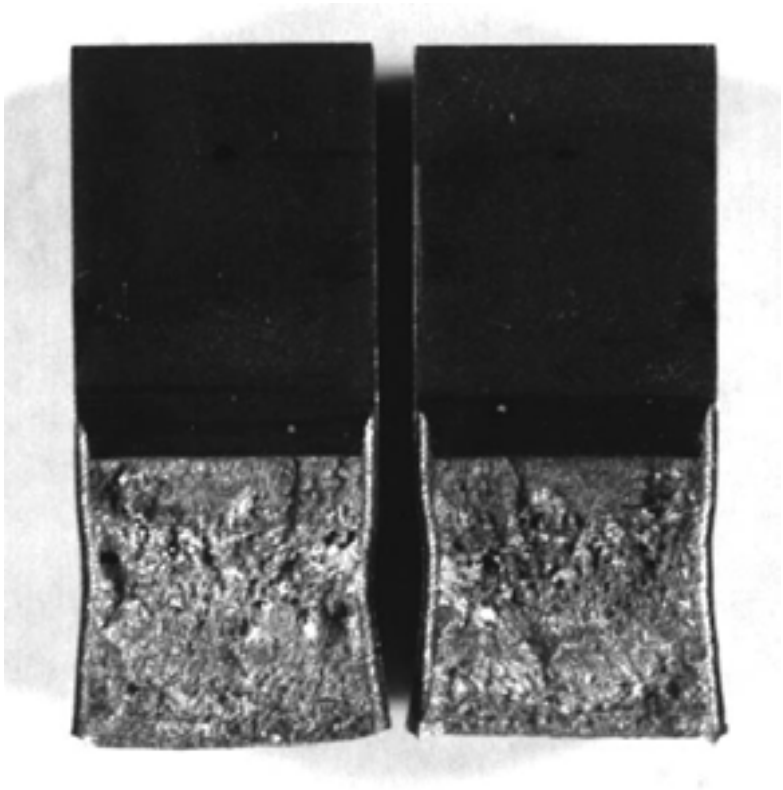

Figure A-2.2. Fracture surface of specimen Y4–02 tested at 288°C

Table A-3. Test data for specimen 75–03T of thermally aged CF–8M cast SS tested at 288°C

Test Number	: JR–07	Test Temp.	: 288°C
Material Type	: CF–8M Cast SS	Heat Number	: 75
Aging Temp.	: 400°C	Aging Time	: 10,000 h
Irradiation Temp.	: –	Fluence	: –
Thickness	: 6.51 mm	Net Thickness	: 5.90 mm
Width	: 11.98 mm	Flow Stress	: 410.0 MPa
Modulus E	: 180 GPa		
Initial Crack	: 7.28 mm	Init. a/W	: 0.61 (Measured)
Final Crack	: 9.35 mm	Final a/W	: 0.78 (Measured)
Final Crack	: 8.72 mm	Final a/W	: 0.73 (Compliance)

	Load	Deflection	Unloading Compliance		DC Potential Method	
No.	(kN)	(mm)	J (kJ/m^2)	Δa (mm)	J (kJ/m^2)	Δa (mm)
0	0.0436	0.000				
1	1.0106	0.057	2.0	-0.105	3.3	0.002
2	1.3193	0.128	10.0	-0.144	10.4	0.006
3	1.5284	0.209	18.5	0.064	19.9	0.012
4	1.8202	0.385	43.2	-0.115	44.1	0.027
5	1.9252	0.476	54.0	0.075	57.9	0.035
6	2.0155	0.569	65.1	0.293	72.7	0.044
7	2.0982	0.659	88.7	-0.130	87.7	0.053
8	2.1654	0.753	103.9	-0.069	103.8	0.063
9	2.2201	0.849	118.4	0.005	120.8	0.073
10	2.2704	0.946	131.8	0.116	138.2	0.084
11	2.2922	1.045	148.4	0.162	156.3	0.095
12	2.2904	1.147	166.6	0.184	171.4	0.205
13	2.2895	1.247	185.9	0.177	183.9	0.336
14	2.2695	1.351	200.2	0.276	195.7	0.491
15	2.2375	1.455	217.3	0.316	207.2	0.638
16	2.2228	1.558	237.1	0.309	219.2	0.766
17	2.1885	1.663	249.8	0.409	232.0	0.884
18	2.1151	1.770	262.2	0.505	243.1	1.033
19	1.9839	1.883	267.4	0.686	248.8	1.253
20	1.9150	1.991	273.7	0.828	251.1	1.479
21	1.8491	2.099	276.1	1.010	255.4	1.660
22	1.7651	2.208	280.7	1.159	260.9	1.832
23	1.6387	2.322	271.7	1.442	261.9	2.074

Power–Law Fit $J = C(\Delta a)^n$

Unloading Compliance	J_{Ic} : 225 kJ/m^2	(11 Data)	
Coeff. C : 277 kJ/m^2	Exponent n : 0.19	Fit Coeff. R : 0.748	
DC Potential Method	J_{Ic} : 180 kJ/m^2	(9 Data)	
Coeff. C : 233 kJ/m^2	Exponent n : 0.22	Fit Coeff. R : 0.972	

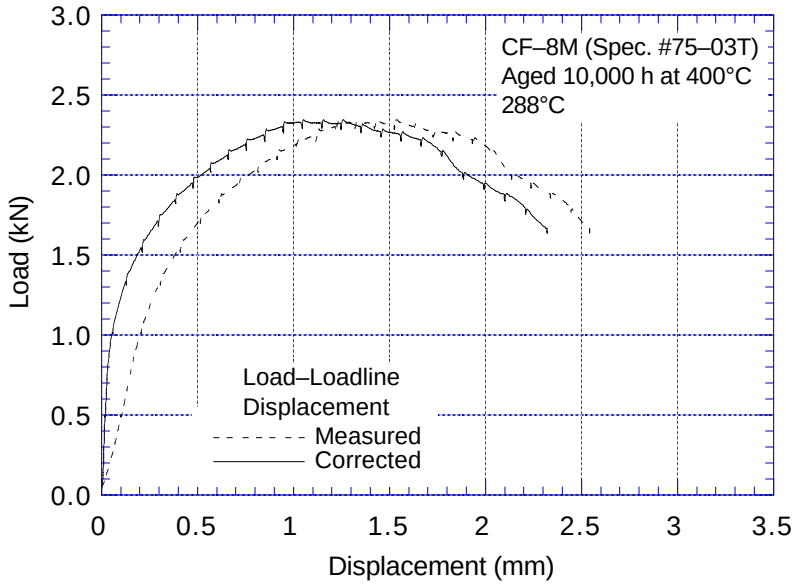

Figure A-3.1. Load-vs.-loadline displacement curve for specimen 75–03T of thermally aged CF–8M cast SS tested at 288°C

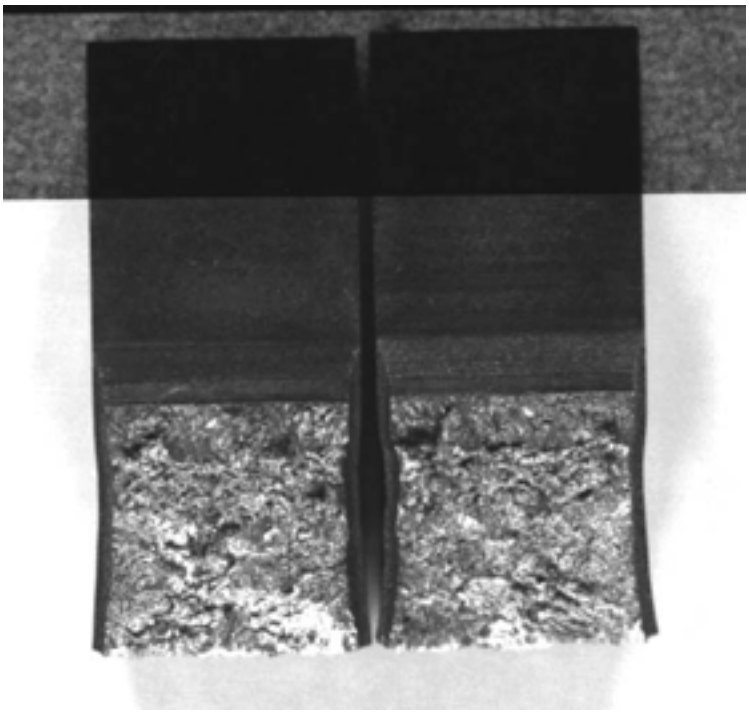

Figure A-3.2. Fracture surface of specimen 75–03T tested at 288°C

Table A-4. Test data for specimen 75–04T of thermally aged CF–8M cast SS tested at 288°C

Test Number	: JR–08	Test Temp.	: 288°C
Material Type	: CF–8M Cast SS	Heat Number	: 75
Aging Temp.	: 400°C	Aging Time	: 10,000 h
Irradiation Temp.	: –	Fluence	: –
Thickness	: 6.51 mm	Net Thickness	: 5.87 mm
Width	: 11.98 mm	Flow Stress	: 410.0 MPa
Modulus E	: 180 GPa		
Initial Crack	: 7.79 mm	Init. a/W	: 0.65 (Measured)
Final Crack	: 9.89 mm	Final a/W	: 0.83 (Measured)
Final Crack	: 10.07 mm	Final a/W	: 0.84 (Compliance)

	Load	Deflection	Unloading Compliance		DC Potential Method	
No.	(kN)	(mm)	J (kJ/m^2)	Δa (mm)	J (kJ/m^2)	Δa (mm)
0	0.0436	0.000				
1	0.4938	0.033	0.9	-0.198	1.0	0.000
2	1.9252	0.829	92.5	-0.063	99.8	0.062
3	2.0155	0.978	111.2	0.062	121.8	0.151
4	2.0982	1.128	131.3	0.171	142.9	0.246
5	2.1654	1.279	154.1	0.238	164.1	0.347
6	2.2201	1.436	179.8	0.284	185.3	0.458
7	2.2704	1.592	203.9	0.348	203.5	0.595
8	2.2922	1.752	222.6	0.474	220.4	0.738
9	2.2904	1.911	234.5	0.648	232.7	0.908
10	2.2895	2.071	240.6	0.857	245.4	1.048
11	2.2695	2.230	248.0	1.027	258.4	1.175
12	2.2375	2.387	254.8	1.188	269.7	1.299
13	2.2228	2.544	268.4	1.278	283.7	1.390
14	2.1885	2.705	265.5	1.531	295.1	1.520
15	2.1151	2.866	265.4	1.694	301.9	1.651
16	1.9839	3.032	255.1	1.968	304.6	1.819
17	1.9150	3.192	241.8	2.176	300.8	1.978
18	1.8491	3.351	242.7	2.283	299.1	2.108

Power–Law Fit $J = C(\Delta a)^n$

Unloading Compliance	J_{Ic}	: 197 kJ/m^2	(10 Data)
Coeff. C : 248 kJ/m^2	Exponent n	: 0.20	Fit Coeff. R : 0.931
DC Potential Method	J_{Ic}	: 154 kJ/m^2	(10 Data)
Coeff. C : 246 kJ/m^2	Exponent n	: 0.39	Fit Coeff. R : 0.997

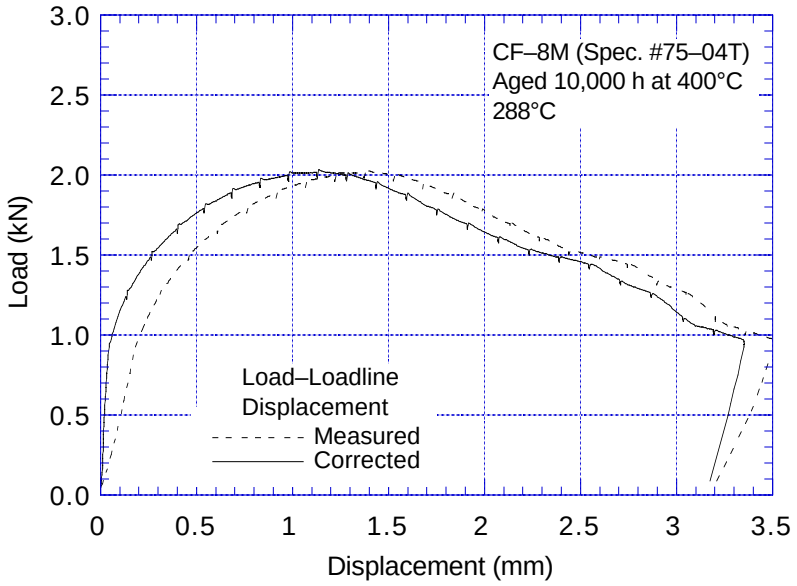

Figure A-4.1. Load-vs.-loadline displacement curve for specimen 75–04T of thermally aged CF–8M cast SS tested at 288°C

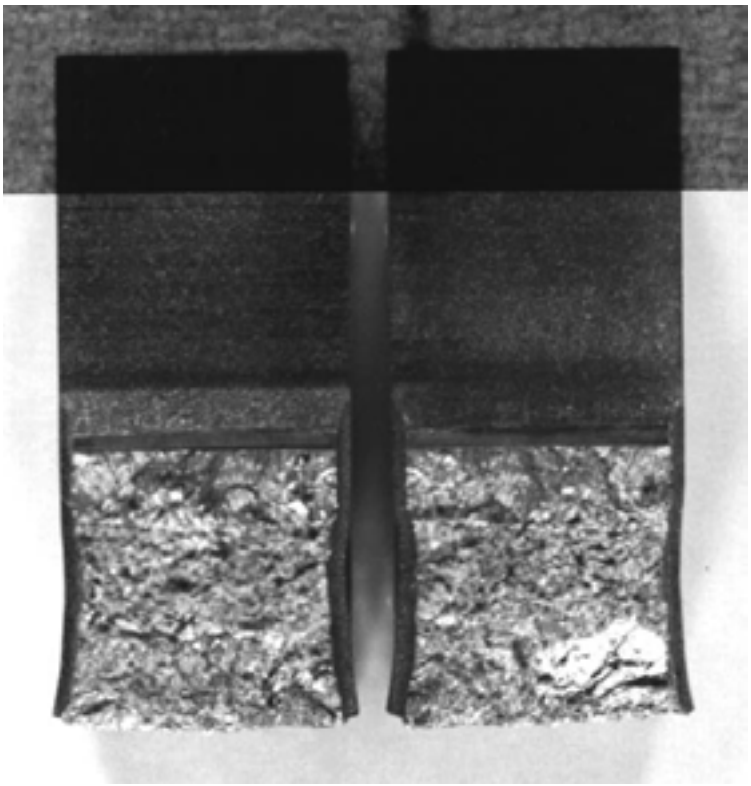

Figure A-4.2. Fracture surface of specimen 75–04T tested at 288°C

Table A-5. Test data for specimen 75–10T of thermally aged CF–8M cast SS tested at 288°C

Test Number	: JR–32	Test Temp.	: 288°C
Material Type	: CF–8M Cast SS	Heat Number	: 75
Aging Temp.	: 400°C	Aging Time	: 10,000 h
Irradiation Temp.	: –	Fluence	: –
Thickness	: 6.50 mm	Net Thickness	: 5.82 mm
Width	: 12.01 mm	Flow Stress	: 410.0 MPa
Modulus E	: 180 GPa		
Initial Crack	: 6.08 mm	Init. a/W	: 0.51 (Measured)
Final Crack	: 8.75 mm	Final a/W	: 0.73 (Measured)
Final Crack	: 8.81 mm	Final a/W	: 0.72 (Compliance)

No.	Load (kN)	Deflection (mm)	Unloading Compliance		DC Potential Method	
			J (kJ/m^2)	Δa (mm)	J (kJ/m^2)	Δa (mm)
0	0.0885	0.000				
1	2.7615	0.368	58.5	-0.496	55.8	0.038
2	2.9091	0.458	69.1	-0.195	73.0	0.044
3	3.0341	0.550	85.9	-0.051	91.6	0.055
4	3.1404	0.642	98.7	0.264	110.7	0.062
5	3.2116	0.739	118.4	0.331	128.6	0.195
6	3.2370	0.838	142.7	0.266	146.8	0.309
7	3.2792	0.937	167.1	0.209	164.9	0.426
8	3.3219	1.035	178.9	0.461	183.9	0.514
9	3.3099	1.135	204.2	0.415	203.3	0.609
10	3.2659	1.240	216.2	0.654	221.5	0.747
11	3.2468	1.345	232.5	0.794	239.6	0.865
12	3.1347	1.454	258.7	0.787	257.3	0.999
13	2.9554	1.567	269.0	1.005	270.9	1.185
14	2.8420	1.677	282.7	1.143	282.5	1.363
15	2.7179	1.788	287.7	1.380	294.9	1.511
16	2.6173	1.896	296.5	1.552	306.6	1.656
17	2.4656	2.008	294.4	1.841	316.7	1.812
18	2.2673	2.123	305.2	1.977	322.8	2.000
19	2.1098	2.235	304.0	2.215	325.3	2.194
20	1.9790	2.345	308.0	2.383	327.9	2.367
21	1.8358	2.458	307.8	2.581	330.7	2.530
22	1.7366	2.567	311.3	2.731	334.8	2.667

Power–Law Fit $J = C(\Delta a)^n$

Unloading Compliance	J_{Ic} : 181 kJ/m^2	(11 Data)	
Coeff. C : 258 kJ/m^2	Exponent n : 0.30	Fit Coeff. R : 0.914	
DC Potential Method	J_{Ic} : 146 kJ/m^2	(11 Data)	
Coeff. C : 246 kJ/m^2	Exponent n : 0.42	Fit Coeff. R : 0.989	

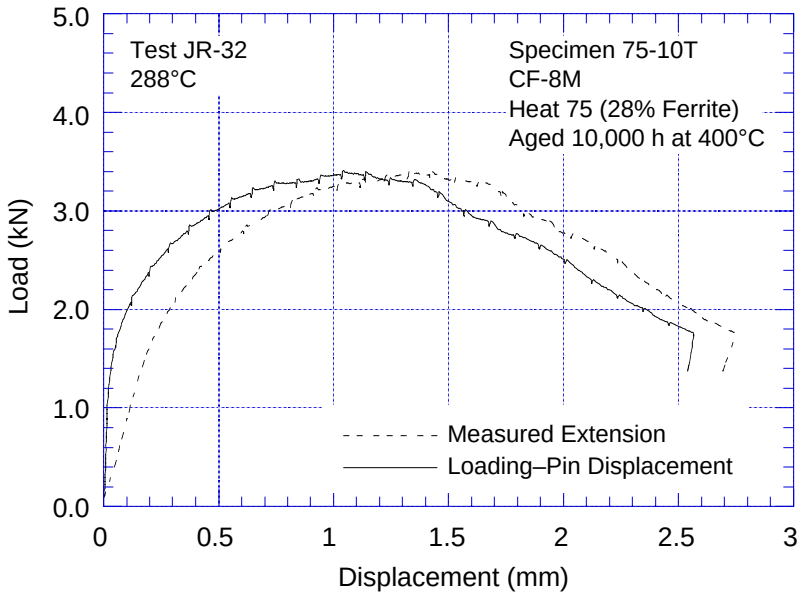

Figure A-5.1. Load-vs.-loadline displacement curve for specimen 75–10T of thermally aged CF–8M cast SS tested at 288°C

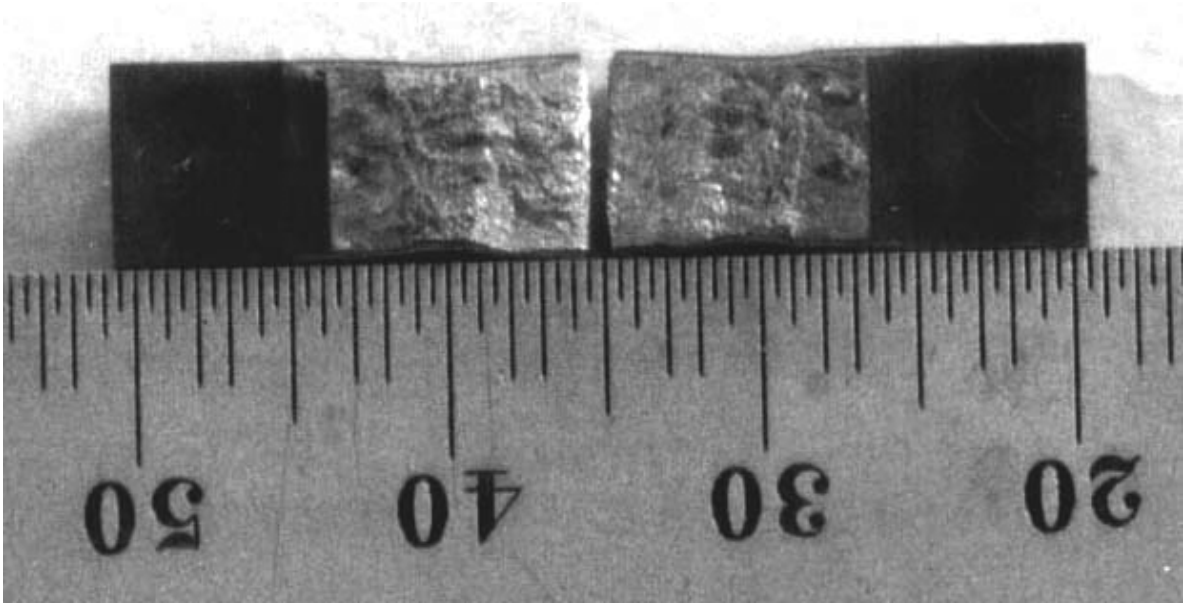

Figure A-5.2. Fracture surface of specimen 75–10T tested at 288°C

Table A-6. Test data for specimen 184–38 of 50% cold–worked Type 316NG SS tested at 288°C

Test Number	: JR–12	Test Temp.	: 288°C
Material Type	: 50% CW 316NG SS	Heat Number	: 18474
Aging Temp.	: –	Aging Time	: –
Irradiation Temp.	: –	Fluence	: –
Thickness	: 6.497 mm	Net Thickness	: 5.819 mm
Width	: 12.032 mm	Flow Stress	: 861.0 MPa
Modulus E	: 175 GPa		
Initial Crack	: 7.14 mm	Init. a/W	: 0.59 (Measured)
Final Crack	: 10.30 mm	Final a/W	: 0.86 (Measured)
Final Crack	: 9.64 mm	Final a/W	: 0.80 (Compliance)

	Load	Deflection	Unloading Compliance		DC Potential Method	
No.	(kN)	(mm)	J (kJ/m^2)	Δa (mm)	J (kJ/m^2)	Δa (mm)
0	0.0445	0.000				
1	1.2522	0.045	2.1	0.048	2.1	0.001
2	1.9296	0.093	7.8	0.055	7.9	0.002
3	2.5430	0.148	17.4	0.023	17.4	0.005
4	3.0577	0.208	30.1	0.184	30.2	0.009
5	3.4665	0.274	45.8	0.169	48.0	0.092
6	3.2041	0.389	72.5	0.522	79.8	0.589
7	2.9932	0.505	93.9	0.779	99.0	1.069
8	2.2784	0.658	115.2	1.169	118.1	1.733
9	1.8362	0.792	121.5	1.594	121.3	2.257
10	1.5115	0.919	136.3	1.903	126.9	2.728
11	1.2219	1.046	113.0	2.501	134.4	3.160

Power–Law Fit	$J = C(\Delta a)^n$		
Unloading Compliance	J_{Ic} : 51 kJ/m^2	(5 Data)	
Coeff. C : 102 kJ/m^2	Exponent n : 0.46	Fit Coeff. R : 0.989	
DC Potential Method	J_{Ic} : 61 kJ/m^2	(5 Data)	
Coeff. C : 97 kJ/m^2	Exponent n : 0.30	Fit Coeff. R : 0.995	

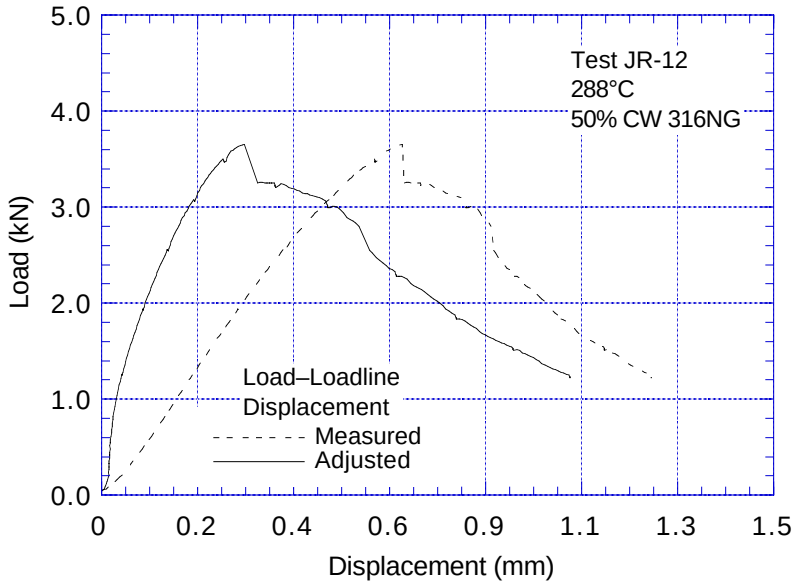

Figure A-6.1. Load-vs.-loadline displacement curve for specimen 184–38 of 50% cold–worked Type 316NG SS tested at 288°C

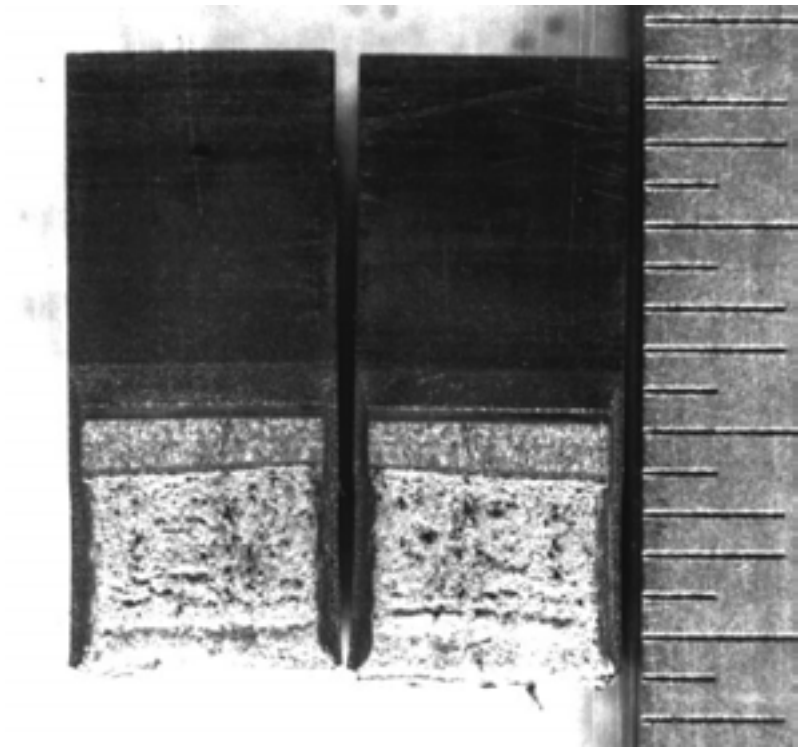

Figure A-6.2. Fracture surface of specimen 184–38 tested at 288°C

Table A-7. Test data for specimen 184–40 of 50% cold–worked Type 316NG SS tested at 288°C

Test Number	: JR–19	Test Temp.	: 288°C
Material Type	: 50% CW 316NG SS	Heat Number	: 18474
Aging Temp.	: –	Aging Time	: –
Irradiation Temp.	: –	Fluence	: –
Thickness	: 6.528 mm	Net Thickness	: 5.829 mm
Width	: 12.024 mm	Flow Stress	: 861.0 MPa
Modulus E	: 175 GPa		
Initial Crack	: 7.35 mm	Init. a/W	: 0.61 (Measured)
Final Crack	: 10.28 mm	Final a/W	: 0.86 (Measured)
Final Crack	: 10.01 mm	Final a/W	: 0.82 (Compliance)

	Load	Deflection	Unloading Compliance		DC Potential Method	
No.	(kN)	(mm)	J (kJ/m^2)	Δa (mm)	J (kJ/m^2)	Δa (mm)
0	0.0894	0.000				
1	1.2295	0.083	4.2	0.407	4.3	0.001
2	1.8900	0.126	13.1	0.177	10.0	0.004
3	2.5012	0.174	18.7	0.099	19.0	0.005
4	3.0493	0.230	32.2	0.135	31.9	0.009
5	3.4621	0.304	52.6	0.148	52.3	0.015
6	3.2699	0.419	79.9	0.481	86.3	0.373
7	2.6147	0.568	99.7	1.030	110.4	0.997
8	2.3976	0.634	103.4	1.228	105.4	1.229
9	1.9777	0.715	109.2	1.530	113.1	1.574
10	1.6716	0.788	114.2	1.699	112.9	1.850
11	1.5275	0.850	116.5	1.890	112.8	2.051
12	1.4056	0.910	116.5	2.098	115.3	2.261
13	1.2873	0.971	118.4	2.238	116.1	2.436
14	1.1210	1.037	118.8	2.420	118.1	2.642
15	1.0453	1.094	119.1	2.547	116.2	2.794
16	0.9715	1.152	120.2	2.666	117.6	2.939

Power–Law Fit	$J = C(\Delta a)^n$		
Unloading Compliance	J_{Ic} : 61 kJ/m^2	(8 Data)	
Coeff. C : 96 kJ/m^2	Exponent n : 0.30	Fit Coeff. R : 0.993	
DC Potential Method	J_{Ic} : 81 kJ/m^2	(8 Data)	
Coeff. C : 104 kJ/m^2	Exponent n : 0.17	Fit Coeff. R : 0.989	

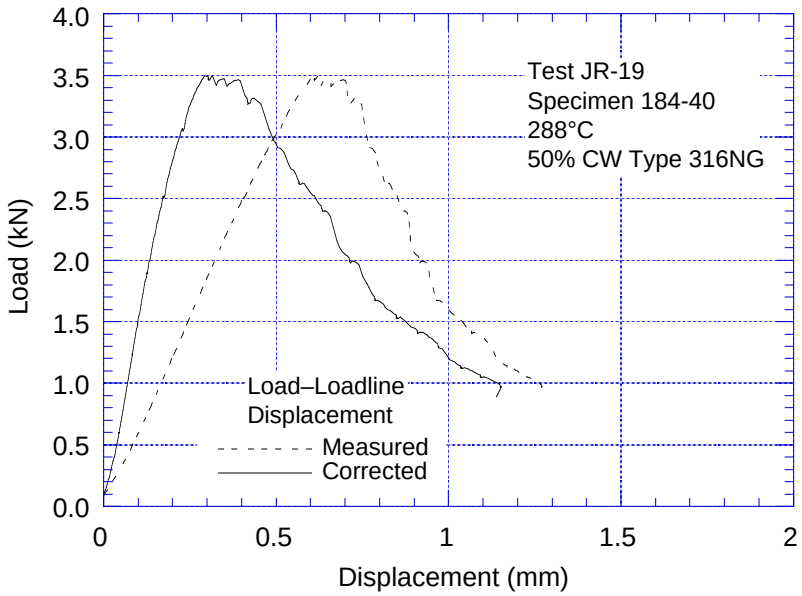

Figure A-7.1. Load-vs.-loadline displacement curve for specimen 184–40 of 50% cold–worked Type 316NG SS tested at 288°C

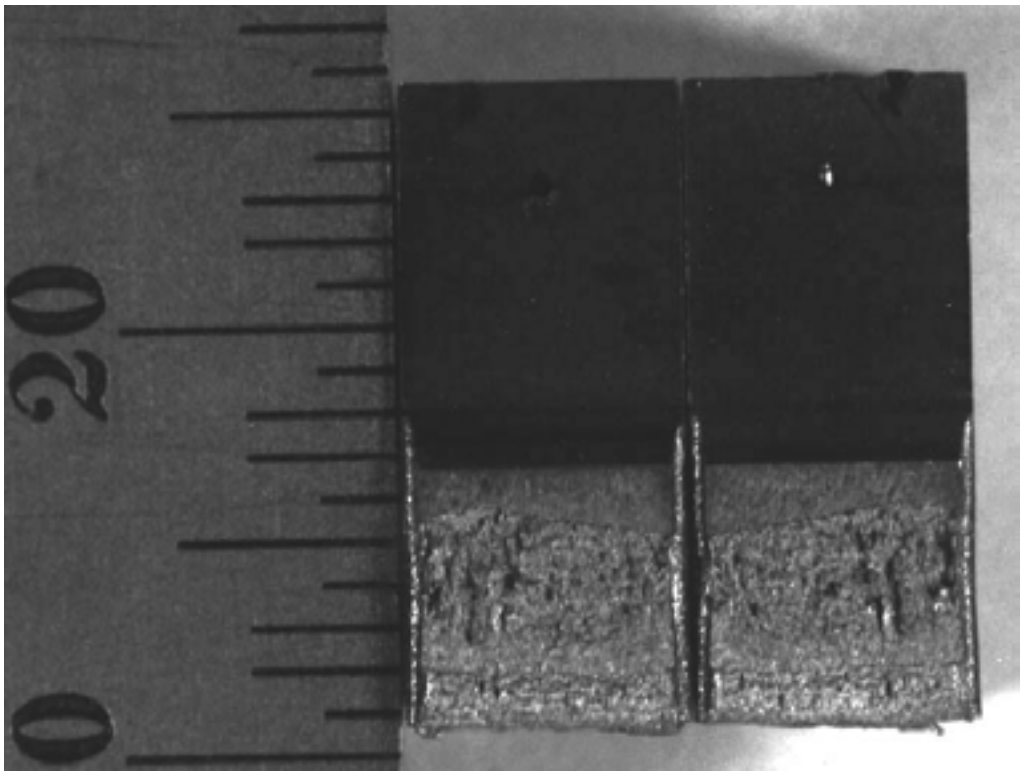

Figure A-7.2. Fracture surface of specimen 184–40 tested at 288°C

Table A-8. Test data for specimen C19–D of nonirradiated Type 304 SS tested at 288°C

Test Number	: JR–27	Test Temp.	: 288°C
Material Type	: Type 304 SS	Heat Number	: C19
Aging Temp.	: –	Aging Time	: –
Irradiation Temp.	: –	Fluence	: –
Thickness	: 6.480 mm	Net Thickness	: 5.890 mm
Width	: 12.000 mm	Flow Stress	: 339.5 MPa
Modulus E	: 175 GPa		
Initial Crack	: 7.28 mm	Init. a/W	: 0.61 (Measured)
Final Crack	: 7.63 mm	Final a/W	: 0.64 (Measured)
Final Crack	: 7.70 mm	Final a/W	: 0.64 (Compliance)

No.	Load (kN)	Deflection (mm)	Unloading Compliance		DC Potential Method	
			J (kJ/m^2)	Δa (mm)	J (kJ/m^2)	Δa (mm)
0	0.089	0.000				
1	1.214	0.247	21.8	-0.001	21.8	0.016
2	1.279	0.342	31.5	-0.027	31.2	0.023
3	1.346	0.435	40.3	0.056	40.9	0.030
4	1.407	0.582	56.5	0.070	57.0	0.042
5	1.515	0.774	80.0	0.033	79.3	0.059
6	1.607	0.969	102.8	0.087	103.2	0.076
7	1.674	1.166	125.6	0.181	128.6	0.092
8	1.790	1.562	183.4	0.172	182.4	0.135
9	1.852	1.761	210.0	0.232	210.9	0.155
10	1.931	1.956	247.1	0.134	239.4	0.182
11	2.025	2.355	300.5	0.254	301.1	0.221
12	2.153	2.852	392.9	0.152	381.1	0.289
13	2.221	3.150	433.5	0.253	432.1	0.319
14	2.294	3.449	464.5	0.434	485.7	0.342
15	2.439	4.045	587.5	0.418	590.0	0.433
16	2.536	4.524			673.8	0.519
17	2.617	5.046			765.5	0.625
18	2.670	5.550			834.9	0.811

Power–Law Fit	$J = C(\Delta a)^n$		
Unloading Compliance	J_{Ic} : 695 kJ/m^2	(9 Data)	
Coeff. C : 765 kJ/m^2	Exponent n : 0.28	Fit Coeff. R : 0.338	
DC Potential Method	(information could not be determined)		

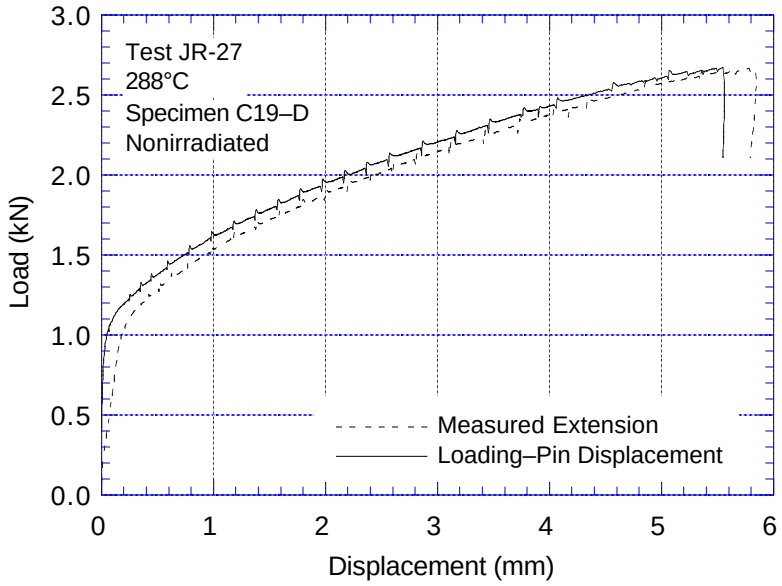

Figure A-8.1. Load-vs.-loadline displacement curve for specimen C19–D of nonirradiated Type 304 SS tested at 288°C

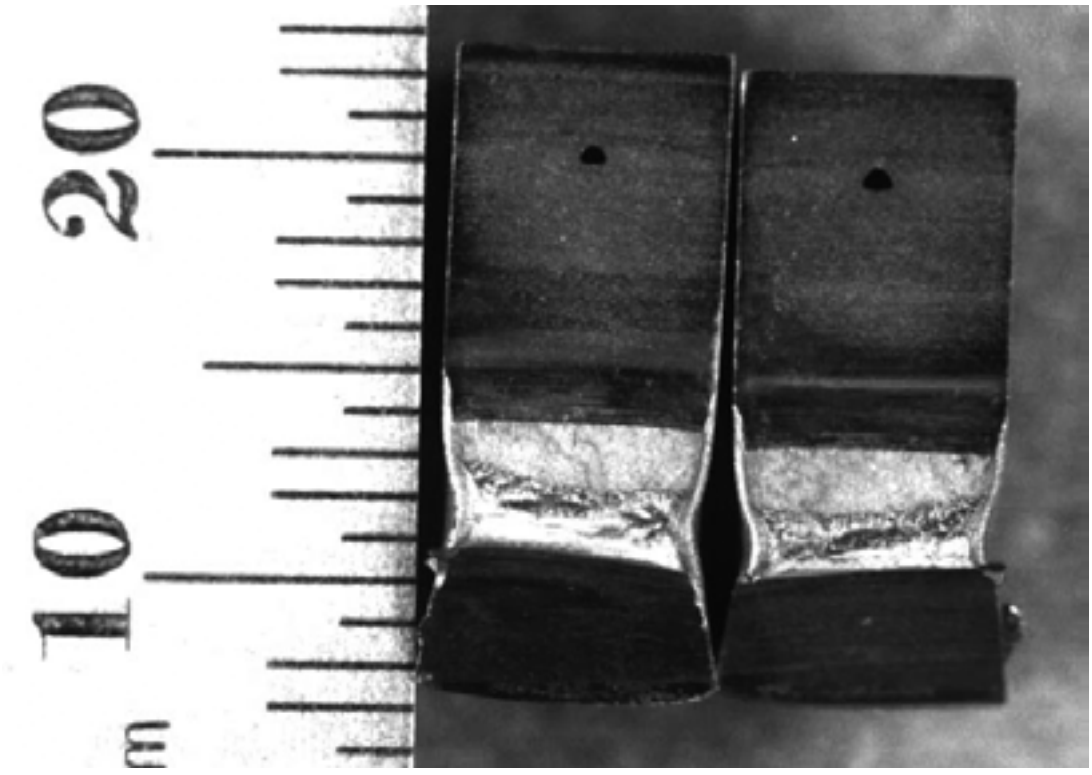

Figure A-8.2. Fracture surface of specimen C19–D tested at 288°C

Table A-9. Test data for specimen C16–C of nonirradiated Type 316 SS tested at 288°C

Test Number	: JR–31	Test Temp.	: 288°C
Material Type	: Type 316 SS	Heat Number	: C16
Aging Temp.	: –	Aging Time	: –
Irradiation Temp.	: –	Fluence	: –
Thickness	: 6.500 mm	Net Thickness	: 5.810 mm
Width	: 11.990 mm	Flow Stress	: 336.0 MPa (estimated)
Modulus E	: 175 GPa		
Initial Crack	: 7.30 mm	Init. a/W	: 0.61 (Measured)
Final Crack	: 7.96 mm	Final a/W	: 0.66 (Measured)
Final Crack	: 7.65 mm	Final a/W	: 0.64 (Compliance)

No.	Load (kN)	Deflection (mm)	Unloading Compliance		DC Potential Method	
			J (kJ/m^2)	Δa (mm)	J (kJ/m^2)	Δa (mm)
0	0.065	0.000			0.0	0.000
1	1.207	0.208	18.9	-0.002	19.0	0.014
2	1.293	0.412	40.2	-0.064	39.5	0.030
3	1.370	0.618	60.7	0.023	61.5	0.045
4	1.426	0.826	82.5	0.103	84.7	0.061
5	1.492	1.023	108.6	0.041	107.8	0.081
6	1.555	1.220	129.2	0.146	132.0	0.096
7	1.620	1.417	152.1	0.219	157.0	0.113
8	1.674	1.615	178.7	0.236	182.9	0.133
9	1.784	2.012	251.4	0.077	236.3	0.187
10	1.831	2.211	278.6	0.095	264.8	0.207
11	1.877	2.410	310.1	0.082	293.7	0.231
12	1.925	2.609	338.6	0.112	323.6	0.252
13	1.977	2.808	373.7	0.081	353.6	0.278
14	2.023	3.007	413.8	0.015	384.0	0.308
15	2.060	3.207	439.0	0.083	416.3	0.327
16	2.100	3.407	469.7	0.108	448.6	0.349
17	2.140	3.607	503.6	0.114	481.1	0.375
18	2.180	3.807	520.0	0.243	515.9	0.387
19	2.219	4.007	555.5	0.249	549.1	0.413
20	2.259	4.207	601.8	0.197	581.4	0.448
21	2.298	4.406	632.6	0.239	616.3	0.471
22	2.330	4.607	646.5	0.371	654.1	0.481
23	2.359	4.808	689.0	0.356	688.2	0.513

Power–Law Fit $J = C(\Delta a)^n$

(information could not be determined)

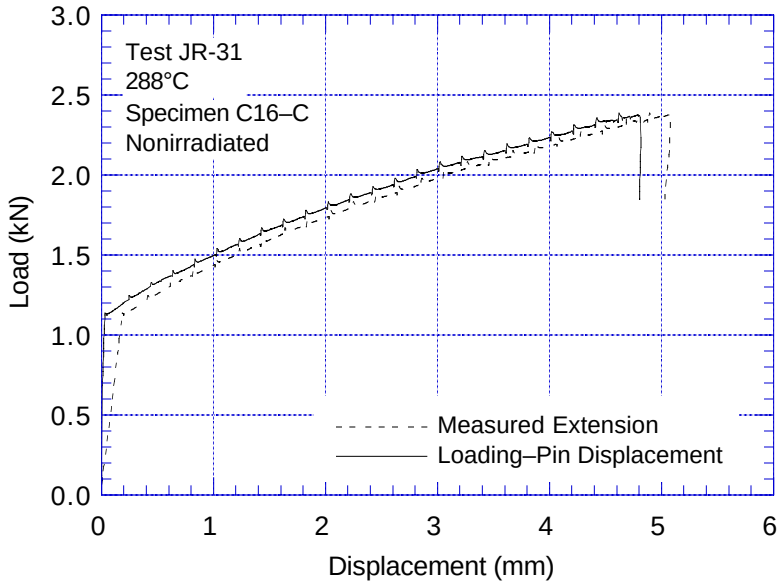

Figure A-9.1. Load-vs.-loadline displacement curve for specimen C16–C of nonirradiated Type 316 SS tested at 288°C

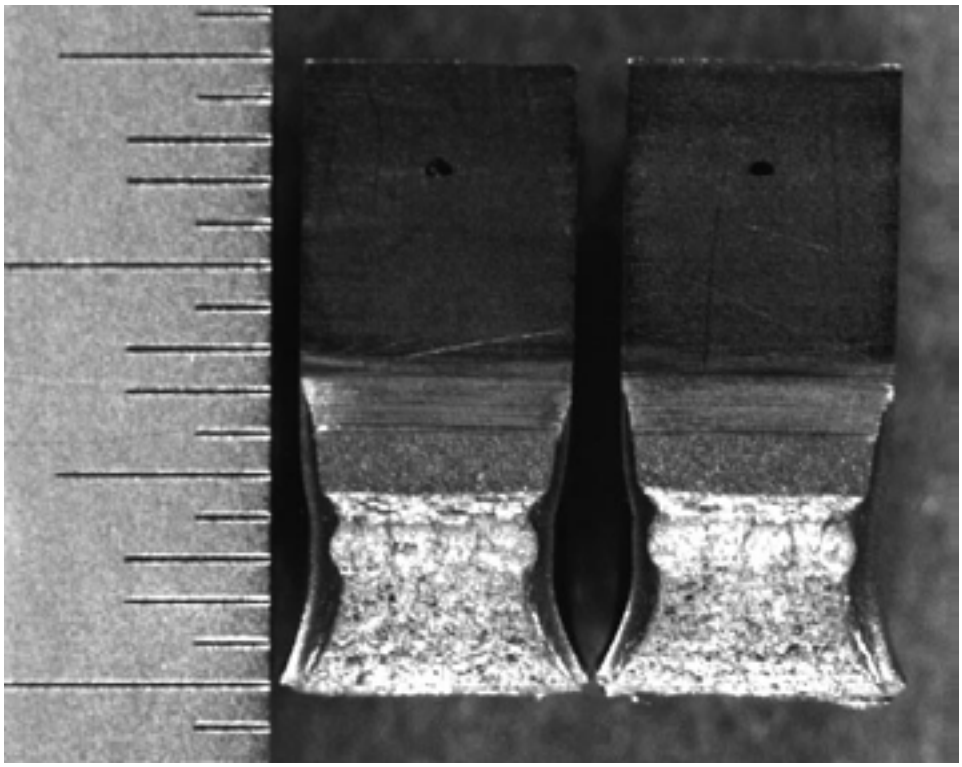

Figure A-9.2. Fracture surface of specimen C16–C tested at 288°C

Table A-10. Test data for specimen C16–D of nonirradiated Type 316 SS tested at 288°C

Test Number	: JR–28	Test Temp.	: 288°C
Material Type	: Type 316 SS	Heat Number	: C16
Aging Temp.	: –	Aging Time	: –
Irradiation Temp.	: –	Fluence	: –
Thickness	: 6.470 mm	Net Thickness	: 5.90 mm
Width	: 11.980 mm	Flow Stress	: 336.0 MPa (estimated)
Modulus E	: 175 GPa		
Initial Crack	: 7.41 mm	Init. a/W	: 0.62 (Measured)
Final Crack	: 7.83 mm	Final a/W	: 0.65 (Measured)
Final Crack	: 7.60 mm	Final a/W	: 0.63 (Compliance)

No.	Load (kN)	Deflection (mm)	Unloading Compliance		DC Potential Method	
			J (kJ/m^2)	Δa (mm)	J (kJ/m^2)	Δa (mm)
0	0.088	0.000			0.0	0.000
1	1.218	0.247	22.5	0.059	23.0	0.017
2	1.304	0.441	43.5	0.007	42.9	0.032
3	1.373	0.637	63.8	0.072	64.1	0.047
4	1.439	0.834	85.4	0.129	86.5	0.064
5	1.501	1.031	109.2	0.140	109.9	0.081
6	1.567	1.228	138.6	0.026	134.1	0.103
7	1.621	1.426	170.1	-0.096	159.3	0.127
8	1.672	1.625	192.1	-0.014	185.7	0.143
9	1.725	1.823	204.8	0.230	213.3	0.152
10	1.772	2.023	230.1	0.287	241.3	0.171
11	1.818	2.222	260.1	0.295	269.7	0.194
12	1.865	2.421	310.7	0.068	297.6	0.231
13	1.908	2.621	332.8	0.169	327.7	0.248
14	1.949	2.820	368.4	0.134	357.8	0.274
15	1.982	3.020	400.4	0.141	388.8	0.298
16	2.019	3.221	428.9	0.182	420.6	0.319
17	2.055	3.420	467.3	0.148	452.3	0.348
18	2.088	3.621	495.4	0.195	484.8	0.369

Power–Law Fit $J = C(\Delta a)^n$
(information could not be determined)

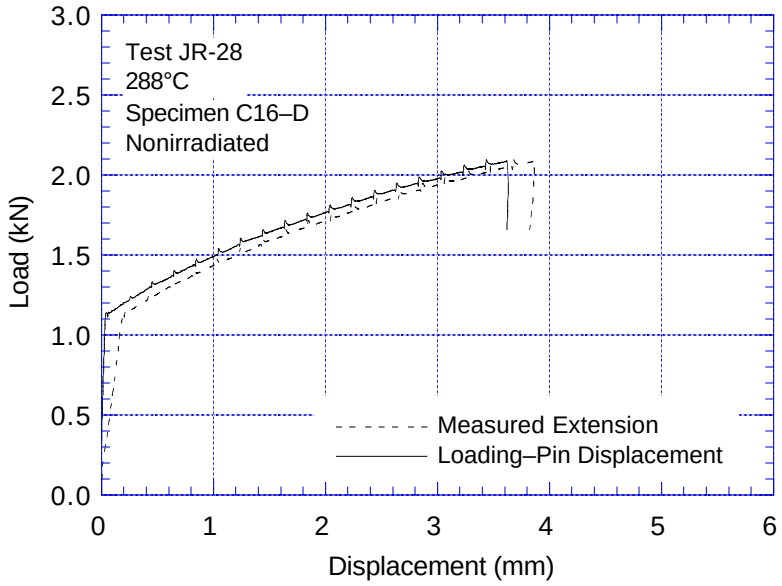

Figure A-10.1. Load-vs.-loadline displacement curve for specimen C16–D of nonirradiated Type 316 SS tested at 288°C

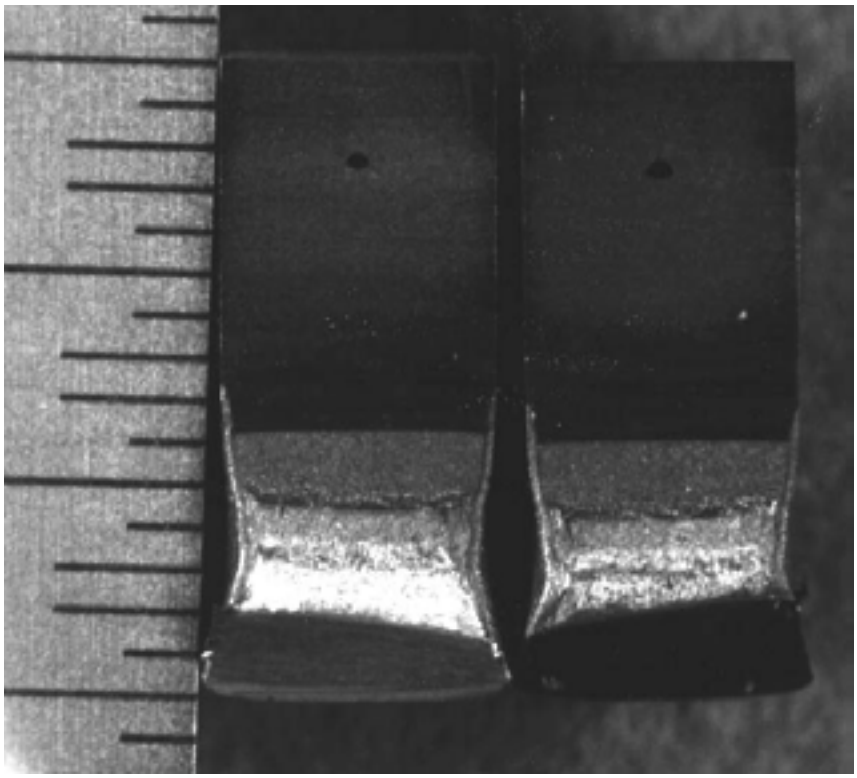

Figure A-10.2. Fracture surface of specimen C16–D tested at 288°C

Table A-11. Test data for specimen L20–D of nonirradiated Type 304 SS tested at 288°C

Test Number	: JR–29	Test Temp.	: 288°C
Material Type	: Type 304L SS (HP)	Heat Number	: L20
Aging Temp.	: –	Aging Time	: –
Irradiation Temp.	: –	Fluence	: –
Thickness	: 6.50 mm	Net Thickness	: 5.89 mm
Width	: 12.00 mm	Flow Stress	: 307.0 MPa (estimated)
Modulus E	: 175 GPa		
Initial Crack	: 7.22 mm	Init. a/W	: 0.60 (Measured)
Final Crack	: 9.52 mm	Final a/W	: 0.79 (Measured)
Final Crack	: 8.84 mm	Final a/W	: 0.74 (Compliance)

	Load	Deflection	Unloading Compliance		DC Potential Method	
No.	(kN)	(mm)	J (kJ/m^2)	Δa (mm)	J (kJ/m^2)	Δa (mm)
0	0.0000	0.000				
1	1.2384	0.028	3.3	-0.704	3.4	0.003
2	1.4995	0.103	8.4	-0.481	11.4	0.007
3	1.6414	0.190	17.4	-0.170	22.1	0.014
4	1.7179	0.285	28.9	0.082	33.0	0.024
5	1.8211	0.581	78.1	0.072	74.0	0.143
6	1.8264	0.682	88.5	0.184	86.6	0.232
7	1.8069	0.786	102.8	0.204	98.4	0.366
8	1.7975	0.888	117.5	0.209	110.0	0.473
9	1.7949	0.991	125.9	0.397	121.8	0.576
10	1.7917	1.092	138.0	0.460	134.0	0.659
11	1.7704	1.196	153.0	0.473	146.4	0.748
12	1.7468	1.300	169.2	0.460	158.1	0.843
13	1.7148	1.405	175.8	0.635	169.6	0.940
14	1.6761	1.510	192.7	0.600	180.3	1.044
15	1.6365	1.615	203.1	0.686	190.0	1.153
16	1.5991	1.720	212.3	0.774	199.3	1.263
17	1.5627	1.825	224.8	0.808	208.5	1.363
18	1.5440	1.929	225.6	0.999	217.8	1.455
19	1.5088	2.033	240.6	0.990	227.2	1.544
20	1.4684	2.139	243.0	1.150	235.9	1.641
21	1.4354	2.244	253.0	1.200	243.8	1.737
22	1.4021	2.349	266.8	1.211	252.5	1.815
23	1.3652	2.454	272.8	1.306	260.8	1.902
24	1.3260	2.559	283.3	1.344	267.3	2.000
25	1.2886	2.665	293.3	1.386	272.9	2.098
26	1.2517	2.770	289.9	1.550	278.1	2.194
27	1.2104	2.876	294.9	1.626	281.8	2.302

Power–Law Fit	$J = C(\Delta a)^n$		
Unloading Compliance	J_{Ic} : 119 kJ/m^2	(19 Data)	
Coeff. C : 236 kJ/m^2	Exponent n : 0.56	Fit Coeff. R : 0.948	
DC Potential Method	J_{Ic} : 78 kJ/m^2	(21 Data)	
Coeff. C : 174 kJ/m^2	Exponent n : 0.60	Fit Coeff. R : 0.998	

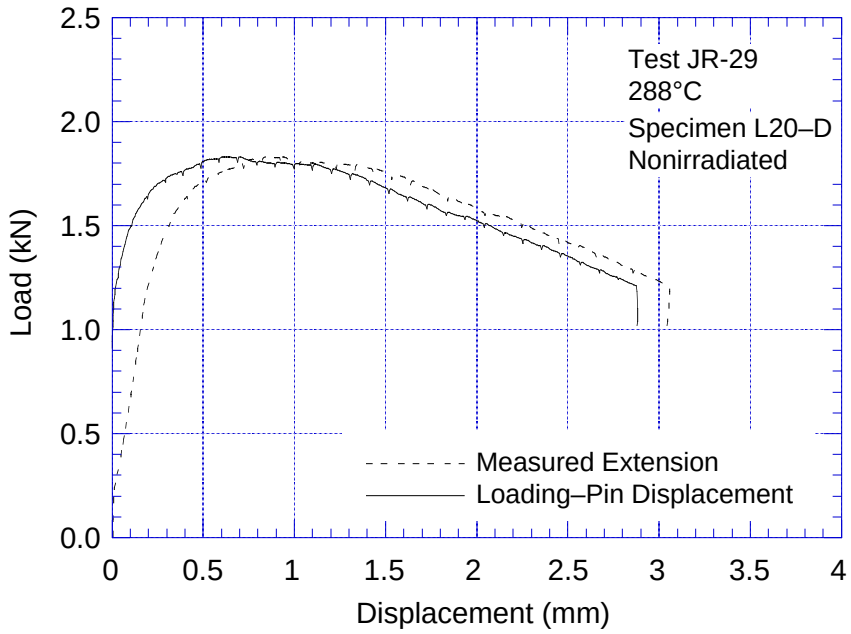

Figure A-11.1. Load-vs.-loadline displacement curve for specimen L20–D of nonirradiated Type 304 SS tested at 288°C

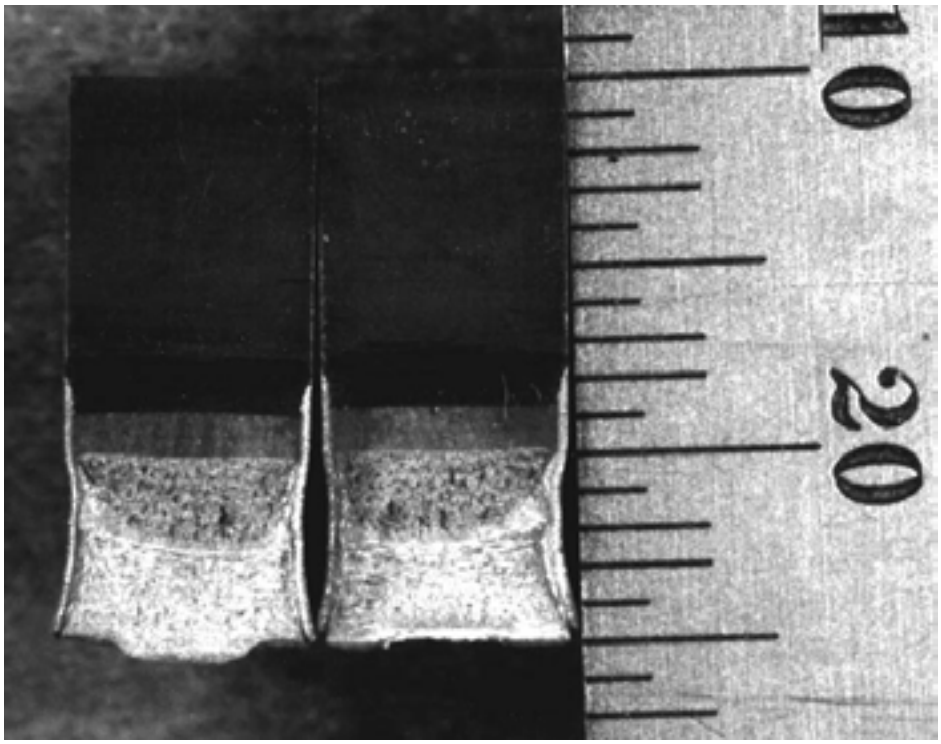

Figure A-11.2. Fracture surface of specimen L20–D tested at 288°C

Table A-12. Test data for specimen L2–C of nonirradiated Type 304 SS tested at 288°C

Test Number	: JR–20	Test Temp.	: 288°C
Material Type	: Type 304 SS	Heat Number	: L2
Aging Temp.	: –	Aging Time	: –
Irradiation Temp.	: –	Fluence	: –
Thickness	: 6.51 mm	Net Thickness	: 5.84 mm
Width	: 11.98 mm	Flow Stress	: 270.5 MPa
Modulus E	: 175 GPa		
Initial Crack	: 7.38 mm	Init. a/W	: 0.61 (Measured)
Final Crack	: 9.17 mm	Final a/W	: 0.76 (Measured)
Final Crack	: 8.08 mm	Final a/W	: 0.75 (Compliance)

	Load	Deflection	Unloading Compliance		DC Potential Method	
No.	(kN)	(mm)	J (kJ/m^2)	Δa (mm)	J (kJ/m^2)	Δa (mm)
0	0.089	0.000				
1	1.300	0.080	6.5	0.237	6.5	0.006
2	1.453	0.169	18.9	0.152	17.1	0.016
3	1.529	0.265	30.2	0.155	29.3	0.028
4	1.596	0.361	43.7	0.126	41.9	0.040
5	1.648	0.459	58.7	0.041	55.2	0.054
6	1.685	0.556	72.5	0.015	68.9	0.067
7	1.717	0.656	87.4	0.027	83.2	0.080
8	1.741	0.756	101.7	0.040	97.7	0.093
9	1.754	0.857	117.1	0.027	112.4	0.107
10	1.769	0.958	130.1	0.082	127.1	0.119
11	1.774	1.059	144.7	0.101	142.1	0.132
12	1.780	1.160	159.9	0.104	157.0	0.146
13	1.775	1.275	176.7	0.120	171.1	0.234
14	1.759	1.379	191.6	0.136	181.6	0.339
15	1.734	1.482	203.5	0.200	192.3	0.432
16	1.708	1.586	214.2	0.277	201.9	0.542
17	1.692	1.688	227.3	0.310	211.0	0.651
18	1.666	1.793	238.6	0.372	220.9	0.747
19	1.619	1.898	243.2	0.518	230.0	0.850
20	1.580	2.001	252.5	0.593	237.2	0.973
21	1.544	2.105	260.8	0.676	244.9	1.075
22	1.504	2.209	265.5	0.798	253.0	1.173
23	1.461	2.315	275.3	0.859	259.4	1.289
24	1.411	2.470	283.6	1.006	270.8	1.429
25	1.353	2.627	292.9	1.132	280.0	1.577
26	1.280	2.785	299.8	1.271	286.5	1.741
27	1.219	2.942	304.8	1.417	292.3	1.893

Power–Law Fit	$J = C(\Delta a)^n$		
Unloading Compliance	J_{Ic}	: 237 kJ/m^2	(13 Data)
Coeff. C : 283 kJ/m^2	Exponent n	: 0.20	Fit Coeff. R : 0.988
DC Potential Method	J_{Ic}	: 186 kJ/m^2	(15 Data)
Coeff. C : 243 kJ/m^2	Exponent n	: 0.27	Fit Coeff. R : 0.996

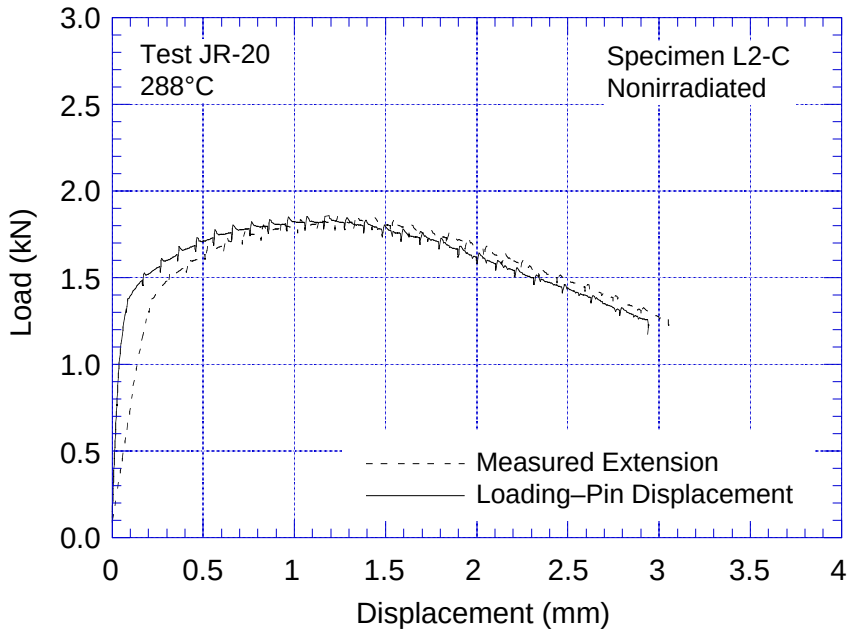

Figure A-12.1. Load-vs.-loadline displacement curve for specimen L2–C of nonirradiated Type 304 SS tested at 288°C

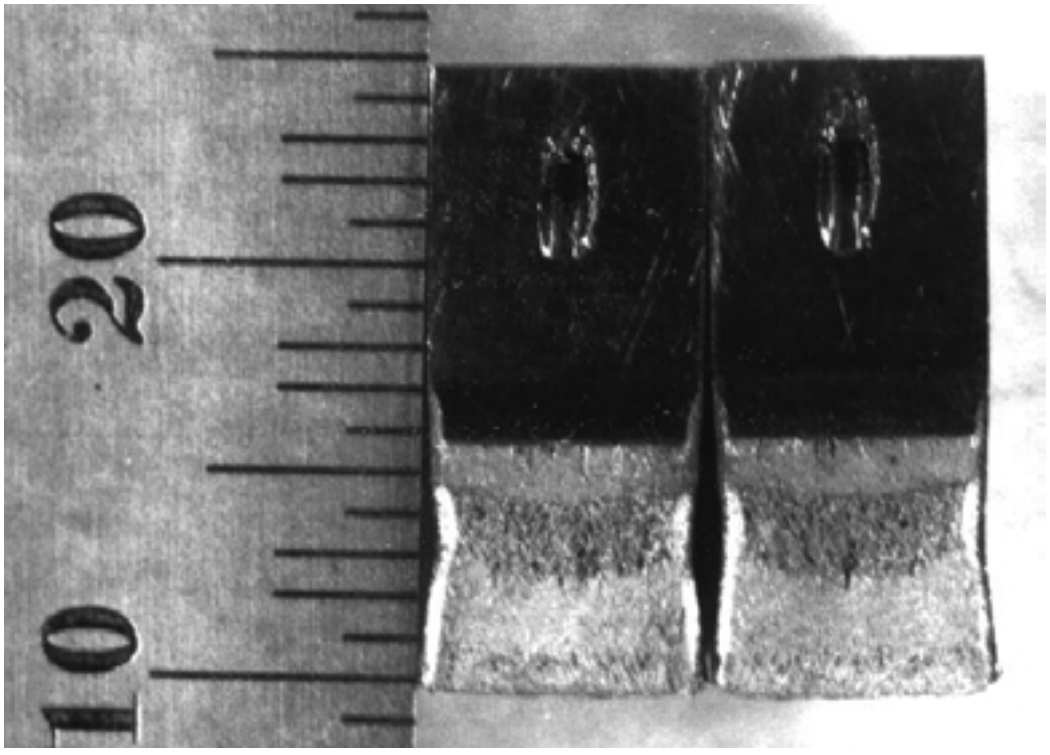

Figure A-12.2. Fracture surface of specimen L2–C tested at 288°C

Table A-13. Test data for specimen L2–E of nonirradiated Type 304 SS tested at 288°C

Test Number	: JR–30	Test Temp.	: 288°C
Material Type	: Type 304 SS	Heat Number	: L2
Aging Temp.	: –	Aging Time	: –
Irradiation Temp.	: –	Fluence	: –
Thickness	: 6.49 mm	Net Thickness	: 5.87 mm
Width	: 12.03 mm	Flow Stress	: 270.5 MPa
Modulus E	: 175 GPa		
Initial Crack	: 7.38 mm	Init. a/W	: 0.61 (Measured)
Final Crack	: 9.17 mm	Final a/W	: 0.76 (Measured)
Final Crack	: 8.08 mm	Final a/W	: 0.75 (Compliance)

	Load	Deflection	Unloading Compliance		DC Potential Method	
No.	(kN)	(mm)	J (kJ/m^2)	Δa (mm)	J (kJ/m^2)	Δa (mm)
0	0.0885	0.000				
1	1.1441	0.052	4.2	0.027	4.2	0.004
2	1.2273	0.144	13.0	0.049	13.1	0.012
3	1.3033	0.238	23.0	-0.020	22.6	0.021
4	1.3669	0.334	32.8	0.057	32.9	0.030
5	1.4225	0.430	44.4	-0.014	43.7	0.041
6	1.4741	0.527	55.9	-0.022	55.0	0.052
7	1.5226	0.624	65.5	0.102	66.7	0.061
8	1.5627	0.722	78.0	0.088	78.8	0.072
9	1.6022	0.820	88.5	0.185	91.2	0.082
10	1.6347	0.918	99.6	0.261	102.2	0.173
11	1.6534	1.019	116.8	0.150	114.1	0.218
12	1.6743	1.118	123.1	0.371	126.3	0.266
13	1.6908	1.219	142.0	0.244	138.8	0.312
14	1.7019	1.320	147.3	0.468	151.2	0.362
15	1.7095	1.421	159.3	0.523	163.8	0.411
16	1.7166	1.522	175.1	0.512	176.2	0.463
17	1.7192	1.630	185.8	0.619	189.7	0.512
18	1.7143	1.732	203.4	0.584	201.9	0.568
19	1.6899	1.835	211.2	0.715	213.6	0.633
20	1.6690	1.938	228.6	0.688	224.1	0.709
21	1.6561	2.041	255.8	0.535	235.1	0.771
22	1.6458	2.143	242.8	0.899	246.1	0.835
23	1.6276	2.246	263.8	0.819	256.8	0.899
24	1.6009	2.350	277.7	0.848	266.7	0.971
25	1.5867	2.453	284.1	0.949	276.6	1.037
26	1.5529	2.557	307.0	0.874	285.8	1.113
27	1.5280	2.661	305.2	1.049	294.6	1.185
28	1.4928	2.765	318.5	1.064	302.9	1.261
29	1.4599	2.870	314.4	1.244	310.9	1.335
30	1.4265	2.975	322.2	1.307	316.6	1.412
31	1.3963	3.080	335.2	1.329	325.3	1.489
32	1.3705	3.184	341.3	1.406	332.3	1.559
33	1.3300	3.289	334.7	1.579	339.7	1.627
34	1.2771	3.396	340.4	1.649	345.0	1.710
35	1.2371	3.501	348.0	1.706	349.1	1.792

Power–Law Fit	$J = C(\Delta a)^n$			
Unloading Compliance	J_{Ic}	: 154 kJ/m^2	(25 Data)	
Coeff. C : 275 kJ/m^2	Exponent n	: 0.54	Fit Coeff. R	: 0.866
DC Potential Method	J_{Ic}	: 159 kJ/m^2	(19 Data)	
Coeff. C : 268 kJ/m^2	Exponent n	: 0.49	Fit Coeff. R	: 0.997

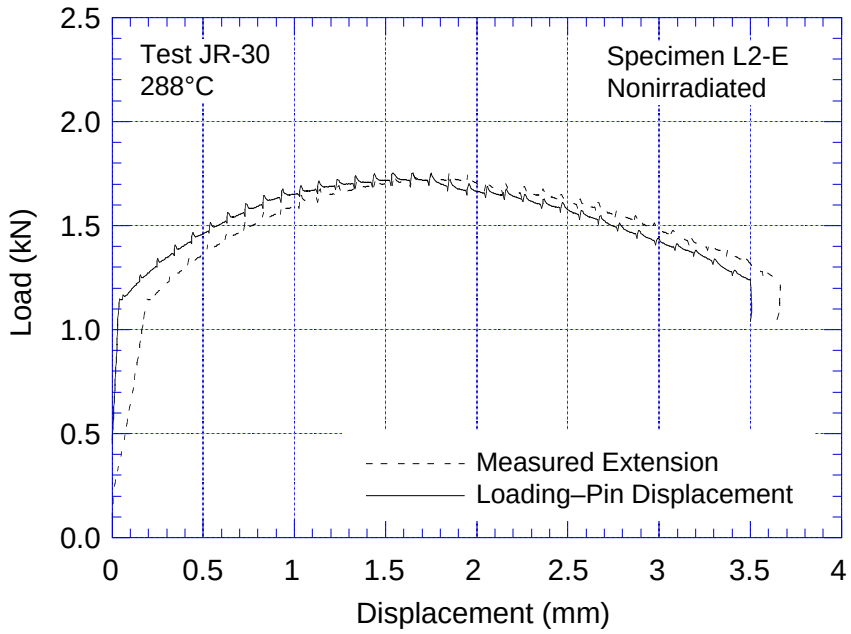

Figure A-13.1. Load-vs.-loadline displacement curve for specimen L2–E of nonirradiated Type 304 SS tested at 288°C

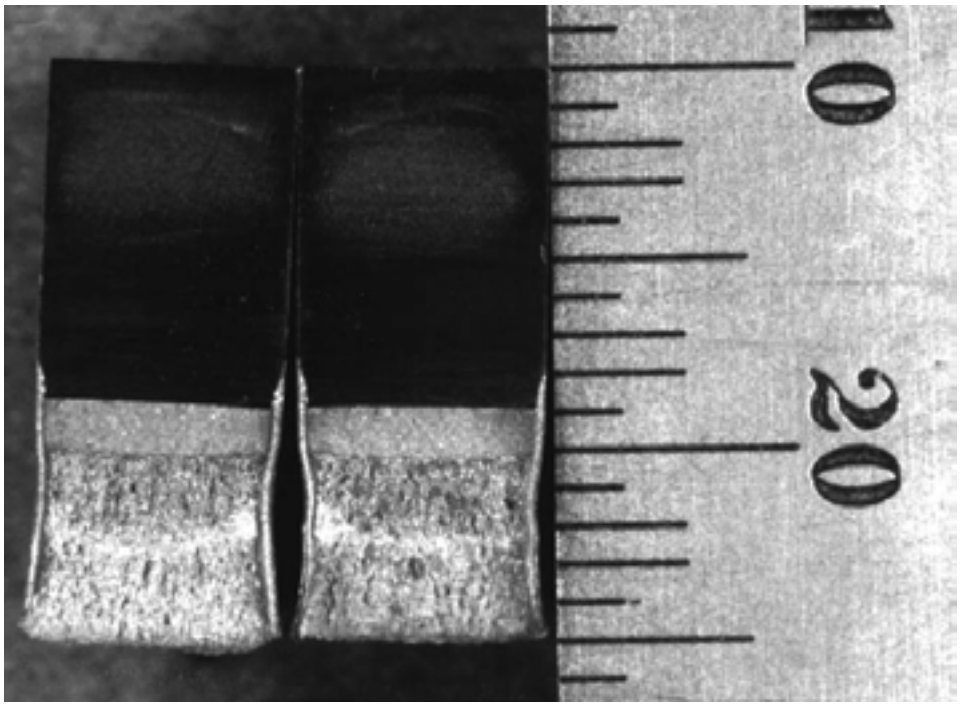

Figure A-13.2. Fracture surface of specimen L2–E tested at 288°C

Table A-14. Test data for specimen C19–A of irradiated Type 304 SS tested at 288°C

Test Number	: JRI–21	Test Temp.	: 288°C
Material Type	: Type 304 SS	Heat Number	: C19
Aging Temp.	: –	Aging Time	: –
Irradiation Temp.	: 288°C	Fluence	: 0.3×10^{21} n/cm^2
Thickness	: 6.50 mm	Net Thickness	: 5.85 mm
Width	: 12.00 mm	Flow Stress	: 618.0 MPa
Modulus E	: 175 GPa	Effective Flow Stress	: 478.8 MPa
Initial Crack	: 7.45 mm	Init. a/W	: 0.62 (Measured)
Final Crack	: 8.84 mm	Final a/W	: 0.74 (Measured)
Final Crack	: 8.32 mm	Final a/W	: 0.69 (Compliance)

No.	Load (kN)	Deflection (mm)	Unloading Compliance		DC Potential Method	
			J (kJ/m^2)	Δa (mm)	J (kJ/m^2)	Δa (mm)
0	0.088	0.000				
1	2.618	1.094	204.8	0.000	204.3	0.107
2	2.637	1.194	226.8	0.000	226.0	0.118
3	2.658	1.295	249.3	0.000	248.1	0.130
4	2.673	1.395	271.4	0.000	270.1	0.140
5	2.687	1.497	294.4	0.000	292.7	0.153
6	2.702	1.597	316.8	0.000	314.9	0.164
7	2.701	1.699	339.5	0.000	337.1	0.179
8	2.706	1.802	356.2	0.068	360.2	0.188
9	2.705	1.902	372.4	0.132	382.8	0.196
10	2.708	2.004	405.3	0.044	405.0	0.213
11	2.705	2.104	427.5	0.050	430.1	0.227
12	2.698	2.207	438.3	0.152	453.5	0.232
13	2.680	2.310	461.9	0.149	475.0	0.251
14	2.666	2.414	486.0	0.147	487.4	0.336
15	2.645	2.516	507.6	0.158	499.7	0.415
16	2.613	2.619	522.2	0.215	510.7	0.502
17	2.589	2.723	545.4	0.215	521.8	0.587
18	2.562	2.827	566.4	0.227	531.2	0.681
19	2.526	2.931	585.2	0.252	544.1	0.748
20	2.460	3.037	570.7	0.467	555.4	0.829
21	2.425	3.143	580.0	0.541	565.2	0.913
22	2.395	3.246	587.8	0.623	575.7	0.987
23	2.354	3.351	608.1	0.639	586.4	1.062
24	2.332	3.454	637.1	0.607	595.9	1.138
25	2.267	3.561	633.3	0.741	604.7	1.220
26	2.218	3.666	652.0	0.757	611.3	1.307
27	2.166	3.771	649.6	0.874	617.3	1.393

Power–Law Fit	$J = C(\Delta a)^n$		
Unloading Compliance	J_{Ic} : 599 kJ/m^2	(15 Data)	
Coeff. C : 661 kJ/m^2	Exponent n : 0..15	Fit Coeff. R : 0.834	
DC Potential Method	J_{Ic} : 507 kJ/m^2	(17 Data)	
Coeff. C : 579 kJ/m^2	Exponent n : 0.17	Fit Coeff. R : 0.975	

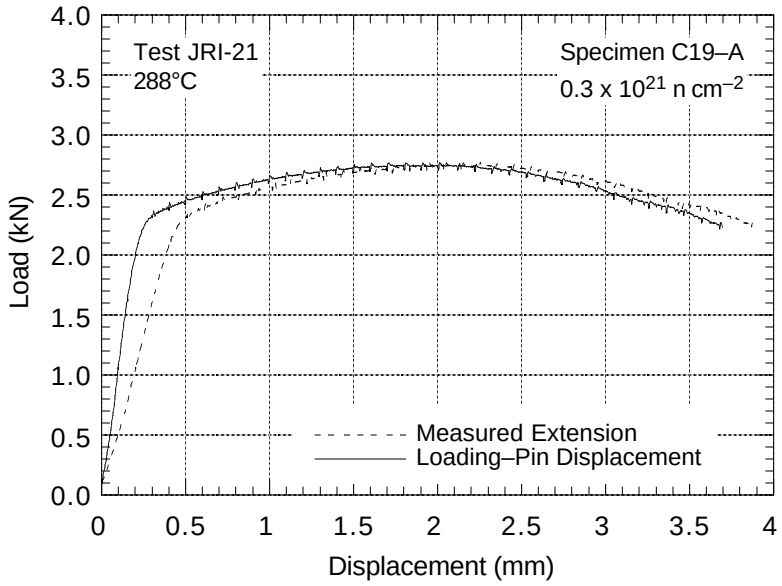

Figure A-14.1 Load-vs.-loadline displacement curve for specimen C19–A of irradiated Type 304 SS tested at 288°C

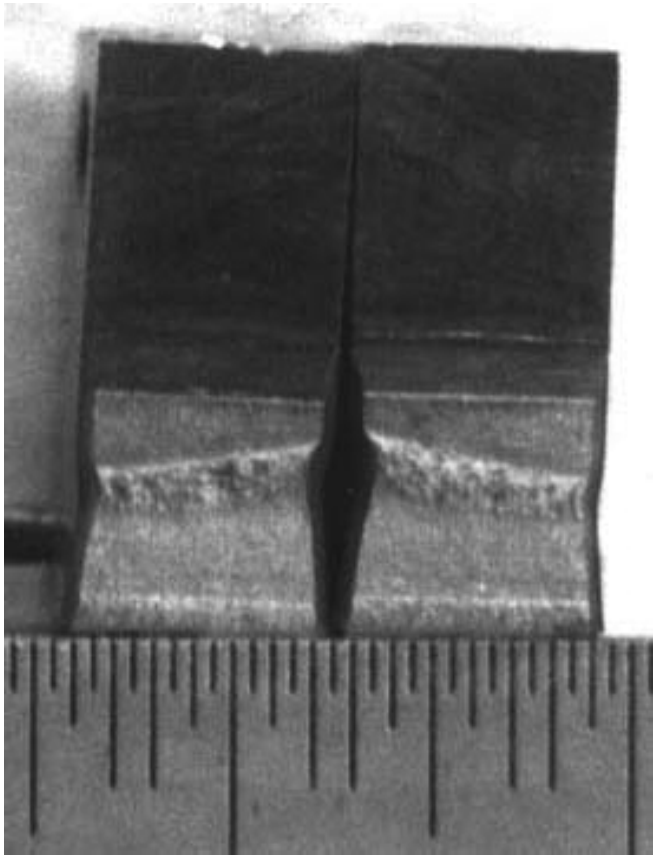

Figure A-14.2 Fracture surface of specimen C19–A tested at 288°C

Table A-15. Test data for specimen C19–B of irradiated Type 304 SS tested at 288°C

Test Number	: JRI–23	Test Temp.	: 288°C
Material Type	: Type 304 SS	Heat Number	: C19
Aging Temp.	: –	Aging Time	: –
Irradiation Temp.	: 288°C	Fluence	: 0.9×10^{21} n/cm^2
Thickness	: 6.50 mm	Net Thickness	: 5.85 mm
Width	: 12.00 mm	Flow Stress	: 759.5 MPa
Modulus E	: 175 GPa	Effective Flow Stress	: 549.5 MPa
Initial Crack	: 7.36 mm	Init. a/W	: 0.61 (Measured)
Final Crack	: 9.40 mm	Final a/W	: 0.78 (Measured)
Final Crack	: 9.01 mm	Final a/W	: 0.75 (Compliance)

	Load	Deflection	Unloading Compliance		DC Potential Method	
No.	(kN)	(mm)	J (kJ/m^2)	Δa (mm)	J (kJ/m^2)	Δa (mm)
0	0.088	0.000				
1	1.971	0.125	9.7	-0.014	9.8	0.004
2	2.630	0.176	19.2	-0.376	19.1	0.007
3	3.185	0.236	26.7	-0.041	33.1	0.010
4	3.544	0.311	52.4	0.055	53.7	0.020
5	3.643	0.404	78.0	0.081	80.5	0.030
6	3.636	0.519	110.5	0.159	114.3	0.043
7	3.589	0.624	142.0	0.119	144.7	0.055
8	3.527	0.729	172.2	0.155	174.6	0.067
9	3.469	0.836	205.8	0.095	204.6	0.080
10	3.426	0.941	233.9	0.143	233.5	0.091
11	3.341	1.047	259.4	0.199	262.3	0.101
12	3.266	1.153	281.3	0.294	285.4	0.210
13	3.195	1.259	309.3	0.296	304.8	0.309
14	3.124	1.366	335.0	0.334	324.7	0.397
15	3.058	1.472	357.7	0.390	344.5	0.479
16	2.959	1.581	384.2	0.405	363.8	0.566
17	2.880	1.689	404.9	0.467	381.4	0.657
18	2.793	1.796	416.2	0.590	397.9	0.746
19	2.709	1.903	440.3	0.599	413.7	0.832
20	2.647	2.009	461.1	0.640	428.7	0.918
21	2.539	2.169	486.0	0.730	452.1	1.040
22	2.431	2.329	508.4	0.819	471.2	1.169
23	2.284	2.491	524.1	0.941	487.7	1.301
24	2.184	2.649	538.6	1.048	503.1	1.416
25	2.060	2.811	550.1	1.167	515.4	1.550
26	1.951	2.970	552.7	1.318	522.6	1.694
27	1.834	3.131	559.7	1.436	529.4	1.823
28	1.743	3.290	569.4	1.534	537.1	1.939
29	1.657	3.449	574.7	1.647	546.4	2.041

Power–Law Fit $J = C(\Delta a)^n$

Unloading Compliance	J_{Ic} : 368 kJ/m^2	(16 Data)	
Coeff. C : 513 kJ/m^2	Exponent n : 0.33	Fit Coeff. R : 0.948	
DC Potential Method	J_{Ic} : 313 kJ/m^2	(17 Data)	
Coeff. C : 442 kJ/m^2	Exponent n : 0.32	Fit Coeff. R : 0.996	

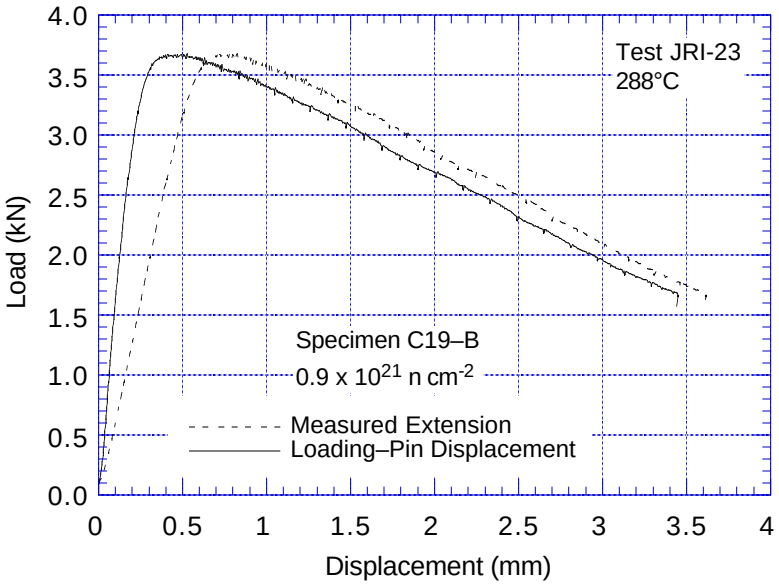

Figure A-15.1 Load-vs.-loadline displacement curve for specimen C19–B of irradiated Type 304 SS tested at 288°C

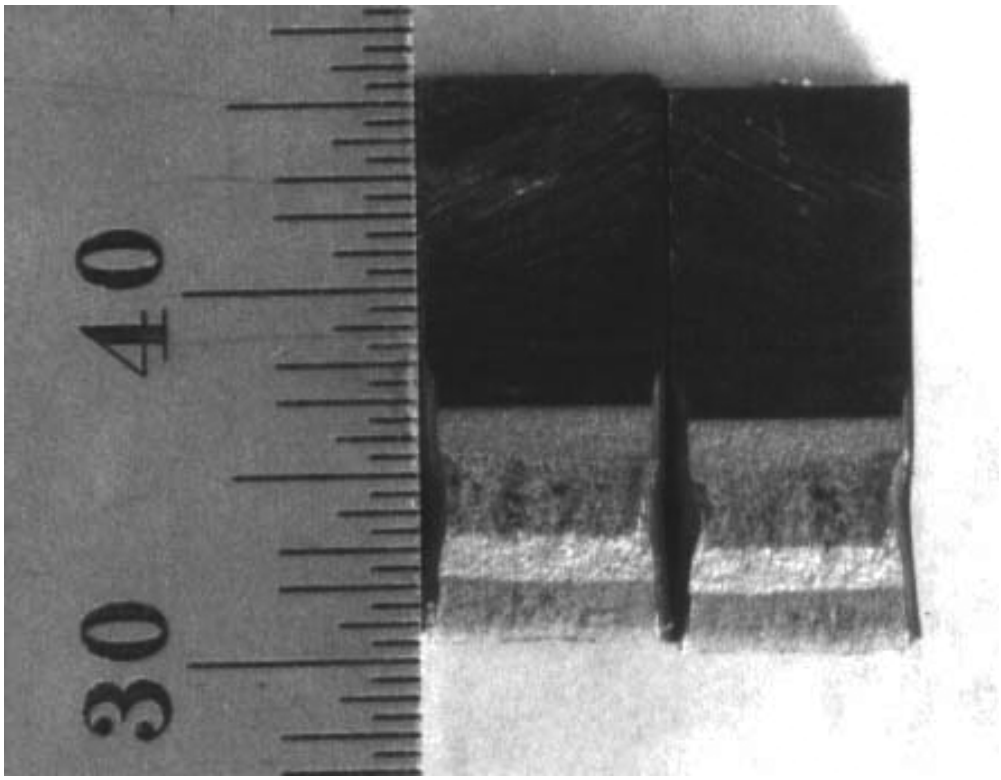

Figure A-15.2 Fracture surface of specimen C19–B tested at 288°C

Table A-16. Test data for specimen C19–C of irradiated Type 304 SS tested at 288°C

Test Number	: JRI–33	Test Temp.	: 288°C
Material Type	: Type 304 SS	Heat Number	: C19
Aging Temp.	: –	Aging Time	: –
Irradiation Temp.	: 288°C	Fluence	: 2.0 x 10^{21} n/cm^2
Thickness	: 6.50 mm	Net Thickness	: 5.85 mm
Width	: 12.00 mm	Flow Stress	: 794.0 MPa
Modulus E	: 175 GPa	Effective Flow Stress	: 566.8 MPa
Initial Crack	: 7.38 mm	Init. a/W	: 0.61 (Measured)
Final Crack	: 9.20 mm	Final a/W	: 0.77 (Measured)
Final Crack	: 9.13 mm	Final a/W	: 0.76 (Compliance)

	Load	Deflection	Unloading Compliance		DC Potential Method	
No.	(kN)	(mm)	J (kJ/m^2)	Δa (mm)	J (kJ/m^2)	Δa (mm)
0	0.089	0.000				
1	0.621	0.040	1.1	-0.254		
2	0.930	0.061	2.1	-0.011		
3	1.251	0.082	4.3	0.047		
4	1.586	0.106	7.3	-0.034		
5	1.911	0.129	10.3	-0.078		
6	2.234	0.156	14.3	-0.103		
7	2.543	0.182	19.2	-0.381		
8	2.839	0.210	23.2	-0.388		
9	3.108	0.240	29.1	-0.253		
10	3.352	0.273	35.0	-0.176		
11	3.540	0.310	42.9	-0.090		
12	3.668	0.350	52.3	-0.044		
13	3.718	0.397	64.4	0.038		
14	3.691	0.449	78.8	0.003		
15	3.627	0.504	96.1	0.006		
16	3.546	0.558	110.7	0.072		
17	3.412	0.668	140.4	0.102		
18	3.232	0.781	168.7	0.168		
19	3.070	0.893	190.6	0.311		
20	2.926	1.004	212.8	0.387		
21	2.746	1.118	228.3	0.575		
22	2.569	1.232	239.9	0.762		
23	2.426	1.343	248.2	0.956		
24	2.294	1.453	256.6	1.122		
25	2.166	1.564	269.5	1.230		
26	2.073	1.672	280.5	1.351		
27	1.963	1.780	297.9	1.445		
28	1.871	1.889	306.0	1.523		
29	1.795	1.997	318.9	1.599		
30	1.700	2.105	329.9	1.680		
31	1.625	2.212	340.0	1.757		

Power–Law Fit $J = C(\Delta a)^n$

Unloading Compliance J_{Ic} : 188 kJ/m^2 (15 Data)

Coeff. C : 268 kJ/m^2 Exponent n : 0.28 Fit Coeff. R : 0.967

DC Potential Method (information could not be determined)

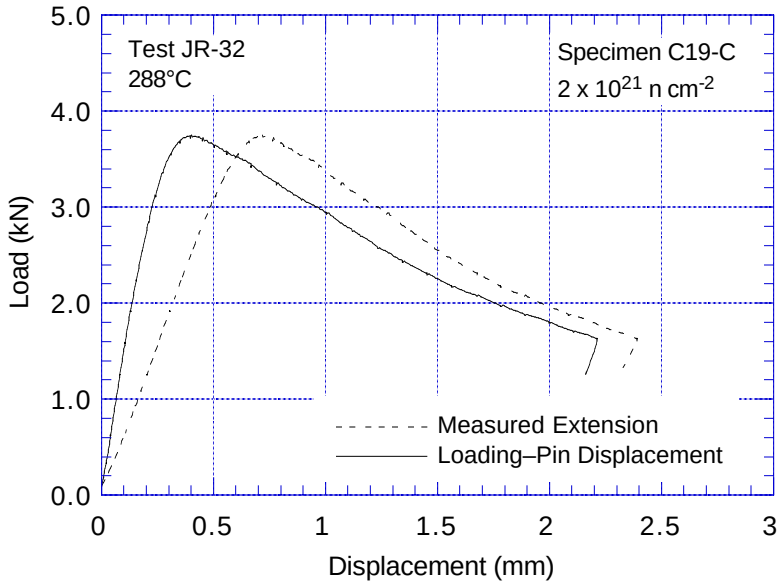

Figure A-16.1 Load-vs.-loadline displacement curve for specimen C19–C of irradiated Type 304 SS tested at 288°C

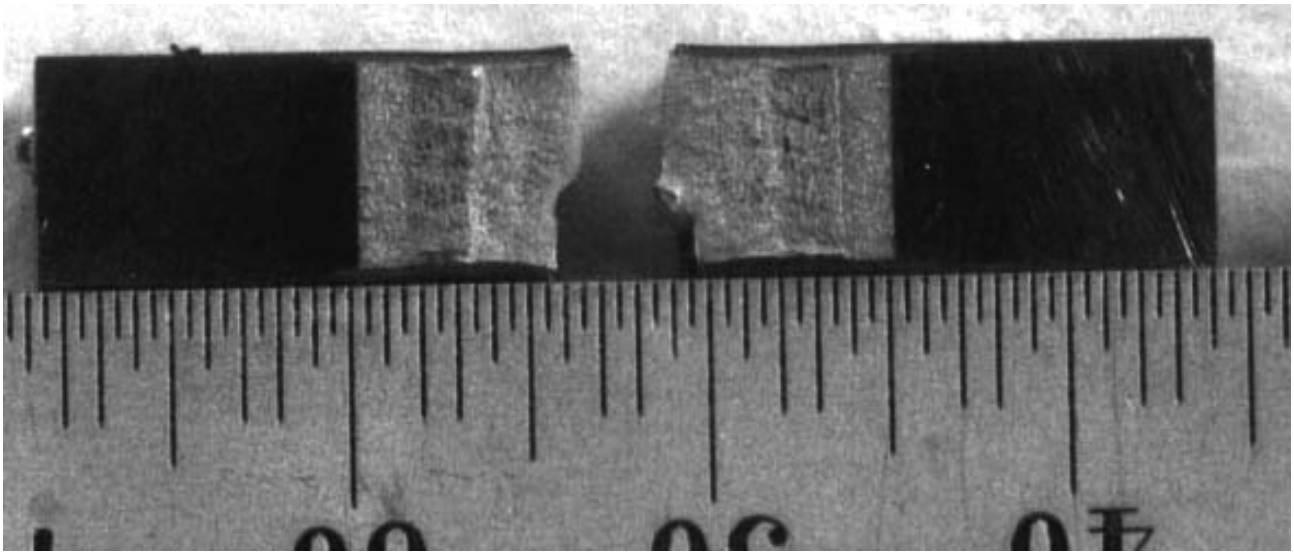

Figure A-16.2 Fracture surface of specimen C19–C tested at 288°C

Table A-17. Test data for specimen C16–A of irradiated Type 316 SS tested at 288°C

Test Number	: JR–26	Test Temp.	: 288°C
Material Type	: Type 316 SS	Heat Number	: C16
Aging Temp.	: –	Aging Time	: –
Irradiation Temp.	: 288°C	Fluence	: 0.9 x 10^{21} n/cm^2
Thickness	: 6.50 mm	Net Thickness	: 5.85 mm
Width	: 12.00 mm	Flow Stress	: 590.0 MPa
Modulus E	: 175 GPa	Effective Flow Stress	: 463.0 MPa
Initial Crack	: 7.28 mm	Init. a/W	: 0.61 (Measured)
Final Crack	: 8.73 mm	Final a/W	: 0.73 (Measured)
Final Crack	: 8.36 mm	Final a/W	: 0.70 (Compliance)

No.	Load (kN)	Deflection (mm)	Unloading Compliance		DC Potential Method	
			J (kJ/m^2)	Δa (mm)	J (kJ/m^2)	Δa (mm)
0	0.089	0.000				
1	2.527	0.212	33.3	0.054	26.6	0.015
2	2.702	0.275	42.4	0.066	39.8	0.019
3	2.755	0.347	59.3	0.004	55.6	0.026
4	2.785	0.421	74.5	0.024	72.0	0.033
5	2.807	0.496	89.8	0.097	88.7	0.039
6	2.810	0.572	106.4	0.099	105.4	0.047
7	2.812	0.649	123.1	0.136	122.8	0.054
8	2.821	0.725	141.0	0.117	139.8	0.062
9	2.832	0.801	159.6	0.097	156.9	0.070
10	2.818	0.880	176.6	0.126	174.5	0.077
11	2.823	0.955	191.1	0.184	191.4	0.084
12	2.821	1.031	207.2	0.202	208.3	0.091
13	2.800	1.136	230.7	0.217	230.0	0.139
14	2.805	1.236	255.9	0.189	249.9	0.183
15	2.784	1.338	279.1	0.198	269.6	0.234
16	2.785	1.441	294.0	0.310	289.0	0.290
17	2.770	1.544	313.2	0.356	307.9	0.346
18	2.745	1.647	343.0	0.293	327.1	0.397
19	2.720	1.751	354.0	0.430	345.8	0.456
20	2.693	1.853	378.8	0.410	363.3	0.515
21	2.655	1.957	402.9	0.413	380.8	0.576
22	2.619	2.063	414.2	0.521	398.1	0.638
23	2.573	2.169	430.2	0.580	414.7	0.703
24	2.539	2.273	455.9	0.561	430.3	0.767
25	2.512	2.378	479.9	0.561	445.4	0.834
26	2.480	2.482	498.3	0.595	461.4	0.888
27	2.444	2.588	513.3	0.648	477.9	0.941
28	2.393	2.693	512.5	0.796	493.9	0.994
29	2.351	2.797	532.4	0.807	506.3	1.051
30	2.292	2.904	550.9	0.836	521.0	1.111
31	2.230	3.010	560.4	0.911	532.4	1.188
32	2.180	3.117	568.0	0.989	543.1	1.260
33	2.128	3.223	584.6	1.016	554.5	1.325
34	2.081	3.328	596.2	1.068	565.4	1.390
35	2.040	3.429	613.3	1.086	575.4	1.453

Power–Law Fit $J = C(\Delta a)^n$

Unloading Compliance	J_{Ic} : 353 kJ/m^2	(12 Data)	
Coeff. C : 607 kJ/m^2	Exponent n : 0.52	Fit Coeff. R : 0.848	
DC Potential Method	J_{Ic} : 299 kJ/m^2	(14 Data)	
Coeff. C : 490 kJ/m^2	Exponent n : 0.45	Fit Coeff. R : 0.997	

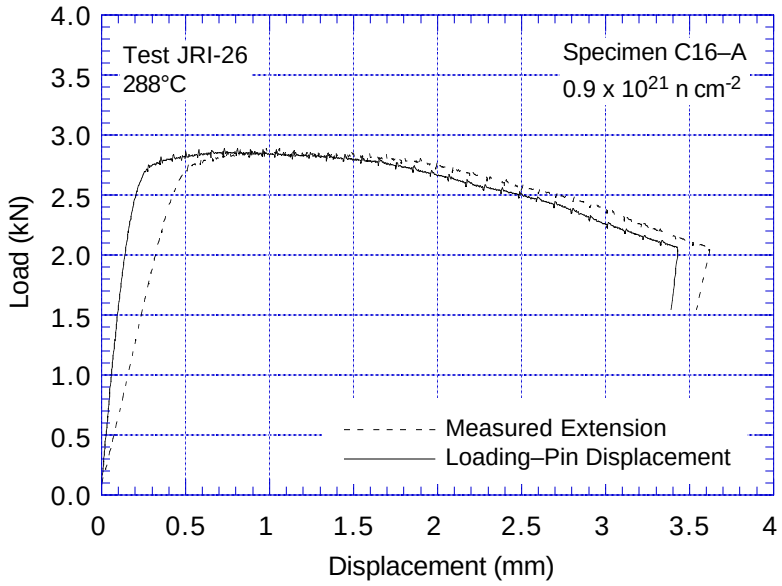

Figure A-17.1 Load-vs.-loadline displacement curve for specimen C16–A of irradiated Type 316 SS tested at 288°C

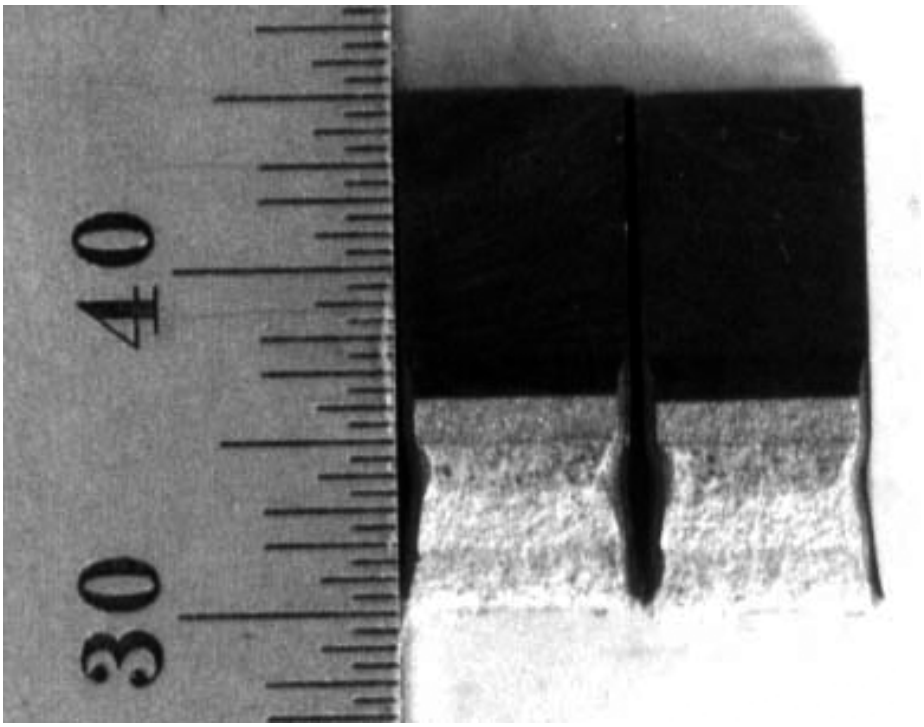

Figure A-17.2 Fracture surface of specimen C16–A tested at 288°C

Table A-18. Test data for specimen L20–A of irradiated Type 304 SS tested at 288°C

Test Number	: JR–22	Test Temp.	: 288°C
Material Type	: Type 304 SS	Heat Number	: L20
Aging Temp.	: –	Aging Time	: –
Irradiation Temp.	: 288°C	Fluence	: 0.3 x 10^{21} n/cm^2
Thickness	: 6.50 mm	Net Thickness	: 5.85 mm
Width	: 2.00 mm	Flow Stress	: 270.5 MPa
Modulus E	: 175 GPa		
Initial Crack	: 7.38 mm	Init. a/W	: 0.61 (Measured)
Final Crack	: 9.17 mm	Final a/W	: 0.76 (Measured)
Final Crack	: 8.08 mm	Final a/W	: 0.75 (Compliance)

No.	Load (kN)	Deflection (mm)	Unloading Compliance		DC Potential Method	
			J (kJ/m^2)	Δa (mm)	J (kJ/m^2)	Δa (mm)
0	0.089	0.000				
1	1.300	0.080	6.5	0.237	6.5	0.006
2	1.453	0.169	18.9	0.152	17.1	0.016
3	1.529	0.265	30.2	0.155	29.3	0.028
4	1.596	0.361	43.7	0.126	41.9	0.040
5	1.648	0.459	58.7	0.041	55.2	0.054
6	1.685	0.556	72.5	0.015	68.9	0.067
7	1.717	0.656	87.4	0.027	83.2	0.080
8	1.741	0.756	101.7	0.040	97.7	0.093
9	1.754	0.857	117.1	0.027	112.4	0.107
10	1.769	0.958	130.1	0.082	127.1	0.119
11	1.774	1.059	144.7	0.101	142.1	0.132
12	1.780	1.160	159.9	0.104	157.0	0.146
13	1.775	1.275	176.7	0.120	171.1	0.234
14	1.759	1.379	191.6	0.136	181.6	0.339
15	1.734	1.482	203.5	0.200	192.3	0.432
16	1.708	1.586	214.2	0.277	201.9	0.542
17	1.692	1.688	227.3	0.310	211.0	0.651
18	1.666	1.793	238.6	0.372	220.9	0.747
19	1.619	1.898	243.2	0.518	230.0	0.850
20	1.580	2.001	252.5	0.593	237.2	0.973
21	1.544	2.105	260.8	0.676	244.9	1.075
22	1.504	2.209	265.5	0.798	253.0	1.173
23	1.461	2.315	275.3	0.859	259.4	1.289
24	1.411	2.470	283.6	1.006	270.8	1.429
25	1.353	2.627	292.9	1.132	280.0	1.577
26	1.280	2.785	299.8	1.271	286.5	1.741
27	1.219	2.942	304.8	1.417	292.3	1.893

Power–Law Fit	$J = C(\Delta a)^n$		
Unloading Compliance	J_{Ic}	: 237 kJ/m^2	(13 Data)
Coeff. C : 283 kJ/m^2	Exponent n	: 0.20	Fit Coeff. R : 0.988
DC Potential Method	J_{Ic}	: 186 kJ/m^2	(15 Data)
Coeff. C : 243 kJ/m^2	Exponent n	: 0.27	Fit Coeff. R : 0.996

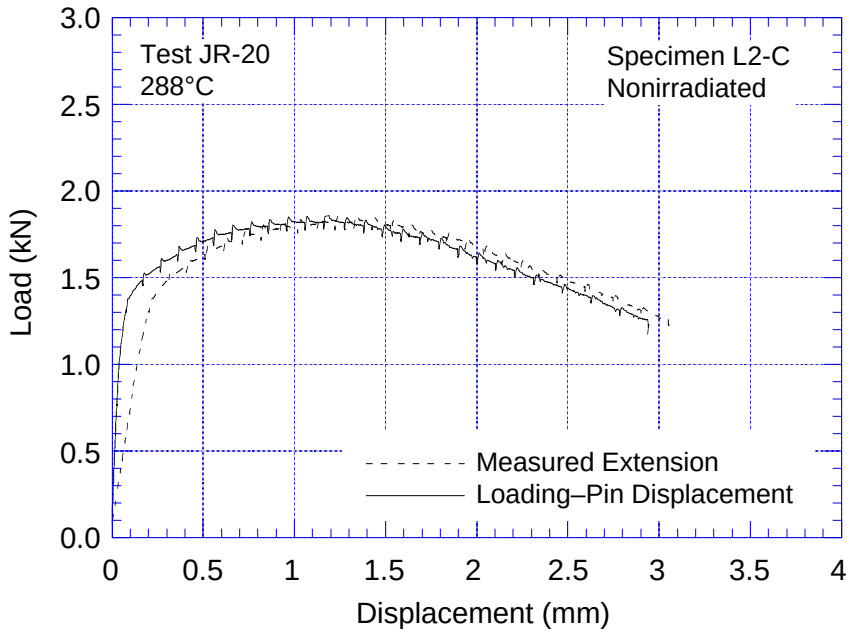

Figure A-18.1. Load-vs.-loadline displacement curve for specimen L20–A of irradiated Type 304 SS tested at 288°C

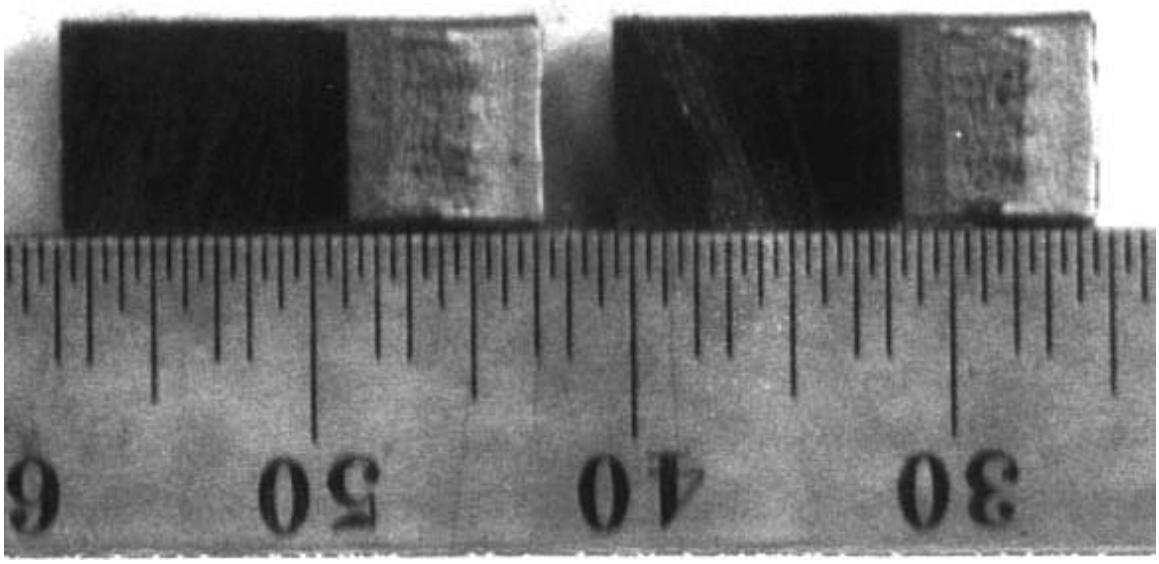

Figure A-18.2. Fracture surface of specimen L20–A tested at 288°C

Table A-19. Test data for specimen L20–B of irradiated Type 304 SS tested at 288°C

Test Number	: JR–24	Test Temp.	: 288°C
Material Type	: Type 304 SS	Heat Number	: L20
Aging Temp.	: –	Aging Time	: –
Irradiation Temp.	: 288°C	Fluence	: 0.9×10^{21} n/cm^2
Thickness	: 6.51 mm	Net Thickness	: 5.84 mm
Width	: 11.98 mm	Flow Stress	: 270.5 MPa
Modulus E	: 175 GPa		
Initial Crack	: 7.38 mm	Init. a/W	: 0.61 (Measured)
Final Crack	: 9.17 mm	Final a/W	: 0.76 (Measured)
Final Crack	: 8.08 mm	Final a/W	: 0.75 (Compliance)

No.	Load (kN)	Deflection (mm)	Unloading Compliance		DC Potential Method	
			J (kJ/m^2)	Δa (mm)	J (kJ/m^2)	Δa (mm)
0	0.089	0.000				
1	1.300	0.080	6.5	0.237	6.5	0.006
2	1.453	0.169	18.9	0.152	17.1	0.016
3	1.529	0.265	30.2	0.155	29.3	0.028
4	1.596	0.361	43.7	0.126	41.9	0.040
5	1.648	0.459	58.7	0.041	55.2	0.054
6	1.685	0.556	72.5	0.015	68.9	0.067
7	1.717	0.656	87.4	0.027	83.2	0.080
8	1.741	0.756	101.7	0.040	97.7	0.093
9	1.754	0.857	117.1	0.027	112.4	0.107
10	1.769	0.958	130.1	0.082	127.1	0.119
11	1.774	1.059	144.7	0.101	142.1	0.132
12	1.780	1.160	159.9	0.104	157.0	0.146
13	1.775	1.275	176.7	0.120	171.1	0.234
14	1.759	1.379	191.6	0.136	181.6	0.339
15	1.734	1.482	203.5	0.200	192.3	0.432
16	1.708	1.586	214.2	0.277	201.9	0.542
17	1.692	1.688	227.3	0.310	211.0	0.651
18	1.666	1.793	238.6	0.372	220.9	0.747
19	1.619	1.898	243.2	0.518	230.0	0.850
20	1.580	2.001	252.5	0.593	237.2	0.973
21	1.544	2.105	260.8	0.676	244.9	1.075
22	1.504	2.209	265.5	0.798	253.0	1.173
23	1.461	2.315	275.3	0.859	259.4	1.289
24	1.411	2.470	283.6	1.006	270.8	1.429
25	1.353	2.627	292.9	1.132	280.0	1.577
26	1.280	2.785	299.8	1.271	286.5	1.741
27	1.219	2.942	304.8	1.417	292.3	1.893

Power–Law Fit		$J = C(\Delta a)^n$		
Unloading Compliance		J_{Ic}	: 237 kJ/m^2	(13 Data)
Coeff. C	: 283 kJ/m^2	Exponent n	: 0.20	Fit Coeff. R : 0.988
DC Potential Method		J_{Ic}	: 186 kJ/m^2	(15 Data)
Coeff. C	: 243 kJ/m^2	Exponent n	: 0.27	Fit Coeff. R : 0.996

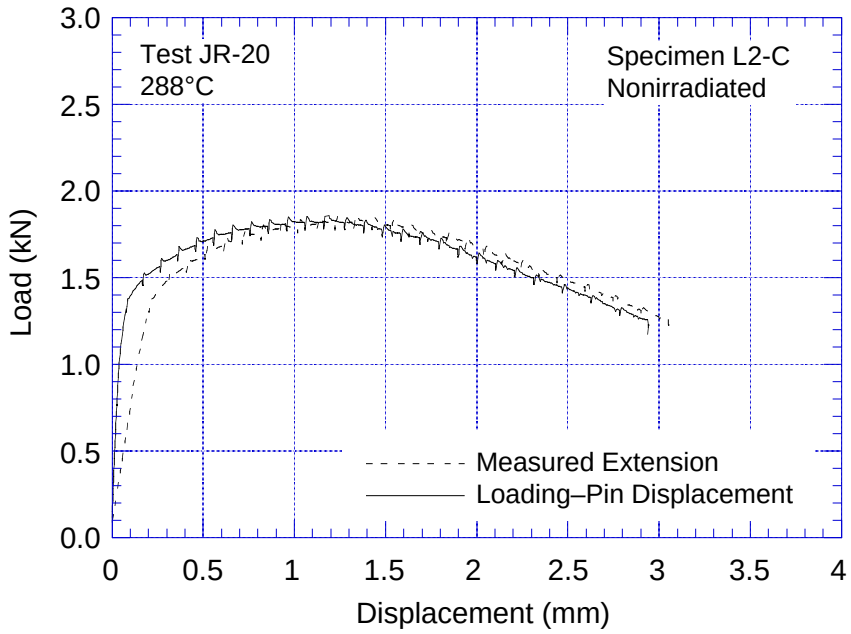

Figure A-19.1. Load-vs.-loadline displacement curve for specimen L20–B of irradiated Type 304 SS tested at 288°C

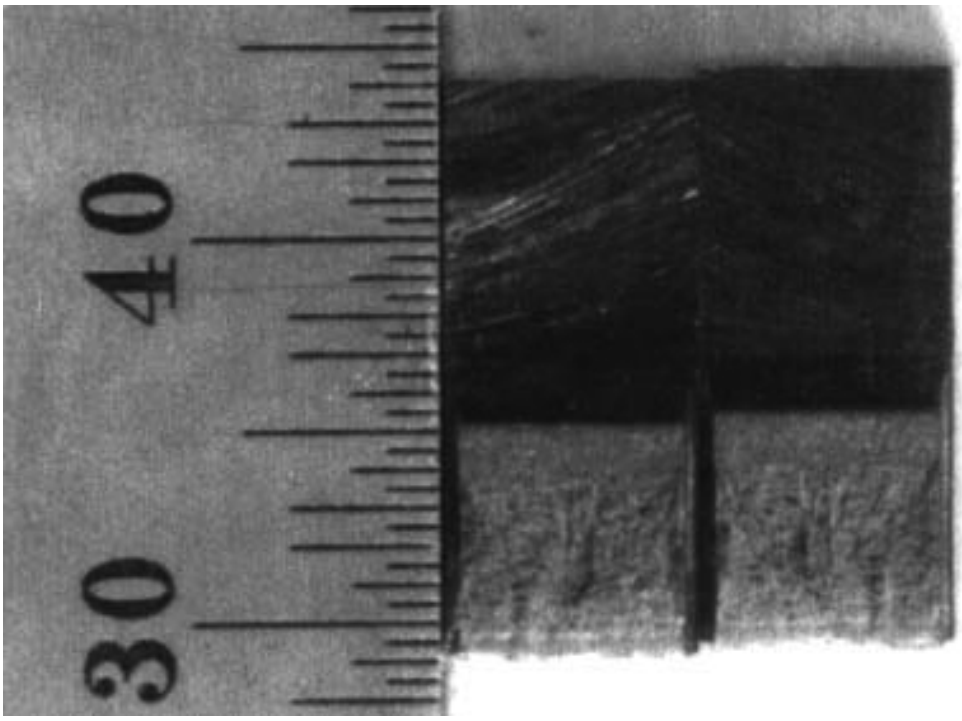

Figure A-19.2. Fracture surface of specimen L20–B tested at 288°C

Table A-20. Test data for specimen L2–A of irradiated Type 304 SS tested at 288°C

Test Number	: JR–25	Test Temp.	: 288°C
Material Type	: Type 304 SS	Heat Number	: L2
Aging Temp.	: –	Aging Time	: –
Irradiation Temp.	: 288°C	Fluence	: 0.9×10^{21} n/cm^2
Thickness	: 6.51 mm	Net Thickness	: 5.84 mm
Width	: 11.98 mm	Flow Stress	: 270.5 MPa
Modulus E	: 175 GPa		
Initial Crack	: 7.38 mm	Init. a/W	: 0.61 (Measured)
Final Crack	: 9.17 mm	Final a/W	: 0.76 (Measured)
Final Crack	: 8.08 mm	Final a/W	: 0.75 (Compliance)

No.	Load (kN)	Deflection (mm)	Unloading Compliance		DC Potential Method	
			J (kJ/m^2)	Δa (mm)	J (kJ/m^2)	Δa (mm)
0	0.089	0.000				
1	1.300	0.080	6.5	0.237	6.5	0.006
2	1.453	0.169	18.9	0.152	17.1	0.016
3	1.529	0.265	30.2	0.155	29.3	0.028
4	1.596	0.361	43.7	0.126	41.9	0.040
5	1.648	0.459	58.7	0.041	55.2	0.054
6	1.685	0.556	72.5	0.015	68.9	0.067
7	1.717	0.656	87.4	0.027	83.2	0.080
8	1.741	0.756	101.7	0.040	97.7	0.093
9	1.754	0.857	117.1	0.027	112.4	0.107
10	1.769	0.958	130.1	0.082	127.1	0.119
11	1.774	1.059	144.7	0.101	142.1	0.132
12	1.780	1.160	159.9	0.104	157.0	0.146
13	1.775	1.275	176.7	0.120	171.1	0.234
14	1.759	1.379	191.6	0.136	181.6	0.339
15	1.734	1.482	203.5	0.200	192.3	0.432
16	1.708	1.586	214.2	0.277	201.9	0.542
17	1.692	1.688	227.3	0.310	211.0	0.651
18	1.666	1.793	238.6	0.372	220.9	0.747
19	1.619	1.898	243.2	0.518	230.0	0.850
20	1.580	2.001	252.5	0.593	237.2	0.973
21	1.544	2.105	260.8	0.676	244.9	1.075
22	1.504	2.209	265.5	0.798	253.0	1.173
23	1.461	2.315	275.3	0.859	259.4	1.289
24	1.411	2.470	283.6	1.006	270.8	1.429
25	1.353	2.627	292.9	1.132	280.0	1.577
26	1.280	2.785	299.8	1.271	286.5	1.741
27	1.219	2.942	304.8	1.417	292.3	1.893

Power–Law Fit		$J = C(\Delta a)^n$		
Unloading Compliance		J_{Ic}	: 237 kJ/m^2	(13 Data)
Coeff. C	: 283 kJ/m^2	Exponent n	: 0.20	Fit Coeff. R : 0.988
DC Potential Method		J_{Ic}	: 186 kJ/m^2	(15 Data)
Coeff. C	: 243 kJ/m^2	Exponent n	: 0.27	Fit Coeff. R : 0.996

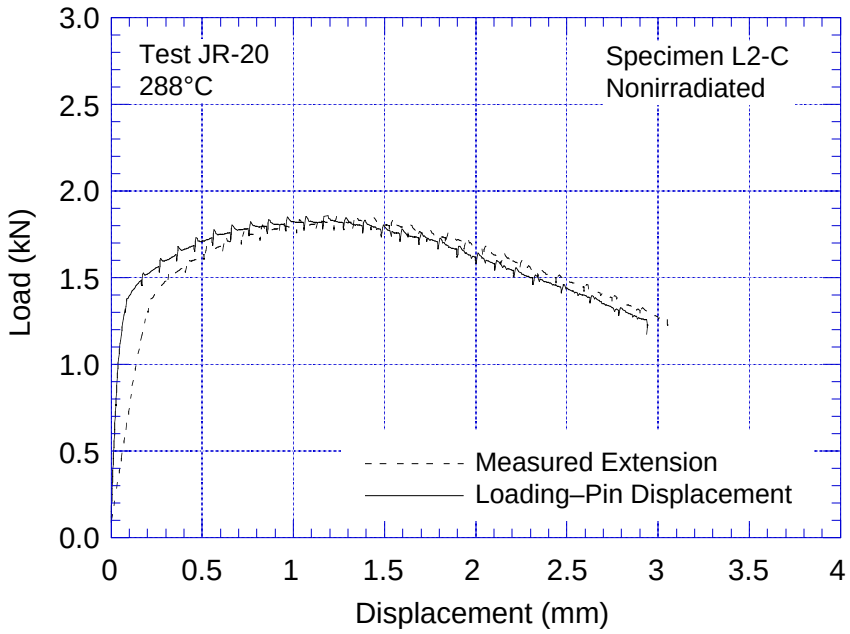

Figure A-20.1. Load-vs.-loadline displacement curve for specimen L2–A of irradiated Type 304 SS tested at 288°C

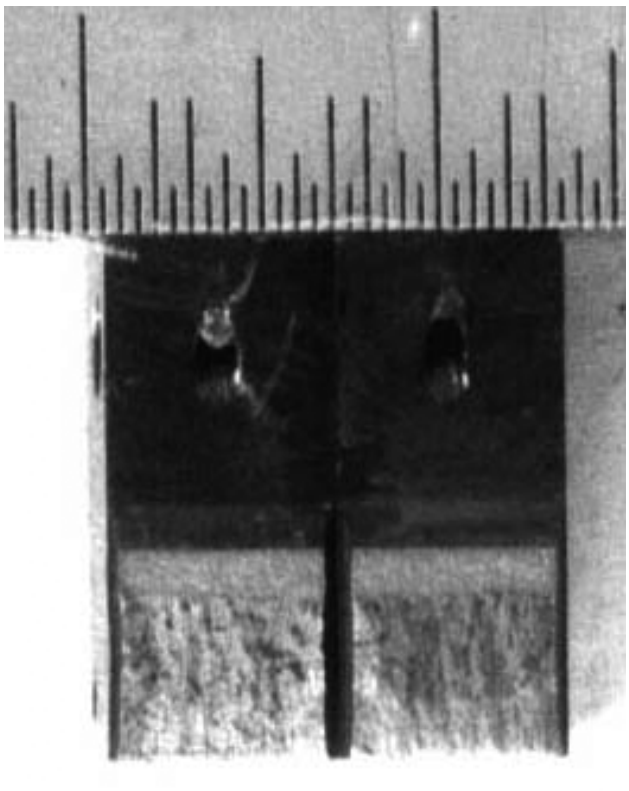

Figure A-20.2. Fracture surface of specimen L2–A tested at 288°C

NRC FORM 335
(2–89)
NRCM 1102,
3201, 3202

U. S. NUCLEAR REGULATORY COMMISSION

BIBLIOGRAPHIC DATA SHEET

(See instructions on the reverse)

1. REPORT NUMBER
(Assigned by NRC. Add Vol., Supp., Rev., and Addendum Numbers, if any.)

NUREG/CR–6826
ANL–03/22

2. TITLE AND SUBTITLE

Fracture Toughness and Crack Growth Rates of Irradiated Austenitic Stainless Steels

3. DATE REPORT PUBLISHED

MONTH	YEAR
August	2003

4. FIN OR GRANT NUMBER

Y6388

5. AUTHOR(S)

O. K. Chopra, E. E. Gruber, and W. J. Shack

6. TYPE OF REPORT

Technical

7. PERIOD COVERED (Inclusive Dates)

8. PERFORMING ORGANIZATION – NAME AND ADDRESS (If NRC, provide Division, Office or Region, U.S. Nuclear Regulatory Commission, and mailing address; if contractor, provide name and mailing address.)

Argonne National Laboratory
9700 South Cass Avenue
Argonne, IL 60439

9. SPONSORING ORGANIZATION – NAME AND ADDRESS *(If NRC, type "Same as above": if contractor, provide NRC Division, Office or Region, U.S. Nuclear Regulatory Commission, and mailing address.)*

Division of Engineering Technology
Office of Nuclear Regulatory Research
U.S. Nuclear Regulatory Commission
Washington, DC 20555–0001

10. SUPPLEMENTARY NOTES

William H. Cullen, Jr., and Carol E. Moyer, NRC Project Managers

11. ABSTRACT (200 words or less)

Austenitic stainless steels (SSs) are used extensively as structural alloys in the internal components of reactor pressure vessels because of their superior fracture toughness properties. However, exposure to high levels of neutron irradiation for extended periods leads to significant reduction in the fracture resistance of these steels. Experimental data are presented on fracture toughness and crack growth rates (CGRs) of austenitic SSs irradiated to fluence levels up to 2.0×10^{21} n/cm^2 (E > 1 MeV) (^{a}3.0 dpa) at ^{a}288°C. Crack growth tests were conducted under cycling loading and long hold time trapezoidal loading in simulated boiling water reactor (BWR) environments, and fracture toughness tests were conducted in air. Neutron irradiation at 288°C decreases the fracture toughness of the steels; the data from commercial heats fall within the scatter band for the data obtained at higher temperatures. In addition, the results indicate significant enhancement of CGRs of the irradiated steels in normal water chemistry BWR environment; the CGRs for irradiated steels are a factor of ^{a}5 higher than the disposition curve proposed for sensitized austenitic SSs. The rates decreased by more than an order of magnitude in low–dissolved–oxygen BWR environment.

12. KEY WORDS/DESCRIPTORS *(List words or phrases that will assist researchers in locating this report.)*

Fracture Toughness
J–R Curve
Crack Growth Rate
Neutron Irradiation
BWR Environment
Dissolved Oxygen
Austenitic Stainless Steels

13. AVAILABILITY STATEMENT
Unlimited

14. SECURITY CLASSIFICATION
(This Page)
Unclassified
(This Report)
Unclassified

15. NUMBER OF PAGES

16.ICE PR

NRC FORM 335 (2–89)

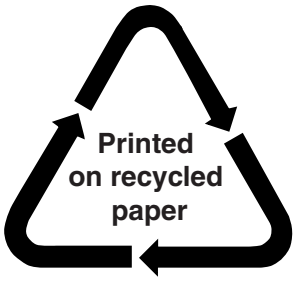

Federal Recycling Program